Giuseppe Marulo

Fatigue life assessment of thin-walled welded joints

Tesi di Laurea Magistrale

Università di Pisa

Luglio 2014

Università di Pisa

Dipartimento di Ingegneria Civile e Industriale

Corso di Laurea Magistrale in Ingegneria dei Veicoli

Fatigue life assessment of thin-walled welded joints

Tesi di

Giuseppe Marulo

Relatori

Prof. Ing. F. Frendo
Prof. Ing. L. Bertini
Ing. A. Tomasella

Sessione Laurea 09 Luglio 2014
Anno Accademico 2013/2014

Contents

Chapter 1

Introduction and summary

1.1 Introduction

The importance of fuel economy in vehicle's design is rapidly increasing. The heightened fuel prices are not the only reason. Also pollution and green house gasses emissions are strictly correlated to the amount of fuel utilized. In the next years most countries will adopt laws enforcing limits on green house gasses for light vehicles. This will affect vehicle's design in many ways, one of which is lightweight design. Disregarding the engine technology a lighter vehicle needs less energy to obtain the same performance of a heavier one. This is especially true in low speed urban contexts, where the resistance force has almost linear dependence on vehicle's mass.

This said lightweight design is a crucial aspect to consider in order to achieve the reduction of fuel consumption and the emissions of green house gasses of vehicles. For this reason the use of high strength steel is rapidly increasing for automotive applications. Since they make possible the design of components with reduced dimensions and so reduced mass. In many cases, welding on those components is unavoidable or at least one of the most used joining technologies. In this prospect fatigue life assessment of thin walled welded structures is one of the field where research is needed. Since fatigue is one of the main causes of failure, and a welded joint is generally a critical spot for fatigue crack nucleation. A better estimation of fatigue life allows for smaller security factors to be applied in design procedures, and so to a better usage of the material.

This makes the background of the present work, that was carried out at the Fraunhofer Institute for Structural Durability and System Reliability LBF in Darmstadt, Hessen.

1.2 Summary

In the present work the theoretical background for fatigue design of welded joints will be briefly summarized. Then the main existing fatigue life assessment methods will be discussed. Specific attention will be given to the effective notch stress theory. A database of fatigue tests on thin walled laser welded joints will be created, containing experimental data from tests performed at the Fraunhofer LBF as well

as data taken from literature. For each specimen in the database the stress field in the welded area will be obtained by means of finite element analysis. In all the models, a reference radius of $r_{ref} = 0.05$ mm will be used to model the notch at the weld root, which is always (in our database) the spot where the fatigue crack starts.

It will be shown that, by means of a properly defined effective stress, results from very different test series can be brought together in an S–N curve with a tight scatter band. Both the stress averaging approach according to Neuber and the critical distance approach according to Taylor will be applied in order to obtain the desired effective stress. Their application will be optimized for thin walled structures using the scatter of the S–N curve as main decisional parameter. A reference S–N curve with a survival probability of 97.5% for both methods will be proposed, which could be utilized in design procedures. The possibility of new more complex kernels for the definition of the effective stresses will be briefly discussed.

In the second chapter an analysis of fatigue concepts, with regard to welded connections, will be summarized. The most popular existing fatigue life assessment methods will be discussed. A more detailed argumentation will be performed for the notch stress method and the effective stress method, as they will be applied in the following of this work. Some aspects of their application to thin walled high static strength structures will be pointed out.

In chapter three, the specimen's categories inserted into the database will be described. Then the application of the notch stress method and the averaged stress methods to real thin walled specimen will be discussed. The structure of the overall work will be outlined, from both the functional and the operational points of view.

The finite element (FE) models by which the stress field in the notch area is obtained will be described in chapter four. The entire test database is too big to study the influence of every possible variation for all the specimens in it. Therefore an accurate study will be performed for only two specimens, in order to better understand the real effects of every possible parameter variation. Then an analysis to all the specimens in the database will be performed, studying the effects of the most effective parameters. Due to the usual scatter of fatigue test data, a big number of tests and a statistical approach are needed to verify each assessment method. Therefore a script to automatically create and analyse the FE models will be created.

In chapter five the fatigue data evaluation will be described. The composition of the database and the most significative parameters characterizing each test series will be reported. A regression method is applied to identify the S–N curve from the experimental data points. Finally the application of several assessment methods to obtain the effective stress for each specimen is discussed.

In chapter six the results obtained, summarized as S–N curves, will be used to validate the assessment methods proposed. The resulting scatter will be assumed as the main parameter for the estimation of the performance of each method.

Finally in chapter seven the more relevant conclusions are summarized. For both the averaged and critical distance methods design oriented S–N reference curves will be proposed. Then some possible future developments are discussed.

Chapter 2

State of the art and research

2.1 Fatigue considerations for welded joints

The present work focuses on the application of existing fatigue life approaches to thin walled high static strength steel welded structures. In the present chapter peculiar aspects of fatigue behaviour for welded joint will be pointed out. Some existing assessment methods will be summarized, and their application to thin walled structures will be analysed.

The behaviour of welded structures under cyclic loads has some peculiar aspects, which may be significantly different in comparison to non-welded structures. An accurate discussion on this subject can be found in [12] and [14], some parts of which will be summarized here. The aspects that will be discussed are:

1. crack nucleation and propagation;

2. stress concentration factor;

3. residual and medium stress;

4. influence of material yield strength.

2.1.1 Crack nucleation and propagation

Generally speaking, it is possible to subdivide the fatigue life of a component in two phases:

- crack nucleation;

- crack propagation.

For small components with high stress levels and no initial imperfections the crack nucleation phase tends to be much greater than the crack propagation one. The opposite behaviour is shown by bigger components with lower stress levels which are generally produced with technological processes that can not exclude the presence of initial imperfections. Unfortunately real cases tend to be somewhere in between the two opposite behaviours.

The number of cycles needed for crack nucleation can be assessed comparing the local stress with the S-N (Wöhler) curves for that material. The crack propagation life is usually evaluated with fracture mechanics based methods.

As reported in [8] there are different fatigue design strategies for welded joints, under constant amplitude loading, predominantly defined by the fatigue method analysis, inspection and monitoring in service:

- infinite life design;

- safe life design;

- fail safe design;

- damage tolerant design.

Infinite and safe life design are based on the assumption that initially the joint is free of imperfections. No monitoring in service is specified. The first one is based on keeping all fatigue actions under the resistance fatigue limit or threshold value, and is fitted for fatigue actions which are almost uniform and act at a very high cycles. For both of them a high survival probability has to be provided. Damage tolerant design is based on the assumption of the presence of crack as large as the the detection level of the non-destructive testing method applied. Fracture mechanics is used to calculate the life cycles to failure. From the number of cycles, inspection intervals are derived. This strategy generally allows the best results in terms of weight reduction, but the regular testing required is to expensive for most applications, such as automotive ones. Fail safe design is based on statically over-determined or redundant structures. In case of fatigue failure, redistribution of forces provides an emergency life, so that the failure can be detected and repaired. This strategy gives the best results in terms of safety considerations, but the use of redundant structures lead to a significative increase in terms of weight and cost of the structure. Thus this method is not generally used in the automotive sector.

The present work is focused on thin walled high strength structures for automotive applications, under constant amplitude loading. Therefore infinite or safe life design strategies will be adopted.

When designing a component loaded with variable amplitude, a damage accumulation rule is needed. Generally the linear Palmegren-Miner sum is adopted. In this case no fatigue limit is thought to occur, therefore no infinite life design is possible.

2.1.2 Stress concentration factor

The considerations in the present section must be understood under the hypothesis of linear elastic material behaviour. In a welded joint there are three main causes of stress concentration:

- geometrical;

- metallurgical;

- weld imperfections.

The geometry of the joint and of the weld seam plays a big role in determining the local elastic stress value ($K_t = 4 - 6$ are common values). There exists many different weld geometry, so it is not easy to discuss the matter from a general point of view. However it is possible to say that, in each kind of joint, one of the most significative geometrical parameters is the radius at the weld root and toe. Some of its characteristics are:

- a smaller radius leads to a higher stress values

- the real radius value depends on the welding process more than on the shell thickness

- the real radius value is not easy to measure and can significantly change along the weld seam

The differences existing between the filling material and the base material, but even the difference between melted and non-melted material if no filling is used, leads to some variation of material properties, such as Young's and Poisson's modulus, in the area near the welding. This affects the stress field in the same way a geometrical notch does, creating areas were the stress is higher than the nominal one. But the stress concentration factors are generally quite low compared to the ones obtained from geometrical notches. Especially if no filling material is used and a post welding heat treatment has been performed.

The welding process itself is known to possibly produce a large number of different imperfections. Imperfections can create spots with high stress concentration factors or even cracks which have to be analysed with fracture mechanics approaches. If placed near the weld root or toe, they can interact with the stress field in that area, generally increasing the stress concentration factor. However experimental researches carried out so far have shown that, if the imperfections are under usual technological limits, fatigue cracks tend to start from the weld toe or root. This leads to the hypothesis that the effects of geometrical notches are more relevant than the one caused by weld imperfections.

The above mentioned considerations are the main hypothesis that lead to assess the fatigue life of a welded joint analysing the stress field at the weld root or toe with methods derived from notch stress concentration factors assessment, such as the Neuber theory [13]. This methods will be discussed in more detail on sec. 2.3.2.

2.1.3 Residual and mean stress

In order to completely define the loading two parameters [1] are needed, the most used one in welded joint analysis are:

- the load amplitude

$$L_a = \frac{L_{MAX} - L_{min}}{2} \tag{2.1}$$

---

[1]under the hypothesis of sinusoidal trend and no effects of the frequency

- the load ratio

$$R = \frac{L_{min}}{L_{MAX}} \tag{2.2}$$

Other commonly used parameter are:

- load range

$$\Delta L = L_{MAX} - L_{min} \tag{2.3}$$

- medium load

$$L_{med} = \frac{L_{MAX} + L_{min}}{2} \tag{2.4}$$

It is possible to define similar parameters for the stresses. If we assume the stress to be linearly proportional with the load, the ratio does not change. Therefore there is generally no distinction between the stress ratio and the load ratio, and the symbol R is used for both of them.

If there are no residual stresses the load ratio has a wide effect on the fatigue life. Generally speaking: decreasing the load ratio (increasing the mean load) the endurable number of cycles at the same load range decreases.

2.1.4 Influence of material yield strength

Most fatigue life assessment methods for welded joints do not regard the endurable static stress of the base material as a relevant parameter. There are several reasons for this choice. First of all welded joints are severely notched components. It is widely known that in fatigue life evaluation of notched components the *notch stress concentration factor* K_t is replaced by the *fatigue notch factor* K_f, which is defined by [11]:

$$K_f = 1 + (K_t - 1)\, q \tag{2.5}$$

where the notch sensitivity q is a material dependent parameter, and it is generally bigger for materials with an higher static stress strength, leading to a bigger K_f. Therefore the increase in fatigue life is smaller than what could be expected looking only at the static strengths of two different steels.

Furthermore the static strength increases the number of cycles needed for the nucleation of a crack, but has only little effects on the crack growth rate. In welded joint as discussed in [12] the main part of fatigue life is given by the crack growth phase, which is only slightly influenced by the static strength.

This said, the yield stress or ultimate stress is surely one of the parameters influencing the fatigue life, but it is not one of the most relevant.

2.2 Existing fatigue life assessment methods

In [8] and [14] is possible to find a detailed description of the more commonly used fatigue life assessment methods, together with useful recommendations for their application. In that work the effects of improvement techniques and weld imperfections are discussed and guidance is given for the estimation of their influence on the fatigue strength. Here only the basic concepts about the fatigue life assessment methods, will be summarized.

2.2.1 Nominal stress method

The nominal stress is defined as the average stress in a welded joint, calculated by an agreed formula. In the IIW recommendations [8], a list of structural details is given. For each one of them the FAT value is stated. Which is the characteristic value of the stress range at two million cycles regarding a survival probability of $P_\sigma = 97.5\%$ and a stress ratio of $R = 0.5$.

This method is based on the assumption that the S-N curve of all welded joints has the same course (Fig. 2.1). The knee point is placed at $N_b = 1 \cdot 10^7$ cycles and a slope of $k = 3$ is chosen. Based on experimental results, in the last years the resolution to drop the idea of a general fatigue limit has been taken [9]. A continuous decline of the fatigue resistance of about 10% per decade was assumed, which leads to a slope of $k^* = 22$. This leaves only one degree of freedom to the S–N curve, that is the vertical position, which is determined by the fatigue class (FAT).
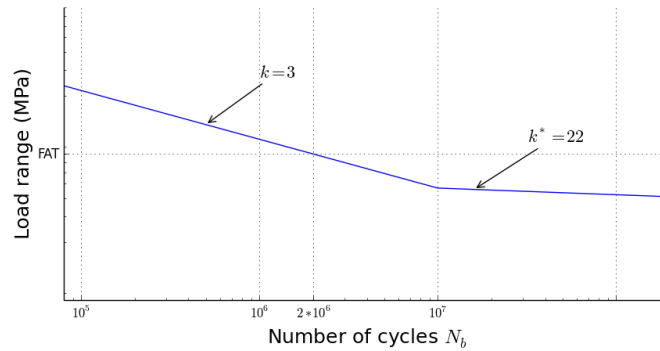

Figure 2.1: Fatigue design curve

At a first glance the nominal stress method could look simple to use, but there are several drawbacks. The most relevant one is that it is not always possible to define a nominal stress. For example in a node of a tubular structure or when the welding is not plane, it is not possible to define a nominal stress with the beam theory.

Another problem is the possible variation of stress in the section under consideration. Macro-geometrical notch effects in the vicinity of the welded joint have to be taken into account, but the distinction between stress concentrations, which have to be considered or not, is not always clear. This problem is even more important when using finite element analysis (FEA), because FEA provides notch stress and not nominal stress. Up to now, no common code or guidance is available, which guides the designer in determining nominal stress from FEA results. Furthermore, FEA calculates geometrical stress concentration and so the factor K_t, whereas the effective factor K_f is relevant for fatigue. Since K_t is always bigger than K_f, the error is on the safe side and can only lead to an uneconomic design.

Last but not least specific fatigue data are needed for each structural detail. Variations within the detail in dimensions, welding process etc. are not covered. This reduction of information gives rise to the scatter, and implies that bigger safety

factors need to be used on the load actions, further increasing the uneconomic design problems of this method.

2.2.2 Structural hot spot method

Structural stress comprises all notch effects of the structural detail but not the notch effect caused by the weld profile itself. It is determined as the linear extrapolation of the stress course on the weld toe of the joint (Fig. 2.2). A Cartesian coordinate system is created were the abscissa is the distance from the hot spot and the ordinate is the stress value. The stress values at two points at a fixed distance from the hot spot are evaluated. Then through a linear extrapolation the desired structural stress at the hot spot is obtained.
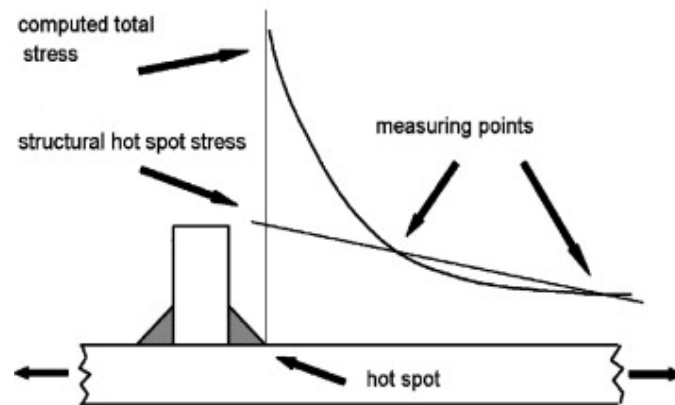

Figure 2.2: Structural hot-spot stress definition [9]

From the above definition some aspects of this method come forward. First of all it is applicable only to surface crack failures. Furthermore, if the stress is obtained by finite element analysis, meshing recommendations should be strictly followed in order to have a comparison between the different analyses.

The fatigue resistance against structural stress is numerically given by two different Wöhler S-N lines, for butt and fillet welds, respectively.
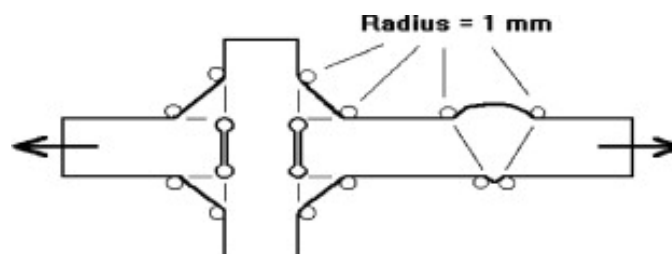
2.2.3 Notch stress method

Figure 2.3: Effective radius [9]

The irregularity of the weld toe and root prevent from a normal determination of the notch stress [9]. Furthermore the elastic notch stress alone is insufficient for

the estimation of fatigue life [15]. This method is based on the determination of an effective notch stress by means of Neuber's micro structural support concept [13]. A section (2.3) of this work will be dedicated to this topic.

When the thickness of the plates forming the joint is $t \geq 5$ mm. The fatigue actions are calculated replacing the irregular notch at welded joints by an effective one with a reference radius of $r_{ref} = 1$ mm. For thin walled joints ($t < 5$ mm), the use of $r_{ref} = 1$ mm will produce a too great weakening of the joint section. Thus a smaller reference radius of $r_{ref} = 0.05$ mm is suggested. Which, according to [20], has its background in the crack tip blunting ([10] and [6]).

The fatigue strength against notch stress can be represented by a S–N curve, whose characteristic depends on the material, on the reference radius and on the equivalent stress hypothesis chosen (Principal stress or von Mises). For example, for a steel specimen with $r_{ref} = 1$ mm under the principal stress hypothesis a FAT 225 is recommended [8]. In [18] it is possible to find a detailed discussion about the reference Wöhler lines for the notch stress method. The suggested FAT values are reported in table 2.1. In [19] a shallower slope for thin steel joints is proposed, with $k = 5.0$ for normal stress and $k = 7.0$ for shear stress.

r_{ref} in mm	1.00	1.00	0.05	0.05
Hypothesis	PSH	von Mises	PSH	von Mises
Steel	225	200	630	560
Aluminium	71	63	180	160
Magnesium	28	25	71	63

All given allowable stress range $\Delta\sigma_{loc}$ are in MPa for $N = 2 \cdot 10^6, R = 0.5, P_s = 97.7\%; k = 3.0, N_k = 1 \times 10^7, k^* = 22.0$

Table 2.1: FAT-values according to the notch stress concept for different reference radii and strength hypothesis (PSH: principal stress hypothesis) [20]

2.2.4 Linear elastic fracture mechanics method

The fracture mechanics method will not be applied in the following of the present work, it is cited here only for the sake of completeness.

Fracture mechanics is suitable for assessment of fatigue life, inspection intervals, crack-like imperfections and the effects of variable amplitude loading.

The calculation of the growth of a crack from a starting length a_i to a final size a_f is performed integrating the Paris power law eq. 2.6.

$$\frac{\mathrm{d}a}{\mathrm{d}N} = C_0 \cdot \Delta K^m \qquad \text{for:} \qquad \Delta K \geq K_{th} \qquad (2.6)$$

Where ΔK is the stress intensity factor (SIF) range, K_{th} is the threshold value, under which no crack propagation is assumed. While C_0 and m are material dependent constants.

The stress intensity factor range ΔK, can be determined directly from FE analysis or by parametric formulae. Both procedures are described in [8].

2.3 Effective stress

"The elastic notch stress alone is insufficient for the estimation if fatigue life of structures" [22]. This statement can be easily understood thinking for example at a structure with a pointed notch, where the elastic stress would reach an infinite value, while the structure retains a finite fatigue life. For this reason the local stress based approaches for the fatigue assessment of notched structures, such as welded joints, are generally performed converting the elastic-linear stress field in the notch area into an effective stress. This can be formally stated as:

$$\sigma_{eff} = \eta \sigma_k, \tag{2.7}$$

where σ_k is the elastic notch stress (some component of the stress tensor), σ_{eff} is the effective stress[2] and η is the notch sensitivity factor. It is theoretically possible to define an infinite number of functions capable of converting the elastic stress field into a fatigue effective one. Looking at the same matter from another point of view, the nominal stress σ_n can be related to the notch and effective stress respectively:

$$\sigma_k = K_t \sigma_n, \qquad \sigma_{eff} = K_f \sigma_n. \tag{2.8}$$

Therefore the notch sensitivity factor η from eq. 2.7 can be thought as the ratio between the fatigue notch factor and the notch stress concentration factor:

$$\eta = \frac{K_f}{K_t}. \tag{2.9}$$

In [22] a general theory based on the functional analysis is developed. Here some aspects of that theory are reported.

The effective stress σ_{eff}, a real number, can be regarded as the result of an adequate mapping of the stress function $\boldsymbol{\sigma}$ into the real space:

$$\sigma_{eff} := \mathcal{F}(\boldsymbol{\sigma}) \in \mathbb{R} \tag{2.10}$$

The map $\mathcal{F}$ is a functional because its arguments are tensor functions, formally $\mathcal{F} : \Sigma \to \mathbb{R}$ where $\Sigma := \{\boldsymbol{\sigma}(\boldsymbol{x}), \boldsymbol{x} \in \Omega\}$ denote the space consisting of all functions of stress tensor defined on the structure Ω.

The functional $\mathcal{F}$ is essentially a property of the considered material. From the Physical point of view, the minimal requirement of homogeneity (in mathematical sense)

$$\mathcal{F}(a\boldsymbol{\sigma}) = a\mathcal{F}(\boldsymbol{\sigma}) \tag{2.11}$$

has to be enforced on $\mathcal{F}$. In other words the effective stress has to increase proportionally to the increase of the external loads.

An additional restriction on $\mathcal{F}$ results if it is applied to a plain specimen in uniform tension. In this case, the effective stress σ_{eff} has to be equal to the

---

[2]The $_{eff}$ subscript is adopted in this work even if a good practice would be to use only one letter subscripts, like σ_e. The reason for this is that the symbol σ_{eff} is adopted in several works on the topic. Also for the r_{ref} symbol the same motivations holds.

nominal stress σ_n. That is

$$\sigma_n = \mathcal{F}(\boldsymbol{\sigma}) \qquad \text{for plain specimens.} \tag{2.12}$$

It is, also, common practice to assume the functional to be linear and continuous

$$\mathcal{F}(a\boldsymbol{\sigma}_1 + b\boldsymbol{\sigma}_2) = a\mathcal{F}(\boldsymbol{\sigma}_1) + b\mathcal{F}(\boldsymbol{\sigma}_2) \ \forall a, b \in \mathbb{R} \wedge \forall \boldsymbol{\sigma}_1, \boldsymbol{\sigma}_2 \in \Sigma. \tag{2.13}$$

This presumption is not really restricting for the most applications because a broad class of existing approaches can be described in this framework.

Finally it is possible[3] to represent the effective stress in its final integral form (eq. 2.14).

$$\sigma_{eff}(\mathbf{x}) = \int_\Omega \mathbf{G}_\mathcal{F}(\mathbf{x}, \bar{\mathbf{x}})\boldsymbol{\sigma}(\bar{\mathbf{x}}) \, \mathrm{d}\Omega_{\bar{\mathbf{x}}}, \qquad \mathbf{x} \in \Omega \tag{2.14}$$

In the above equation, $\mathbf{x}$ is a single point where the functional and then the effective stress are calculated, $\bar{\mathbf{x}}$ is each possible point of the structure Ω, and $\mathbf{G}_\mathcal{F}(\mathbf{x}, \bar{\mathbf{x}})$ plays the role of a weight function. The subscript $\mathcal{F}$ of $\mathbf{G}_\mathcal{F}(\mathbf{x}, \bar{\mathbf{x}})$ empathises its dependence on the functional.

The effective stress obtained with eq. 2.14, thanks to $\mathcal{F}$ being linear and continuous, has the important property to be bounded even if the stress field $\boldsymbol{\sigma}$ has singularities on countable points. According to eq. 2.14 the fatigue effective stress is a non-local parameter, like the micro-structural support concept by Neuber states.

The elasticity theory is based on the Hooke law which correlates the stress in each point of the structure to the strain in the same point, thus it is a local theory. Lattice dynamics describes the deformation behaviour (or precisely movement) of each atom taking into account the influence of its neighbours. A non-local continuum theory is derived where elastic stress results from an integral transform of the strain, thus the stress has no singularities.

2.3.1 Stress averaging by Neuber and critical distance by Taylor

As shown in [22] the existing effective stress assessment methods can be represented by eq. 2.14, choosing the appropriate integral kernel. Both Neuber's and Taylor's assessment methods consider only a component of the stress tensor, the maximum principal stress or the von Mises stress. Therefore a scalar integral Kernel $G_\mathcal{F}(\mathbf{x}, \bar{\mathbf{x}})$ is needed.

The simplest method is the one defined by a constant kernel, formally:

$$G_\mathcal{F}(\mathbf{x}, \bar{\mathbf{x}}) = \begin{cases} \dfrac{1}{\text{mes}(\Omega_x)}, & \forall \bar{\mathbf{x}} \in \Omega_x \subseteq \Omega \\ 0, & \forall \bar{\mathbf{x}} \in \Omega_x \backslash \Omega \end{cases} \tag{2.15}$$

where Ω_x a sub-set of Ω and $\text{mes}(\Omega_x) > 0$ denotes the measure (volume, area or

---

[3]The detailed description of the needed mathematical procedure is discussed by Zhang in [22].

length) of Ω_x. Equipped with this kernel the calculation of the effective stress (eq. 2.14) reduces to:

$$\sigma_{eff}(\mathbf{x}) = \frac{1}{\text{mes}(\Omega_x)} \int_{\Omega_x} \sigma(\bar{\mathbf{x}}) \, d\Omega_{\bar{x}}. \tag{2.16}$$

The difference between Neuber's and Taylor' methods consists in the shape of Ω_x chosen. In 2D- cases Neuber's Ω_x is a line of length ρ^* perpendicular to the surface, from which the famous formula comes:

$$\sigma_{eff}(\mathbf{x}) = \frac{1}{\rho^*} \int_0^{\rho^*} \sigma(\bar{\mathbf{x}}(s)) \, ds. \tag{2.17}$$

Also Taylor's method can be obtained from Eq. 2.14, but now the integration domain is a sphere with a radius of R and its centre at $\mathbf{x} + \mathbf{d} \in \Omega$. $\mathbf{d}$ is a vector starting at $\mathbf{x}$, has a length of d and towards the interior of Σ. If it is imposed $R \to \infty$, the constant kernel $G_{\mathcal{F}}(\mathbf{x}, \bar{\mathbf{x}})$ (Eq. 2.15) becomes the well known Dirac function: $\delta_{\mathbf{x}+\mathbf{d}}$. Therefore the Eq. 2.14 reduces to

$$\sigma_{eff}(\mathbf{x}) = \int_\Omega \delta_{\mathbf{x}+\mathbf{d}} \sigma(\bar{\mathbf{x}}) \, d\Omega_{\bar{\mathbf{x}}} = \sigma(\mathbf{x} + \mathbf{d}) \tag{2.18}$$

in this case $\sigma_{eff}(\mathbf{x})$ simply takes the value of σ at a remote point. Further considerations are reported in [22], they are omitted here for the sake of simplicity.

2.3.2 Fictitious notch rounding

The concept of fictitious notch rounding, developed by Neuber [13], is the basis for the notch stress assessment method (sec. 2.2.3). Neuber's theory, its historical background and more recent theoretical developments are discussed in [15], here follows a brief summary of that work.

Neuber conceived an analytical approach for solving the differential equation system of the linear theory of elasticity, then calculated a closed-form solution for the stress field of several notch shapes. He developed the concept of microstructural support and then the averaged stress approach, which can be formally written as:

$$\sigma_{eff} = \frac{1}{\rho^*} \int_0^{\rho^*} \sigma(x) \, dx \tag{2.19}$$

In order to avoid the integration[4] Neuber formulated the procedure of fictitious notch rounding (fig. 2.4), where the averaged stress on the real notch with a radius ρ is substituted by the maximum stress on a fictitiously enlarged notch radius ρ_f (eq. 2.20).

$$\rho_f = \rho + s\rho^* \tag{2.20}$$

Where the support factor s depends on the loading mode, on the multiaxiality condition at the notch tip and on the applied strength criterion. Also, the notch

---

[4]Neuber wrote his work in 1937, numerical integration was not possible at that time.

opening angle has a considerable influence on s.

The $\rho_f = 1$ mm is obtained assuming the worst case values $\rho = 0$, $s = 2.5$ and the steel micro-support length $\rho^* = 0.4$.
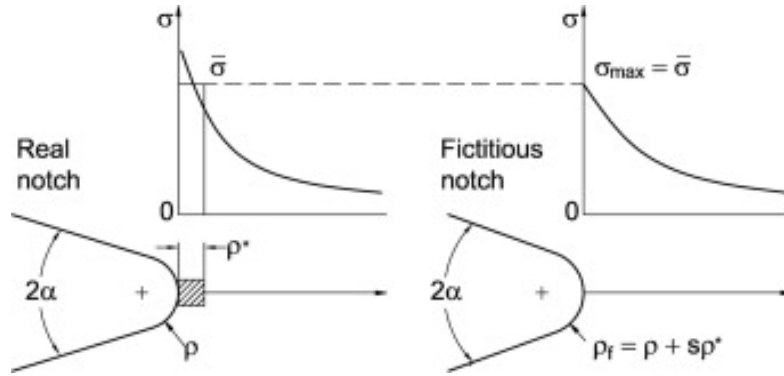

Figure 2.4: Notch stress $\bar{\sigma}$ averaged over ρ^* at real notch radius ρ expressed by maximum notch stress σ_{max} at fictitious notch radius ρ_{f} [15]

2.4 Wöhler or S–N curve

It is widely known that representing experimental results of fatigue tests on a bi-logarithmic coordinate system, with a load related parameter on the ordinate and the number of cycles to failure on the abscissa, a straight regression line is obtained. That is generally referred as Wöhler line and can be formally expressed by the Basquin equation [2]:

$$\sigma = A(N)^{-\frac{1}{k}} \tag{2.21}$$

where the constants A and k defines respectively the height and the slope of the curve.

The mentioned load-related parameter in the above definition can be the load itself, the maximum elastic stress or an effective stress. In (sec. 4.4.1), for the specimens under investigation in the present work, a linear relationship between the load and the elastic stress will be established. While in (sec. 2.3) the property of linearity enforced on the functional $\mathcal{F}$ (eq. 2.13) leads to a linear relationship between the elastic and the effective stress. This said choosing one of the three above mentioned parameters on the ordinate axis will affect the Wöhler line changing the A constant (both value and unit) but not the slope of the curve and so the k value.

2.5 Maximum likelihood regression method

The maximum likelihood method will be used in order to obtain the regression S–N curves for all test series and for the entire database. The main advantage of this method compared to the usual least square method is that even the run-out can

be included in the regression calculation. If no run-out are present the maximum likelihood method gives the same results as the least square method.

This method has been successfully utilized in the analysis of fatigue test results. In [21], the theoretical background is reported and the practical utilization explained.

The procedure, better described in the following section, implies that for each S–N curve[5] the standard deviation σ and then the support function, related to the logarithm of the probability, needs to be calculated based on the position of all experimental points. The curve which posses the maximum support function is the more likely best regression curve. This process implies a big computational effort, furthermore will be applied a number of times in the following chapters. Therefore a script to automatically perform the calculations was implemented. For further discussion, about the practical application of this script, the reader is referred to sec. 5.2 and sec. 6.1, which describes respectively the application of the maximum likelihood method to obtain the load S-N for a single test series and the effective stress S–N curve for all the series in the database.

What follows is a summary of the above cited work of Spindel and Haibach [21].

2.5.1 Calculation of likelihoods and support

The maximum likelihood regression method is based on the assumption that the logarithms of the stress range (or amplitude) follow a normal Gaussian distribution. A set of possible regression curves is created, then for each curve the support function is calculated. The necessary probabilities in the analysis of fatigue data can be calculated in terms of the variable t as:

$$t = \frac{(x - \mu)}{\sigma} \tag{2.22}$$

which is the difference between an observed result x and the assumed mean μ divided by the assumed standard deviation σ[6], where x is the logarithm of the stress range. For each curve to be tested it is possible to calculate the standard deviation. It is thus possible to determine the probability of any given failure directly as the ordinate of the nominal distribution for the point at which the failure occurred. Similarly, the probability of a run-out is given by the cumulative normal probability function[7]. These probabilities can equally be expressed in terms of their logarithms to give the support values. Therefore the contribution to the support from all points in a set of data, irrespective of whether they are failures or run-outs, are then added to give the total support value for the hypothesis considered:

$$\text{SUP} = \sum_{i=1}^{n} \Delta\text{SUP}_i. \tag{2.23}$$

---

[5]As said in sec. 2.4 to describe an S–N curve four parameters are needed.

[6]In this section the symbol σ is adopted to indicate the standard deviation, a common practice in statistics. However, σ is also the universally adopted symbol to indicate the stress. The context in which the σ symbol is placed should leave no ambiguity about its meaning.

[7]This is the probability that no failure occurred up to this point.

The above described procedure returns the value of the support function for each possible regression line, then the most likely one is chosen to be that one with the maximum support function. Please note that an S–N curve as said in sec. 2.4 is described by four parameters, therefore ∞^4 regressions curves are theoretically possible. Obviously it is not possible to calculate the support function for an infinite number of curves. In the realised scripts a set of possible S–N curves is created with discrete variations of each of the four parameters in a range of expected values, in order to reduce the overall computational effort. As an example it would have no meaning to test a curve with a slope of $k = 1000$, because it would be clearly out of the possible range.

2.5.2   Combining sets of results

In [21] the problem of combining sets of results is also discussed. It is stated that two different sets with the same slope could, if put together, lead to a regression curve with a different slope[8]. This difficulty is encountered essentially when the data do not cover the same range of values of the variables as illustrated in Fig. 2.5.

Fig. 2.5a shows two (artificially created) sets of results which describes essentially two parallel S–N lines. The diagram shows regression lines for each set of results and the S–N line for the two sets considered as an unique population, all obtained with the maximum likelihood method. All three are parallel. Fig.2.5b the same three lines are plotted, the method has been applied to same sets, but this time some points were omitted. The top portion of one set is considered with the bottom end of the other. The most likely slopes of the lines have now changed and that of the most likely common line is no longer parallel to the individual lines. The two regression lines for the combined sets are compared in Fig 2.5c.

Obviously a change of the slope when combining several test series with almost the same slope is not a desired output. One of the possible solution to this problem is to calculate a weighted mean value of the slopes of each test series, and then perform the regression using only curves with that fixed slope. This will lead to a loss of support or rather to an increase of the standard deviation.

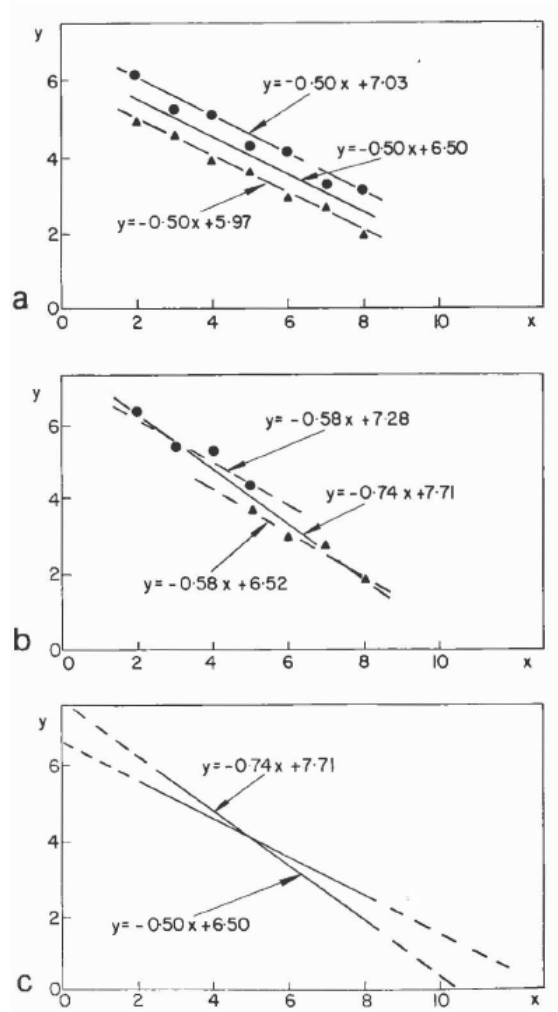[8]This can happen both with the maximum likelihood and the least square methods.

Figure 2.5: Example to demonstrate the difficulties in comparing regression lines or combining data for a common Wöhler line [21]

2.6 Mean stress sensitivity

The reference S–N curves are defined for a stress ratio $R = 0.5$. The reason are tensile residual stresses, that generally are present in welded joints. Under the hypothesis of no residual stresses in the joint, a fatigue life enhancement factor $f(R)$ can be considered. In the design procedures proposed by [8] and [18] the reference curve is multiplied by the factor $f(R) \geq 1$, which produces an increase of the fatigue strength for $R \leq 0.5$. Purpose of our investigation is to obtain a design S–N curve capable to assess the fatigue life of several test series, characterized by different load ratios R. Therefore a $\dfrac{1}{f(R)}$ factor will be applied to the effective stress of each experimental test, obtaining a reduced stress when $R \leq 0.5$.

In the IIW recommendations [8], for components with negligible residual

16

stresses, is suggested:

$$\begin{cases} f(R) = 1.6 & R < -1 \\ f(R) = -0.4R + 1.2 & -1 \leq R \leq 0.5 \\ f(R) = 1 & R > 0.5 \end{cases} \tag{2.24}$$

While Sonsino in [18], for thin welded joints, proposed:

$$\begin{cases} f(R) = 1.32 & R < -1 \\ f(R) = -0.22R + 1.1 & -1 \leq R \leq 0 \\ f(R) = -0.2R + 1.1 & 0 < R \leq 0.5 \\ f(R) = 1 & R > 0.5 \end{cases} \tag{2.25}$$

Both the formulas will be applied, and the results will be discussed in sec.(6.7) of this work.

Chapter 3

Methods for fatigue life assessment of thin-walled welded joints

The present work is focused on establishing an applicable assessment method for thin-walled welded joints, based on the local effective stress theory discussed in sec. 2.3. The effects, if any, of the base material static strength will be discussed.

An experimental investigation has been made on two different kinds of plane specimens. Both are made of 30MnBr5, a high strength steel, and have a plate thickness of $t = 0.9$ mm. From the obtained data, S–N curves have been derived by means of the maximum likelihood regression method (sec. 2.5). A database has been created including the six series experimentally derived and a number of test series of similar specimens taken from literature, plus some tests with a tube specimen (all described in sec. 3.1), for a total of 31 test series which contains 316 experimental points. For each specimen the stress field in the notch area has been calculated by FE analysis. This allows the critical distance and stress averaging approaches (sec. 2.3.1) to be used in order to derive an effective stress. Effective stress - number of cycles couples from the entire database have been plotted together and a regression S–N curve has been derived, for each approach (chapter 6) by the maximum likelihood method. The resulting scatter band for each curve has been calculated, since it can be used as an index to estimate the performance of the corresponding assessment method.

Knowing the S–N curve and its scatter band it is possible to derive a design curve for the assessment method, which is the curve with a survival probability of 97.5%. Here the scatter plays a big role because a S–N curve with a high scatter, can lead to a design curve much lower than another one with the same mean and a lower scatter.

It has to be underlined that increasing the number of series contained inside the database can lead to an increase in the scatter. Therefore the scatter can not be considered an absolute index but a relative one. Or rather the scatter is useful to compare the performance of different assessment methods, but for it to be meaningful every method has to be performed the same database.

In the present chapter the general characteristics of the analysed specimens will be summarized, the general layout described and then the basic principles of the scripts realized to perform all the calculations outlined.
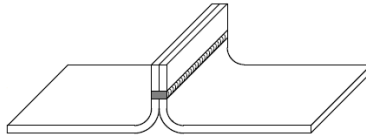
3.1 Specimens

Thin walled welded joints are generally obtained by a laser welding process. The laser allows to concentrate a high amount of energy in a small spot. Thus makes it possible the creation of narrow weld seam, with minimal imperfections and a small heat affected zone. Furthermore it is widely used in the automotive sector because it is easily automated.

In Fig. 3.1 are shown some drawings exemplifying the three categories of specimens analysed in the present work. In the following they will be referred as shear 3.1a, peel 3.1b and tube 3.1c specimens. Even thought the dimensions can vary significantly, those are among the most common categories of thin-walled welded specimens in fatigue oriented investigations.
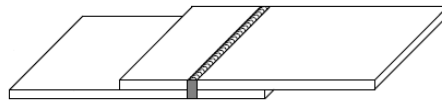
(a) Shear

(b) Peel
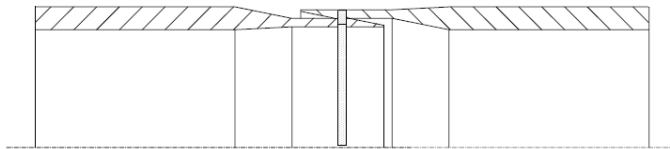
(c) Tube

Figure 3.1: Specimens

3.2 Procedure layout

In fig. 3.2 a diagram representing the overall layout of the present work is shown. The black rectangle contains the process needed in order to obtain the effective stress and the load S–N curve. This part has to be repeated for each test series. Going into detail: the blue rectangles represents the data, while the red one are reserved to the processes performed on those informations. Finally combining the results obtained from all the series it is possible to obtain the effective stress S–N curve (purple box).
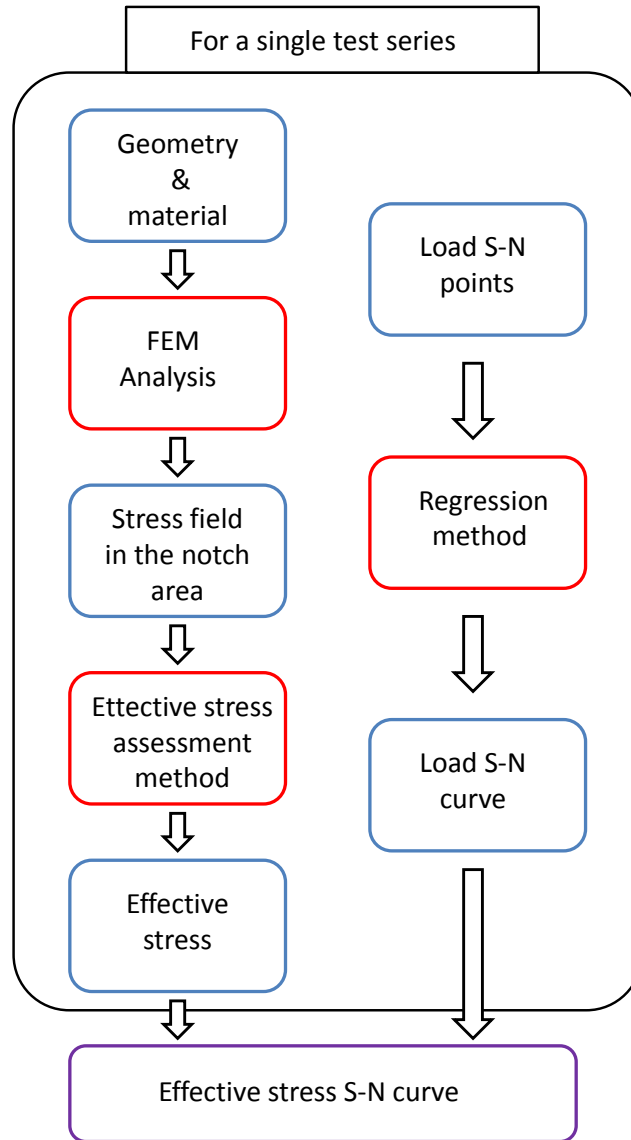
Figure 3.2: Procedure layout

Here a more detailed discussion on the procedure layout, above mentioned follows. The purpose of this section is to give a global view of the overall work. Each step will thoroughly examined in the referred sections. For each test series, given the geometry of the specimen and the properties of the material[1], a FE model can be created (chapter 4),from which it is possible to obtain a numerical description of the elastic stress field in the notch area. It will take the form of a matrix containing the coordinates and the values of the elastic stress components in a finite number of points. Through an effective stress assessment method, is possible to reduce the stress field into a fatigue life related scalar value. The theoretical background for this concept is reported in sec. 2.3, while in sec. 5.3 the application of the methods will be shown.

---

[1]For a linear elastic analysis, only the Young's modulus and the Poisson's ratio are needed.

Also for each test series the maximum likelihood regression (sec. 2.5) method is applied in order to identify the load S–N curve, this operation is described in sec. 5.2.

This done it is possible to draw the effective stress S–N curve containing all the test series. In chap. 6 the curves obtained for each assessment method will be reported. The analysis of those graphs, in particular the width of the scatter band, will allow an estimation of the performance of each assessment method. While the curve with a survival probability $P_\sigma = 97.5\%$ will be assumed as a design curve.

3.3   Scripts

In order to be meaningful an investigation, like the one proposed here, has to be performed on a database as wide as possible. This lead to a large number of data which have to be stored and processed. Therefore a structured database and a set of tools to perform the calculations are needed. This was achieved creating several scripts in the object oriented programming language Python®. An object is a class instance and can be thought as a container for both data and functions generally referred to as methods.

This feature was deeply used, since each test series has been stored as an object (fig. 3.3). This allowed to create the desired database as a list of objects, each containing all the starting data in an easy to access structure. In facts, to retrieve a value from the database it is sufficient to load the corresponding object and state the desired variable name. But this is only the smallest part of the possibilities offered. Since even more useful was the definition of methods for the test series object. As an example this was done for the averaged effective stress, which is obtained integrating the elastic stress course over a path. Obviously the result of this operation depends on the length of the integration domain, called ρ^*. Therefore, storing the elastic stress field inside the object and creating an averaging method, it is possible to obtain the desired effective stress value simply stating the name of the method and the chosen ρ^* value. Furthermore, being all the objects instances of a class, it is possible to expand the definition of the class adding other methods or variable fields. This makes it easy, as an example, to test the performance of new effective stress assessment methods.

Other than the test series object, this approach was used to create all the needed tools. From the implementation of the maximum likelihood regression method to the plotting of the S–N graphs everything has been automatised. Time and effort has been put into creating all this tools for two reasons. First this was the only possible way to perform the investigations showed in the following. Otherwise, creating and analysing a database so big would not have been possible. The second one is that the produced tools are an achievement of the present work even if not related to the results obtained with them. It is a fact that, with minor changes, the classes and other tools implemented for this work could be used in the future for more investigations.
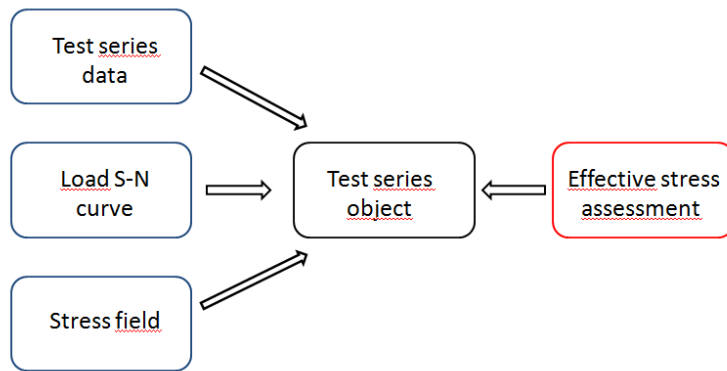
Figure 3.3: database layout

Chapter 4

Local stress field estimation

The needed output of the FEM simulations is the elastic linear stress course in the notch ligament, for it is needed in the effective stress assessments. All the simulations were performed using the software Abaqus 6.12-1®.

In the present work we will analyse three categories of thin walled welded specimens, two different kinds of plate joints and a tube joint, shown in sec. 3.1. In each category there are several specimens which differ principally in plate thickness and width of the gap between the plates. The values of plate thickness vary from $t = 0.8$ mm to $t = 2.0$ mm. A two dimensional finite element model will be utilised, for all the specimens. For the tube specimen we will take advance of its axial symmetry, in order to reduce the model to a two dimensional one containing the section of the tube.

4.1 Notch shape

The tests on all the three category of specimens shows that the crack originates generally from the weld root. For this reason, the internal notch at the weld root and the stress course in that area will be utilized to determine the fatigue strength of the specimens. A reference radius of $r_{ref} = 0.05$ mm will be utilized, this value has been widely used for thin walled joints so a comparison with known results will be possible. Furthermore it fits well with the micro-sections of most of the specimens, being the gap between the two plates approximately $s = 0.1$ mm, for a large number of specimens. Among the suggested internal notch shapes [15], the Keyhole and the U-hole (Fig. 4.1) will be utilized, based on the width of the gap between the two plates. The Keyhole shape will be used for the specimens where non gap exists between the two plates, while the U-notch shape for the specimens where the gap is approximately $s = 0.1$ mm.

The blunt circular V-notch (Fig. 4.2), will be used to compare the results of the FE analysis with the analytical solution found in [23].
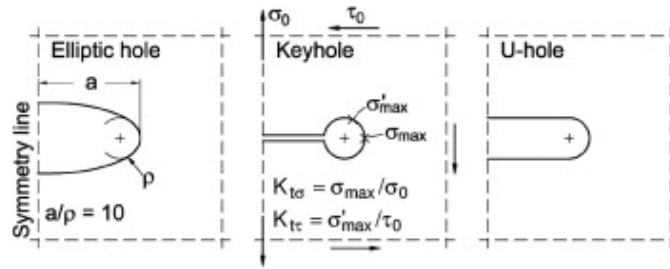
Figure 4.1: Three basic internal notch shapes (elliptical, keyhole, U-notch) under tensile and in-plane shear loading (modes 1 and 2); stress concentration factors $K_{t\sigma}$ and $K_{t\tau}$. [15]
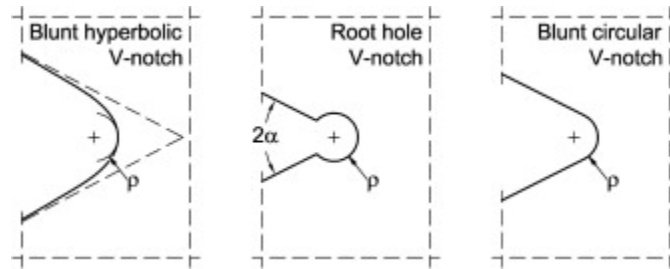
Figure 4.2: Three notch shapes with function-analytical or numerical solutions for fictitious notch rounding. [15]

4.2 Mesh and element type

For the mesh the recommendations found in [3] have been followed. Quadrilateral elements with quadratic shape function have been used. A mapped mesh has been created in the notch area, as shown in (Fig. 4.3). This allows the best results in terms of error on the notch stress value [3], and will make easier the extraction of the stress course. For the peel and shear specimens CPE 8 elements were utilized, while for the tube specimen CAX8R (axial symmetric) elements were chosen. A free mesh has been generated in the other areas of the specimen. Here triangular elements (CPE6 and CAX6 for the axial symmetric tube) with quadratic shape function were allowed. In the transition zone between the mapped mesh and the free mesh an appropriate bias has been imposed, in order to have an overall good mesh quality.

i	32	elements over 360°
V	2	Aspect ratio
Z	1	Factor

Table 4.1: Mesh settings

The mesh parameters chosen are displayed in table 4.1 along with their definition according to [3]. With the above mentioned settings an approximate error of 2% on the notch stress can be assumed. Several simulations have been performed, for each specimen, refining the mesh, in order to validate the results
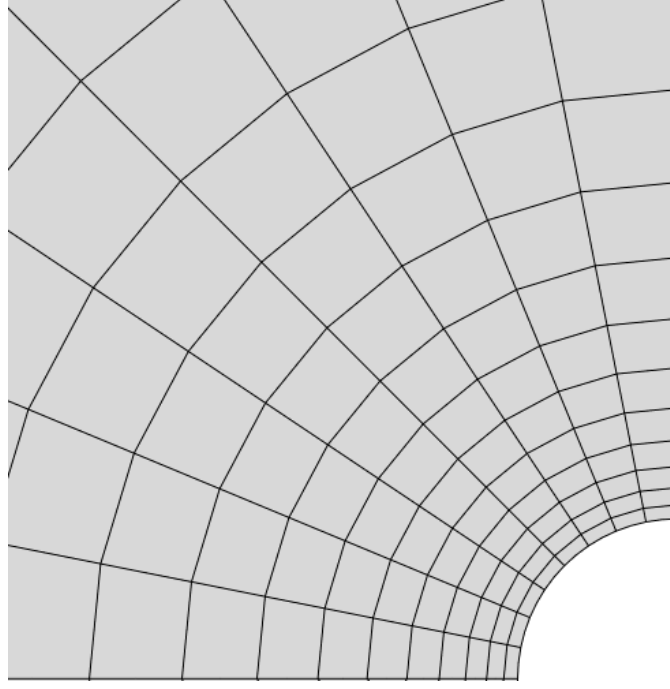
Figure 4.3: Detailed view of the mesh on the notch

obtained. The mesh refinement has been obtained not only increasing the mesh parameters in the notch area, but also decreasing the maximum element size in the free meshed areas and the bias in the transition zone. From the simulations with refined mesh, no significant variations of the stress values were observed, thus confirming the results obtained in [3] for different specimen geometry, comply well with the cases under investigation in the present work.

4.3   Analytical notch model

In order to check the reliability of the FE analysis performed, its results have been compared to the one obtained with the analytical solution found in [23]. For this purpose a simple rectangular plane specimen with a V-shaped notch has been modelled, and loaded with a force perpendicular to the notch (mode I).

The notch sensitivity coefficient η (Eq. 2.7) extracted from the FE analysis is compared with the one calculated with the analytical functions for the blunt circular V-notch, where σ_k is the elastic stress and σ_{eff} is the effective stress, that will be obtained with the Neuber's stress averaging method (Eq. 2.17) Using the Neuber method [13] as reported in [23], the notch sensitivity factor can be brought in the form:

$$\eta = \eta\left(\rho^*, \rho, \omega\right) \tag{4.1}$$

where ρ^* is the micro-support length, ρ is the real radius of the notch and ω is its opening angle (Fig. 4.4). Choosing $\rho^* = 0.4mm$ it is possible, for example, to plot the notch sensitivity factor dependency on ω for different values of ρ as shown in Fig. 4.5. It is possible to obtain the same plot (Fig. 4.6) from the FEM results,
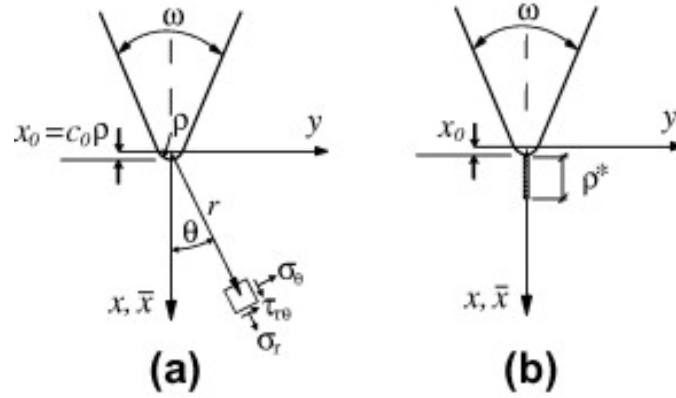
Figure 4.4: (a) Geometry of a V-notch, (b) integration path for the Neuber-method [23]

numerically integrating the stress course with a linear method.
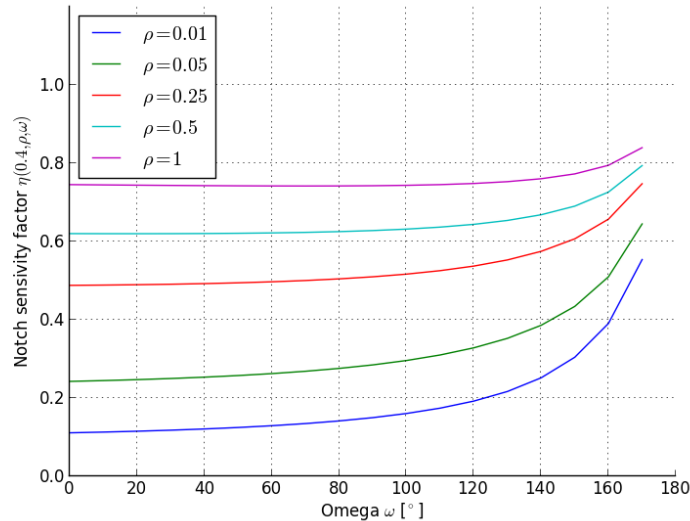
Figure 4.5: $\eta(0.4, \rho, \omega)$ obtained with the analytical solution [23, Fig.4]

Comparing the plots in Figs. 4.5 and 4.6, it is possible to assert that there is a good correlation between the results obtained with the analytical model and the FEM, especially for $\omega < 120°$. For bigger values of ω the accuracy of the FE model drops, this could be caused by the fact that the angle of the radius of curvature at the tip of the notch is very small. Thus allowing very few elements for the mapped mesh region. For the purposes of our analysis this is not a significant limitation, because the internal notches are characterised by an opening angle of $\omega = 0$. So no changes to the mesh have been made to increase the accuracy of the results for big values of ω.

It is important to outline that the overall dimensions of the rectangular body must be big compared to the length of the notch. Because the analytical solution is valid for an infinitely big plate under normal load. The most commonly used integration length is $\rho^* = 0.4mm$ that is the micro-support length for steel which
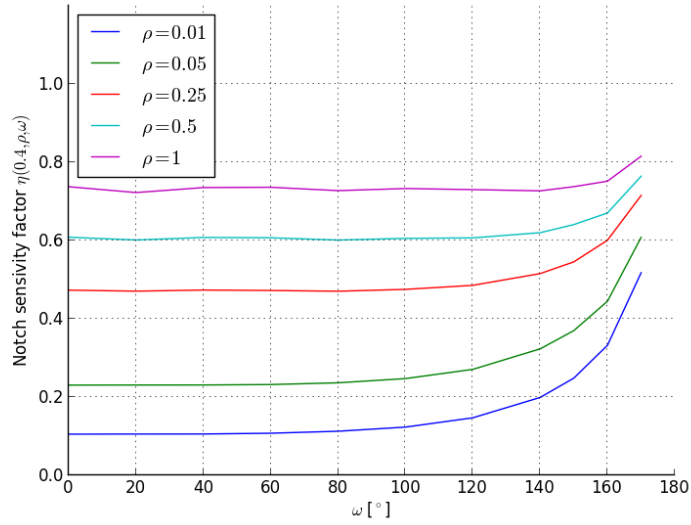
Figure 4.6: $\eta(0.4, \rho, \omega)$ obtained with the FE analysis

leads to the definitions of $r_{ref} = 1mm$ [15]. Such ρ^* value can be considered small enough for thick specimens ($t \geq 5mm$), so the effects of the global stress gradient on local stress gradient can be neglected. This is not true for the thin specimens object of this work where the thickness can drop down to $t = 0.9mm$. The stress course can be imagined as the sum of a non linear stress produced by the notch plus the nominal stress in the section, which can be supposed constant when $\rho^* \ll t$ for every load configuration. This hypothesis does not hold for thinner specimens where $\rho^* \sim t$.

4.4 Model set-up

The entire database is too big to study the influence of every possible variation for all the specimens in it. Therefore it has been decided to perform an accurate study only for two specimens, in order to better understand the real effects of every parameter variation, accepting the hypothesis that the conclusions drawn from those tests will hold for all the specimens in the database.

4.4.1 Linearity check

The relationship between the load and the notch stress will be investigated. This relationship strongly depends on the geometry of the selected specimen. Therefore a sample of each specimen has been tested at different load levels, assuming a geometrically non linear behaviour. The obtained results are plotted in Fig. 4.7, where the blue line represents the non-linear FE model and the red line the linear one. For both the specimens the difference between the two curves is small enough

with a maximum error below 2% on the notch stress. For this reason a linear behaviour will be assumed.

(a) Peel specimen

(b) Shear specimen
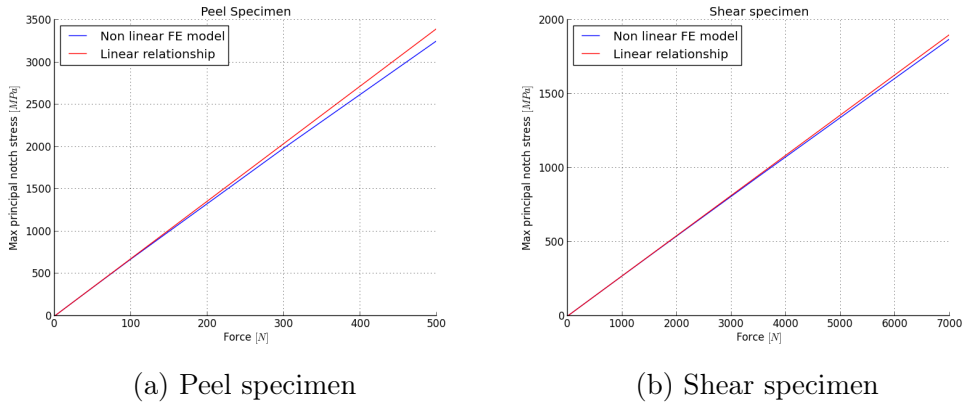
Figure 4.7: Linear versus non linear geometry behaviour

A linear proportionality between load and notch stress greatly simplifies the overall procedure to determine the notch stress. It makes it possible to run only one FE simulation, with a testing load, and extrapolate the desired notch stress for different loads by a simple linear proportion. Moreover, it is not necessary to perform a non linear geometric simulation, therefore reducing the simulation time required. Each model in the database is quite simple but the number of simulations is quite high, making it relevant to reduce the time for each simulation.

4.4.2 Weld seam width

(a) Peel specimen

(b) Shear specimen
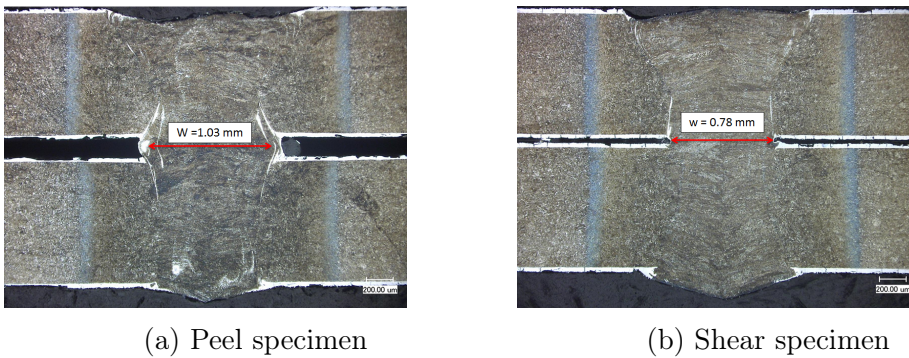
Figure 4.8: Weld width estimation through micro-sections

Along with the reference radius the weld seam width is one of the most relevant factors in determining the effective notch stress. Its numerical value has been determined from the micro-sections available for each specimen (Fig. 4.8). It is important to notice that sometimes it is not easy to fix the exact point where the welding begins or ends due to the characteristic geometrical irregularity of the weld seam. Furthermore taking several sections from the same specimen will lead to not

28

so slightly different values of the weld seam width as well as all the other weld parameters. As plotted in Fig. 4.9 a weld seam width variation affects the peel specimen (30%) much more than the shear specimen (2.5%).
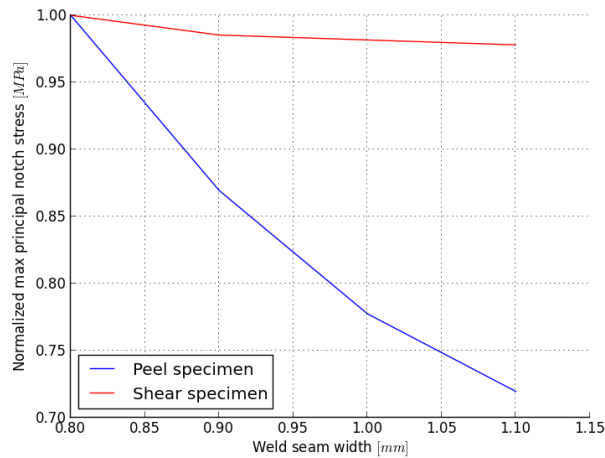
Figure 4.9: Effects of a weld seam width variation on the notch stress

In order to proper investigate the effects of the seam width a three dimensional analysis would be required. The previously reported values are obtained with two dimensional models which implies the hypothesis that all the dimensions do not vary in the third suppressed direction. This surely is a source of error, but implementing a three dimensional model would not solve the problem, because it would require the knowledge of the width in each point of the weld seam.

4.4.3 Positioning errors

Clamping a specimen in the testing machine always produces some positioning errors. It is important to have an idea of the influence of such errors on the notch stress and thus on the fatigue life of the specimen. Knowing the allowed position errors range allows a rational design of the clamping, capable of avoiding influences on the fatigue life while keeping the clamping as easy as possible in order to reduce its costs. Several simulations have been made varying the previously mentioned parameters, the results obtained are plotted in Fig. 4.10. It is possible to say that, whit the allowed precision of standard clamping systems, no significant effects on the fatigue life are expected. A three dimensional model would be required to investigate the effects of other possible positioning errors, such as the angular misalignment.

<div align="center">
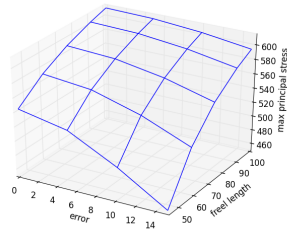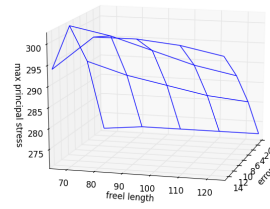
(a) Peel specimen   (b) Shear specimen

Figure 4.10: Effects of positioning errors

</div>

4.5 Scripts

<div align="center">
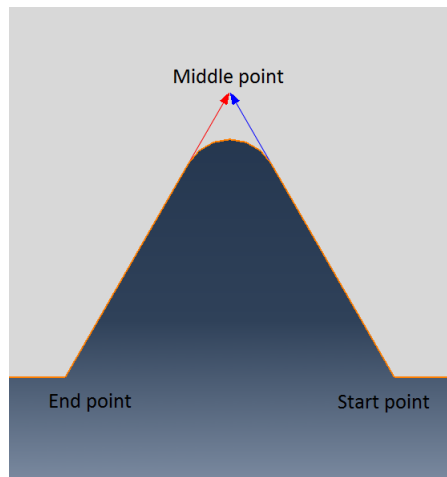
Figure 4.11: Needed points

</div>

Due to the high number of FE models required for the present work, an automated procedure capable of draw and properly mesh the notch is required. This has been achieved creating a Python® script, which is the programming language used by Abaqus®.

The allowed external notch shape are the blunt circular V-notch and the Root hole V-notch (Fig. 4.2), while the internal ones are the Keyhole and the U-hole (Fig. 4.1). The overall script is divided into two parts, first the notch geometry with the desired shape is created then the local mapped mesh is generated. The needed inputs to draw the notch is the position of the three points shown in Fig. 4.11, along with the required notch shape.

Finally the local mesh is generated, as shown in Fig. 4.12. Care has been taken so that the transition between the refined local mesh and the coarser global one is smooth enough, independently on the notch shape chosen.

The script is also capable of finding the maximum stress along the notch reference radius and to extract the stress course in that location on a path perpendicular to the notch surface. Both the maximum principal and von Mises stresses are extracted, and the values obtained are saved on a text file as a table

(a) Blunt circular V-notch

(b) Root hole V-notch

(c) Keyhole notch

(d) H-hole notch
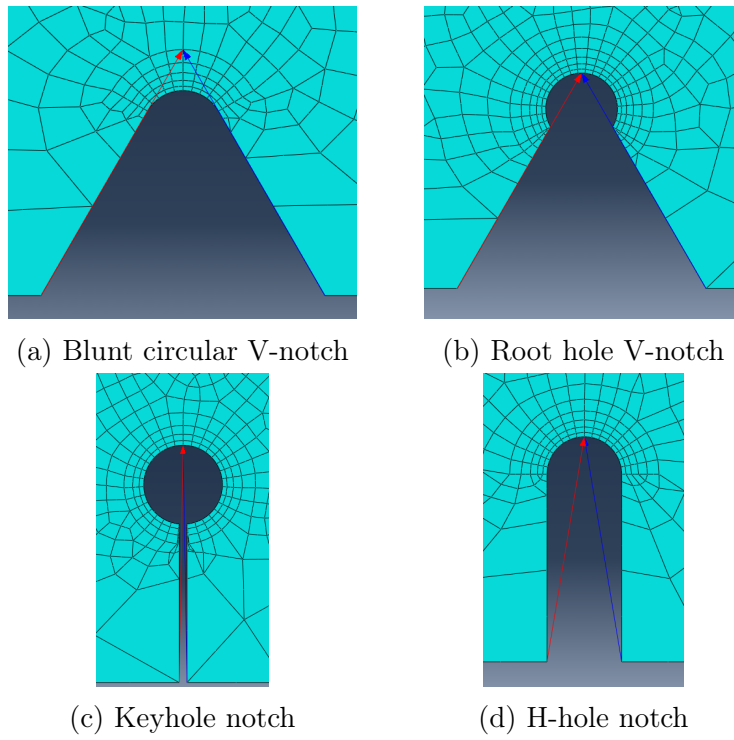
Figure 4.12: Mesh examples

containing the stress values and their coordinates along the path. This output will be later included inside the test series object, for the estimation of the effective stress.

Chapter 5

Evaluation of fatigue data

Due to the statistic nature of fatigue test's results, a number of tests is needed to estimate the fatigue life of a single specimen in relation to the load applied. The array of tests performed on the same specimen will be referred to as a test series. Certainly the specimen's geometry, it's material and the load parameters (amplitude and ratio) are the most relevant variables in defining a test series. But a number of other parameters contribute to define a test series such as: the load frequency, the temperature at which the tests were performed, the technological parameters of the welding and last but not least the criterion which caused the test to stop called failure criterion. For all the test series analysed here the above mentioned criterion was total rupture. However, we can have test were there was no rupture, usually called run-outs. Generally, a low load amplitude is responsible for a run-out. But also the test with a failure of the base material and tests interrupted to measure the crack growth are marked as run-outs. Moreover when a low load amplitude causes a run-out it is possible to test the specimen again whit an increased load, those tests will be marked as retested-run-outs.

5.1   Test series database

In this section some characteristics of the test series inside the database will be reported. They have been subdivided on the basis of the source from which the data are taken. It has been decided to select only specimens that showed a fatigue crack starting from the weld root. Also only tests performed under constant amplitude loading have been included.

Sonsino

- source: Course of SN-curves especially in the high-cycle fatigue regime with regard to component design and safety [17]

- author: C. M. Sonsino

- label: FAT93

- specimen categories: shear (7 series) and peel (3 series)

- material: St14 ($\sigma_y = 313$ MPa)

Eibl

- source: Berechnung der Schwingfestigkeit laserstrahlgeschweißter Feinbleche mit lokalen Konzepten [7]

- author: M. Eibl

- label: FAT01

- specimen categories: shear (4 series), peel (2 series) and tube (3 series)

- material: DC 04 ($\sigma_y = 227$ MPa) and St35 ($\sigma_y = 235$ MPa)

Asim et al.

- source: Fatigue behavior of laser welds in lap-shear specimens of high strength low alloy steel sheets [1]

- author: K. Asim et al.

- label: Asim

- specimen categories: shear (1 series)

- material: J2340 300Y ($\sigma_y = 315$ MPa)

Bruder et al.

- source: Fatigue assessment of seam welds of automotive components by local stress approaches [4]

- author: T. Bruder et al.

- label: A222

- specimen categories: tube (3 series)

- material: S 235 G2T ($\sigma_y = 350$ MPa)

Schmidt et al.

- source: On-line damage detection and monitoring at thin sheet joints for deriving failure criteria [16]

- author: H. Schmidt et al.

- label: A233

- specimen categories: shear (1 series)

- material: Dx52D+Z ($\sigma_y = 246$ MPa)

Super light car

- source: European founded collaborative project "superlight-car" - towards a new generation of light weight automobiles [5]

- author: T. Bruder

- label: SLC

- specimen categories: shear (1 series)

- material: XIP1000 ($\sigma_y = 1000 Mpa$)

Light E body

- source: a research project carried out at the LBF Fraunhofer, not published yet.

- label: LEB

- specimen categories: shear (3 series) and peel (3 series)

- material: 22MnB5 ($\sigma_y = 1000$ MPa)

As said the tests in the Light E body project have been performed at the Fraunhofer LBF, and are not published elsewhere yet. For those tests, with a constant amplitude load, a ratio $R = 0.1$ has been chosen, in order to prevent failures from the base material. Some more informations are reported in appendix A.1. There were two specimen categories: a peel specimen and a shear specimen (Fig.5.1).

(a) Peel specimen   (b) Shear specimen

Figure 5.1: Picture of the tested specimens (removed superficial coating)

The tests where subdivided into three series for the peel specimen and other three series for the shear one, for a total of six test series. Among both the two groups of three series each there is no differences in the nominal dimensions of the specimens. The reasons for splitting the tests were: a different manufacturer (Q series) or the removal of the superficial coating (S series). In Fig. 4.8 the microsections of the specimen tested are shown, and the superficial coating is easily visible. The tests performed after the removal of the coating showed no significant variation of the fatigue life.

5.2   Identification of the S–N curve for a test serie

As said the load - number of cycles curves for each test series have been obtained using the maximum likelihood regression method (sec. 2.5). The theoretical concept of this method is to calculate a support function for each possible line, and choose the one with the maximum value of this function, assuming that this is the most likely one to be the desired regression line.

From the mathematical point of view an S-N curve can be thought as two straight lines, both described by the Basquin equation (eq. 2.21). So four independent parameters are needed in order to fully define the curve, with the notation adopted they are A,A^*,k and k^* where the upper case * refers to the line beyond the knee point. However from the engineering side it is better to translate this set of parameters into a more meaningful one containing: S_k,N_k,k and k^*. Where the lower case k refers to the knee point, so that S_k and N_k are respectively the stress[1] and the number of cycles at the knee point.

No restrictions have been enforced on the three variables S_k,N_k and k, while for k^* only three values have been allowed: $k^* = 22, 45$ and ∞. The first one refers to a decrease of the fatigue strength of 10% per decade which is being proposed by many authors in the last years [8] and [19]. The hypothesis of $k^* = \infty$ comes from the idea of a fatigue limit, while the value $k^* = 45$ was proposed dy Sonsino for thin walled weld specimens, based on experimental tests.

The computer program implemented in this work is able to draw three regression S-N lines for each test series. Here two problems emerge both of which a computer program is not able to solve. First of all a value from the three above mentioned k^* has to be chosen. For a number of test series in the current database this was not really possible, because of the lack of data in the high number of cycles region. Therefore it has been decided to enforce the hypothesis of $k^* = \infty$ on all the test specimens. In average this value has shown the best correlation between the regression line and the experimental points. Not only a common k^* value for all the test series has to be chosen, but it has been found that in some cases the support function of the maximum likelihood method has several local maximums, with slightly different values. In Fig. 5.2 is shown, as an example, the values of the support obtained for a real test series in relation to the number of cycles. It is possible to observe three local maximums located at circa $N_b = 7 \cdot 10^4$, $N_b = 6.5 \cdot 10^5$ and $N_b = 1 \cdot 10^7$.

The main criterion that has been used to choose the N_k value is that specimens made of the same material should show approximately the same position in term of number of cycles for the knee point. For those reasons in some cases not the global but a local maximum has been chosen, accepting a small loss in terms of the support function. In Fig. 5.2 the non regular trend of the support function is due to the fact the variable N_k is not the only parameter that affects the scatter T_σ of the S–N curve and so the support function. A similar trend with local maximums can be expected for the other two free variables (k and S_k) but for those no criterion to choose between several local maximums can be assessed other than the value of the support function.
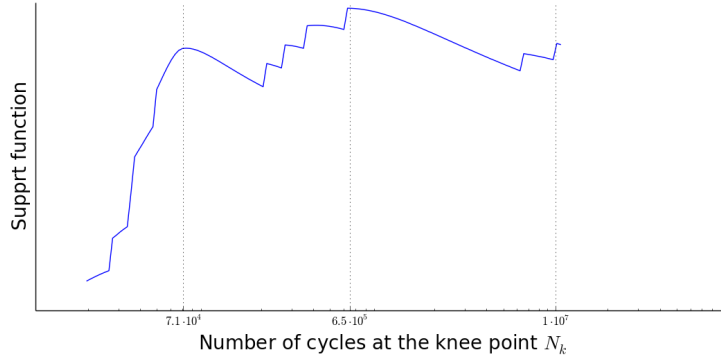
---

[1]Or the load value.

Figure 5.2: Support function versus number of cycles at the knee point

An example of regression S–N curve is shown in Fig. 5.3, in the graph are not only reported the parameters identifying the curve but also the standard deviation related to the curve and some data of the test series such as the name, the load ratio and the frequency at which the load was applied. Moreover the two curves with a survival probability of 10% and 90 % are plotted.
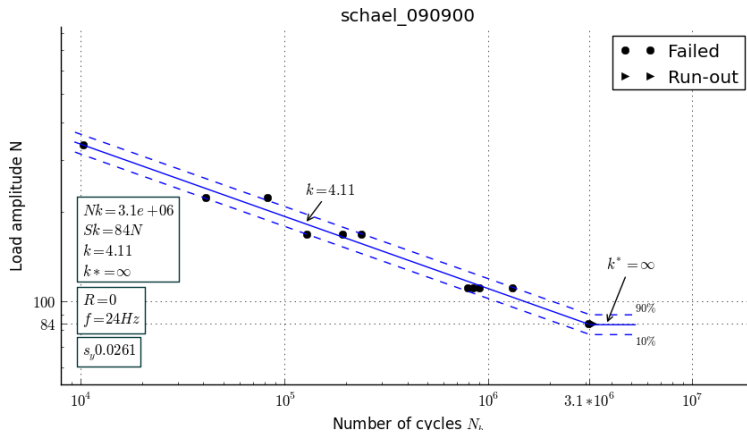

Figure 5.3: Example of regression S-N curve

In appendix A.2 the curves for all the test series in the database are shown. All the graphs are plotted with the same proportion between the axis: the limit values on the abscissa has been fixed and on the ordinate they were chosen as to place the curve in the middle of the available area. This makes possible to easily compare the slope of the various curves. Naturally, having placed the load value on the ordinate axis causes to very different absolute values for this variable (even an order of magnitude).

5.3 Calculation of the effective stress

In sec. 2.3 the theoretical equations which defines the effective stress were reported. The averaged effective stress by Neuber can be calculated by Eq. 2.17, while the critical distance method by Taylor leads to the effective stress defined by Eq. 2.18.

Both equations require as an argument the analytical description stress field in the notch area. In our case, the functions which describes the stress field are not available. All we have is the value such functions assumes in a finite number of points, which is the result of the FE analysis. Therefore the above mentioned equations have been translated from the domain of the continuous functions to the domain of the discrete functions.
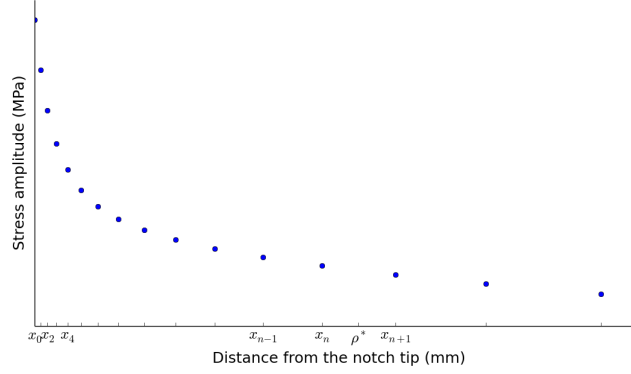
Figure 5.4: Example of stress course obtained from FE analysis

The averaged stress equation 2.17, is transformed into a first order numerical integration described by:

$$\sigma_e = \frac{1}{\rho^*} \left\{ \sum_{i=0}^{n} \left[\frac{\sigma_i + \sigma_{i+1}}{2} (x_{i+1} - x_i) \right] + \left[\frac{\sigma_n + \sigma_{n+1}}{2} (\rho^* - x_n) \right] \right\} \qquad (5.1)$$

where x_i is the distance of the node i from the tip of the notch (Fig. 5.4) and the subscript $_n$ denotes the last available point smaller than ρ^*, so that:

$$x_n < \rho^* < x_{n+1}. \qquad (5.2)$$

For the stress σ the same subscripts has been used. Here the term stress is referred to a single component of the stress tensor, for example the maximum principal stress.

In Eq. 5.1 for each element the mean stress is calculated and multiplied by the length of the element. Since it is not generally possible to have a node at a ρ^* distance from the surface, in the second part of the equation the mean stress in the last element is multiplied by the distance between x_n and ρ^*.

Since the second order elements of the FE model gives a first order description of the stress in each element, the use of an integration formula with an order bigger than one would not be necessary and also not theoretically acceptable. For the same reason a linear interpolation has been used to calculate the critical distance effective stress (eq. 2.18). Which is simply the stress value at a remote distance from the notch tip.

With both methods it is possible to calculate an effective stress along a path, a straight line perpendicular to the notch circumference (Fig. 5.5a). In fig. 5.5b

37
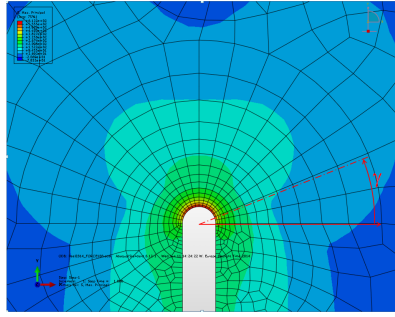
(a) Maximum principal stress
field
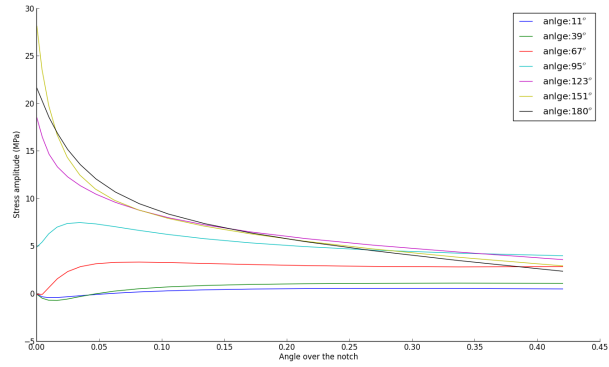
(b) Elastic stress on some paths

Figure 5.5: Peel specimen, both plates $t = 0.9$ mm

the stress curse along several paths is shown.

There is almost no theoretical concepts available to choose of the best path. One possible criterion could be to perform the calculation along a path in the same direction of the fatigue crack. This requires experimental tests to be carried out for every specimen, so can not be proposed in a design oriented assessment method. Furthermore different tests on the same specimen could show cracks growing from different spots and directions, making it difficult to assess a standardized procedure. In the present work two empirical criterion have been investigated. First the path is drawn from the point on the circumference where the elastic stress is maximum. Then the effective stress is calculated on every possible path and it's maximum value is chosen. This second criterion if thought in a design procedure would be the most conservative one.

In figs. 5.6 and 5.7 the elastic stress on the circumference, the effective stresses according to Neuber ($\rho^* = 0.2$ mm) and Taylor ($a_c = 0.1$ mm) are plotted. It is possible to notice that the two above mentioned criterion can lead to different results.
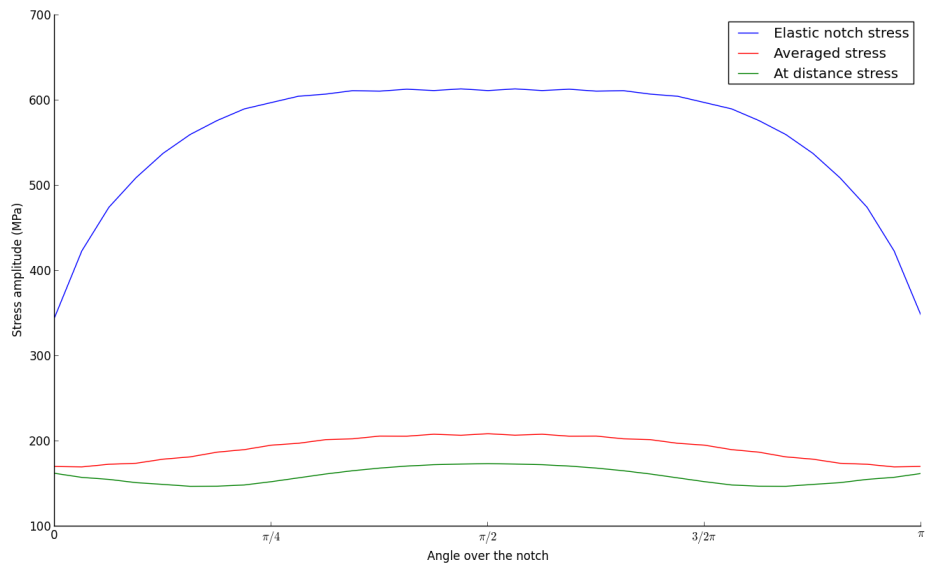
Figure 5.6: Elastic and effective stresses over the notch, peel specimen
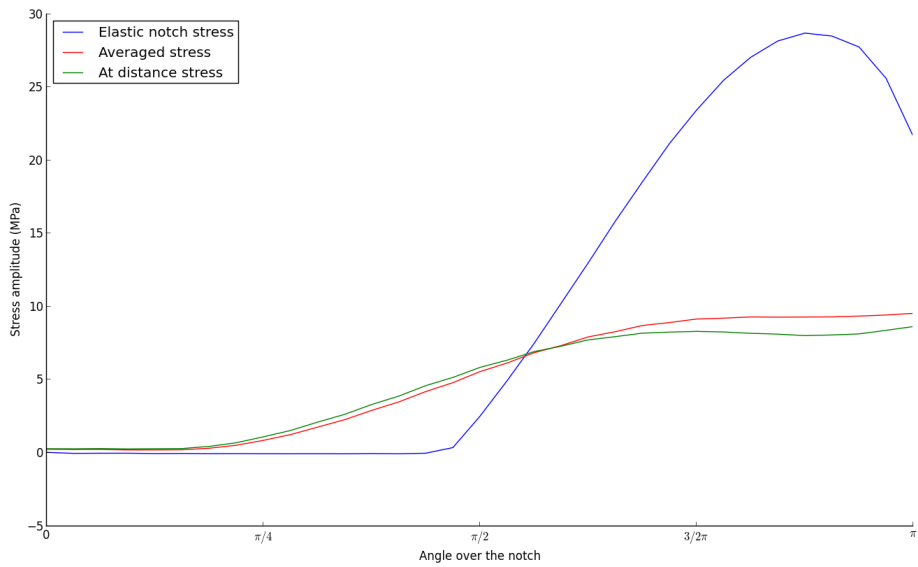
Figure 5.7: Elastic and effective stress over the notch, shear specimen

Chapter 6

Evaluation of fatigue assessment approach

In this chapter the results obtained with each fatigue life assessment method are reported and discussed. Regression lines have been obtained from the entire population inside the database, and have been plotted in the effective stress - number of cycles plane. They have been identified by the inverse exponent k of the Basquin law (eq. 2.21) and the stress value at $N_b = 2 \cdot 10^6$ cycles, to allow comparison with the known FAT values. Then reference curves for design are proposed, which have been calculated from the regression lines with a survival probability of $P_\sigma = 97.5\%$. For al the assessment methods both the maximum principal and the von Mises strength hypothesis have been investigated.

In this chapter will be shown only some examples of the stress-number of cycles graphs obtained. Which will be needed in order to debate the results obtained. For completeness sake all the other graphs will be reported in appendix B.

6.1 Identification of the S–N curve for the database

For most of the test series in the database only a limited number of experimental points after the knee point are available. This makes it difficult to estimate the position of the knee point and the slope of the curve after this point. Therefore it has been decided to include in the regression algorithm only the points with a lesser number of cycles than the knee point of the respective S–N curve. In that way we focus our attention only in the finite fatigue life region.

Even here the S–N curve will be obtained with the maximum likelihood regression method. In the analysed database all the run-outs were caused by a low load amplitude. Therefore they were all after the knee point of the respective curve. So they have been removed in this stage. As said before (sec. 2.5), with the maximum likelihood regression method, when applied to a set of points with no run-outs, one obtains the same exact curve that the least square method would have identified. Therefore in this stage the regression curves obtained are always the one with the minimum possible scatter for the population they are taken from.

6.2 The slope of the reference S–N curve

Before the detailed discussion of the regression lines derived, a section is dedicated to the slope, because all assessment methods share the same value of k.

As discussed in sec. 2.5 the slope obtained with a regression method applied to sets of results from different test series as they would be a single population can lead to a wrong interpretation. For this reason here the slope has been calculated as the mean of the slopes from each test series regression line. A weighted mean has been utilized, were the weights are the number of tests inside the series. Given the linear proportional property of all the utilized effective stress assessment methods, for a single test series the slope does not change if calculated with the load or one of the effective stresses on the ordinate axis.
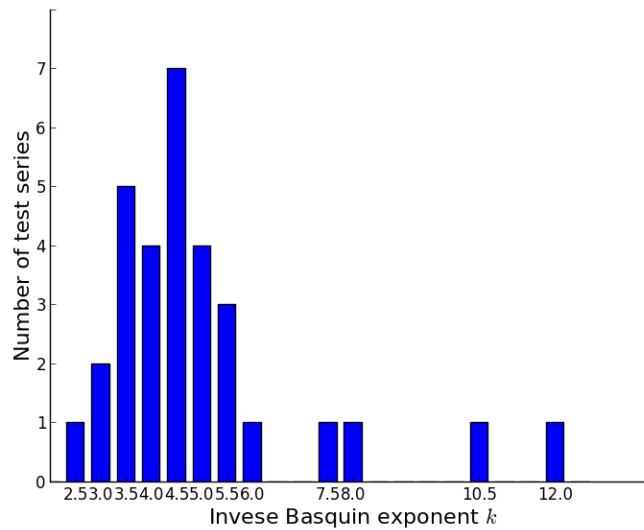
Figure 6.1: Distribution of the slope exponent k

For this two reasons the exponent k has always the same value for each assessment method. Within the current database the slope related exponent has been calculated to be $k = 4.68$. This value is very close to the $k = 5$ proposed by Sonsino et al. [20] for thin walled welded joints under normal stress.

It is interesting to consider the range in which the slope is contained for the test series. In fig. 6.1 a bar plot is showed where the height of each bar is related to the number of test series with the k value reported in the abscissa. Looking at this graph a Gaussian distribution can be hypothesized for the slope k, with a mean value somewhere near 4.5. Some curves with quite different slope can be caused by series obtained from a limited number of test. For example the curve with $k \simeq 12$ is from a series with only five test before the knee point. It is quite obvious that the fewer the test are the worse the regression method results are, in terms of reliability. For this reason a weighted mean was chosen. In fact it allows to assign a smaller weight to the series with fewer test, producing a better estimation of the mean k value.

6.3 Description of the effective stress S–N curve

Referring for example to fig. 6.2, here a description to the common properties of all effective stress-number of cycles graphs is drawn. From each graph a large number can be deducted:

- the effective stress method and the strength criterion

- the scatter T_σ

- the 50% or mean survival probability S–N curve, with its slope

- the number of test series and the total number of tests in the database

- a graphical description of the scatter band, tanks to the 10% and 90% survival probability S–N curves

- the $P_s = 97.5\%$ curve in red

- on the ordinate axis, the effective stress amplitude at $2 \cdot 10^6$ cycles, for the 97.5% and 50% survival probability S–N curves

The names in the legend are composed of three components, separated by underscores ("_") . The first one is a string referring to the source from where the test series was taken (sec. 5.1). The second one is the name of the specimen category as they were defined in sec. 3.1. While the last one is an array of numbers indicating in order the thickness on the plates in mm and the width of the gap also in mm. In some cases a fourth component is present. This denotes test series with slightly different characteristics. For example the "FAT93_shear_090902_uv" series differs from the "FAT93_shear_090902" one for a superficial coating is present. Also for the markers three characteristics needs to be noted:

- the shape, related to the specimen category

- the colour, related to the material

- the shadowing, used to tell apart series with the same shape and colour.

Those graphs are all obtained automatically, meaning that the script written not only plots the curves, but also creates the legend retrieving the label from the database objects, places the tips on the axes and all other informations described above without any intervention from the user.

6.4 Effective stress assessment methods

The effective stress, as explained in sec. 2.3, is a properly defined stress value that is hypothesized to be directly correlated to the fatigue strength of the material. In general it is a function of the stress field in the notch area. However, it is theoretically possible to define a limitless number of kernels to obtain the

effective stress. Here the performance, in terms of resulting scatter, of several well known kernels will be discussed. For the theoretical background the reader is referred to sec. 2.3.1, while a more detailed discussion over the application procedure adopted in the present work can be found in sec. 5.3. In the present work only bi-dimensional linear elastic model have been investigated, under the plain strain hypothesis. This simplifies the stress tensor, which is reduced to a 2×2 matrix. However a strength hypothesis is needed, in order to transform the above mentioned matrix into a scalar value. In the following both the von Mises and the maximum principal criterion will be utilized. Their effects on the fatigue life assessment discussed. Once again the scatter will be assumed as the main performance parameter.

6.4.1 Notch stress

In the past years the $r_{ref} = 0.05$ mm radius approach has been successfully applied to a number of thin-walled welded joints. The small value of the radius prevents cross sectional weakening in most cases. It is placed here, even though rigorously it is not an effective stress. It could be thought as a critical distance effective stress with $a_c = 0$ mm. It is one of the recommended methods by Sonsino [20], as also discussed in sec. 2.2.3. So it is the only one in the present work for which previously obtained endurable notch stress has been established.

Obviously the endurable notch stress is quite higher compared to the one allowed with the $r_{ref} = 1$ mm. In [18] an endurable stress range of $\Delta\sigma_{loc} = 575$ MPa is recommended, for steels under the maximum principal stress. With the von Mises criterion the allowable stress range drops to $\Delta\sigma_{loc} = 512$ MPa. Those values were obtained from S–N curves with a slope of $k = 3$, for a survival probability of $P_s = 97.7\%$. However they can be referred to as comparison values. Under the conditions of plane strain and no shear stresses, the following equation can be written

$$\sigma_{vM} = 0.89 \cdot \sigma_{PSH} \tag{6.1}$$

Where σ_{vM} and σ_{PSH} are respectively the von Mises and the PSH equivalent stresses.

In fig.6.2 is plotted the S–N curve obtained for the database under investigation. Here the von Mises stress hypothesis has been enforced. The analogous graph for the PSH criterion is reported in appendix B for completeness. The curve with $P_s = 97.5\%$ and the FAT 512 proposed by Sonsino are also plotted. In table 6.1 the most relevant results are reported. The lower values and the quite high percentage error related to the FAT values can be ascribed to the high scatter, which makes the $P_\sigma = 97.5\%$ curve to shift downwards. However most of the experimental point lay above the FAT curve, especially in the high cycle region.

Finally the ratio between the PSH and von Mises stresses obtained is 0.88, which is very close to its theoretical value.

	PSH	von Mises
T_σ	2.88	2.87
$\Delta\sigma_{eff}$ (MPa)	492	434
$e\%$ to Sonsino	17%	18%

Table 6.1: Notch stress range (MPa) values at $N_b = 2 \cdot 10^6$ cycles for curves with $P_s = 97.5\%$, $k = 4.68$, $r_{ref} = 0.05$ mm
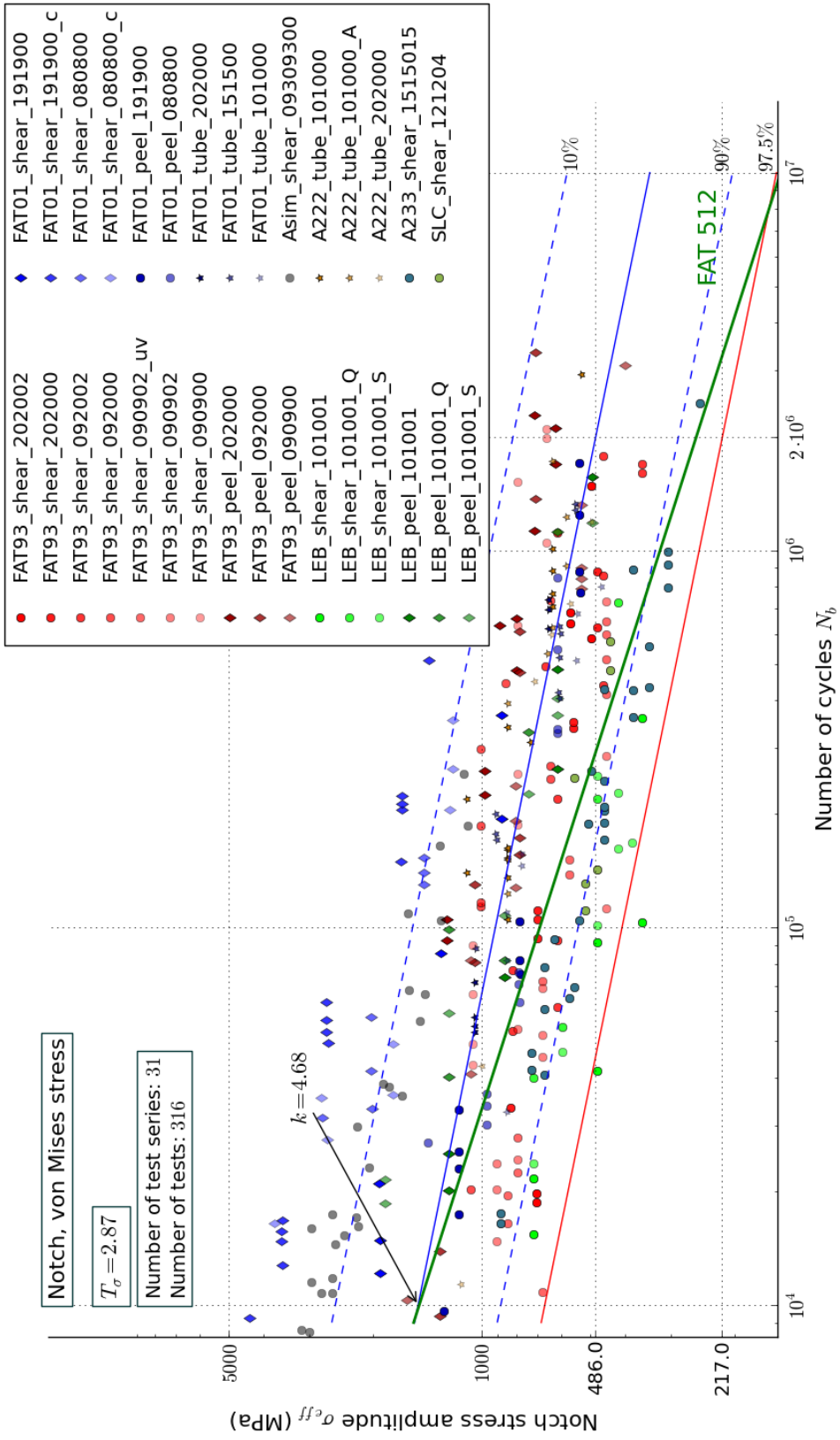
Figure 6.2: Regression curve for maximum notch stress

6.4.2 Averaged effective stress

The theoretical background of this assessment method, originally proposed by Neuber, is reported in sec. 2.3.1. It has to be stated that the integral averaging procedure was meant to be performed on the stress field originated from the real geometry of the notch. In this work it is applied to a modified geometry where the weld root notch radius has been fictitiously enlarged to $r_{ref} = 0.05$ mm. However, as discussed before, the real radius at the weld root is not easily obtained. Therefore using a fixed value for all the specimens is a choice made to make possible a good correlation between the values obtained from different test series.
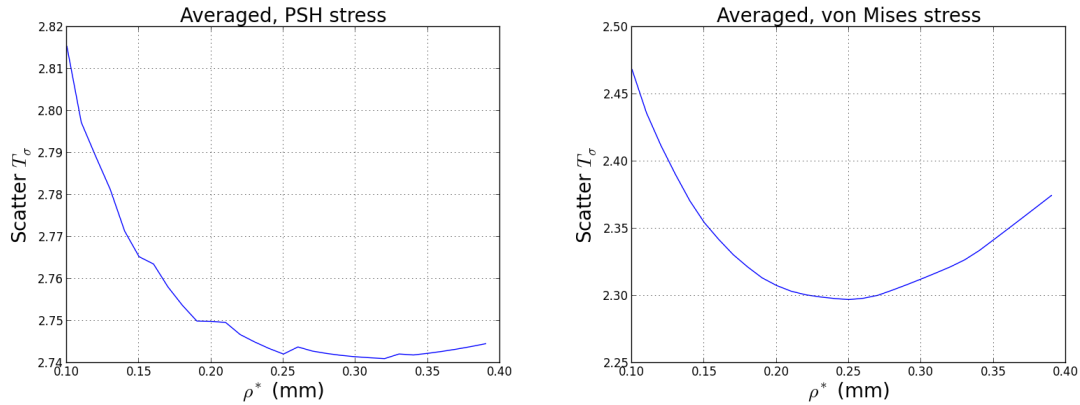
Figure 6.3: Scatter T_σ versus ρ^*

The choice of on which path perform the averaging process is still open (sec. 5.3). Several possibilities appears to be meaningful. A path in the expected crack propagation direction could be theoretically the best choice. But it is not possible to define a standardized procedure able to translate this concept into a numerical value. So this possibility was rejected. Here the averaging was performed on a straight line, perpendicular to the notch surface. Starting from the point where the elastic stress reaches its peak value.

The assessment procedure was performed both with the PSH and the von Mises strength hypothesis. For both the ρ^* value which produces the lowest scatter was searched. In fig. 6.3, the trend of the scatter T_σ when changing ρ^* is plotted.

	PSH	von Mises
T_σ	2.74	2.30
$\Delta\sigma_{eff}$ (MPa)	128	102
ρ^* (mm)	0.32	0.25

Table 6.2: Notch stress range (MPa) values at $N_b = 2 \cdot 10^6$ cycles for curves with $P_s = 97.5\%$, $k = 4.68$, $r_{ref} = 0.05$ mm

In tab. 6.2, the results obtained are reported, while in fig. 6.4 the S–N curve for the von Mises criterion is shown. It is possible to state that the best results

are obtained with the von Mises hypothesis, with a scatter of $T_\sigma = 2.3$. When the PSH hypothesis is used the scatter increases of the 19%. Those optimum values where obtained for a different ρ^*, also reported in tab. 6.2.
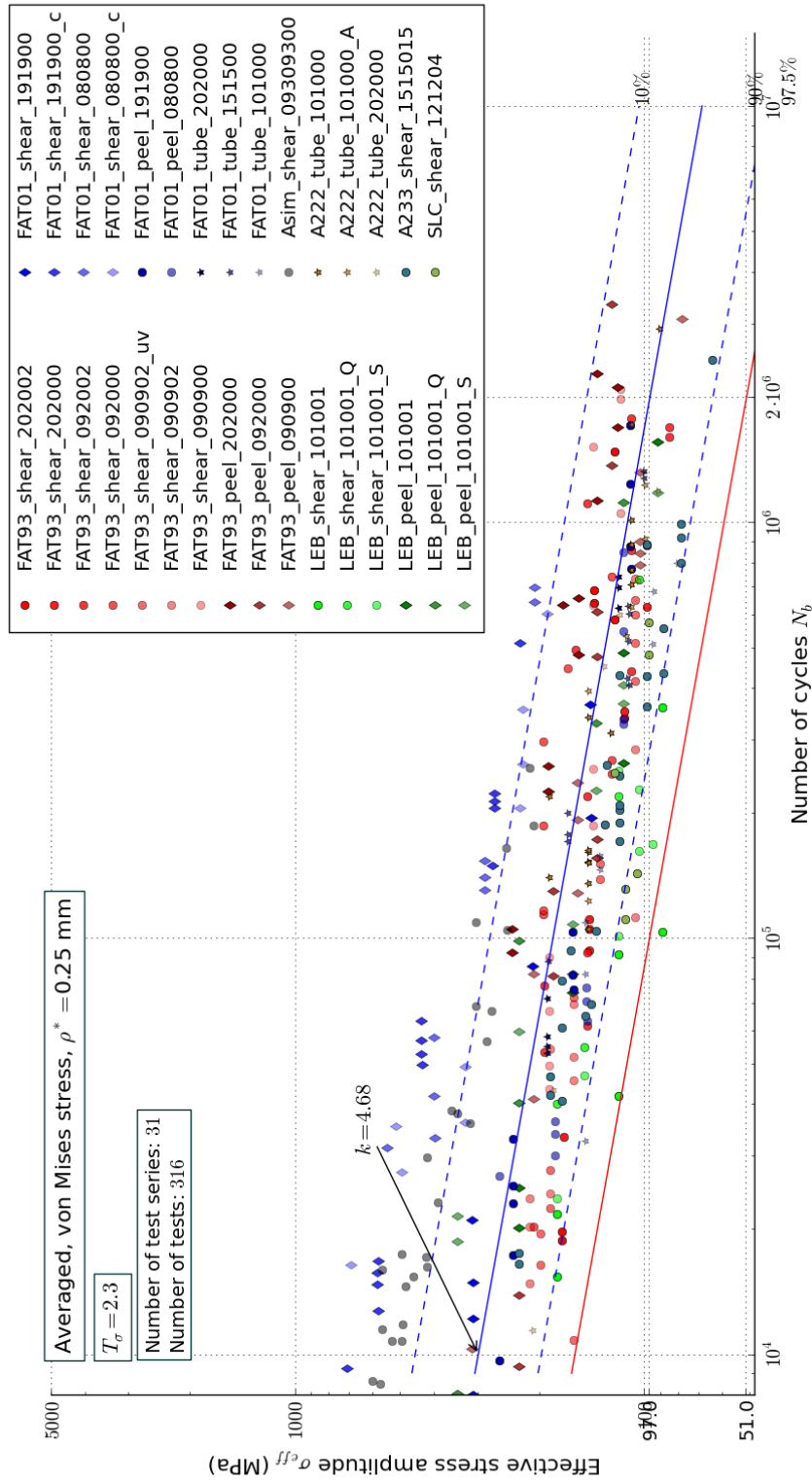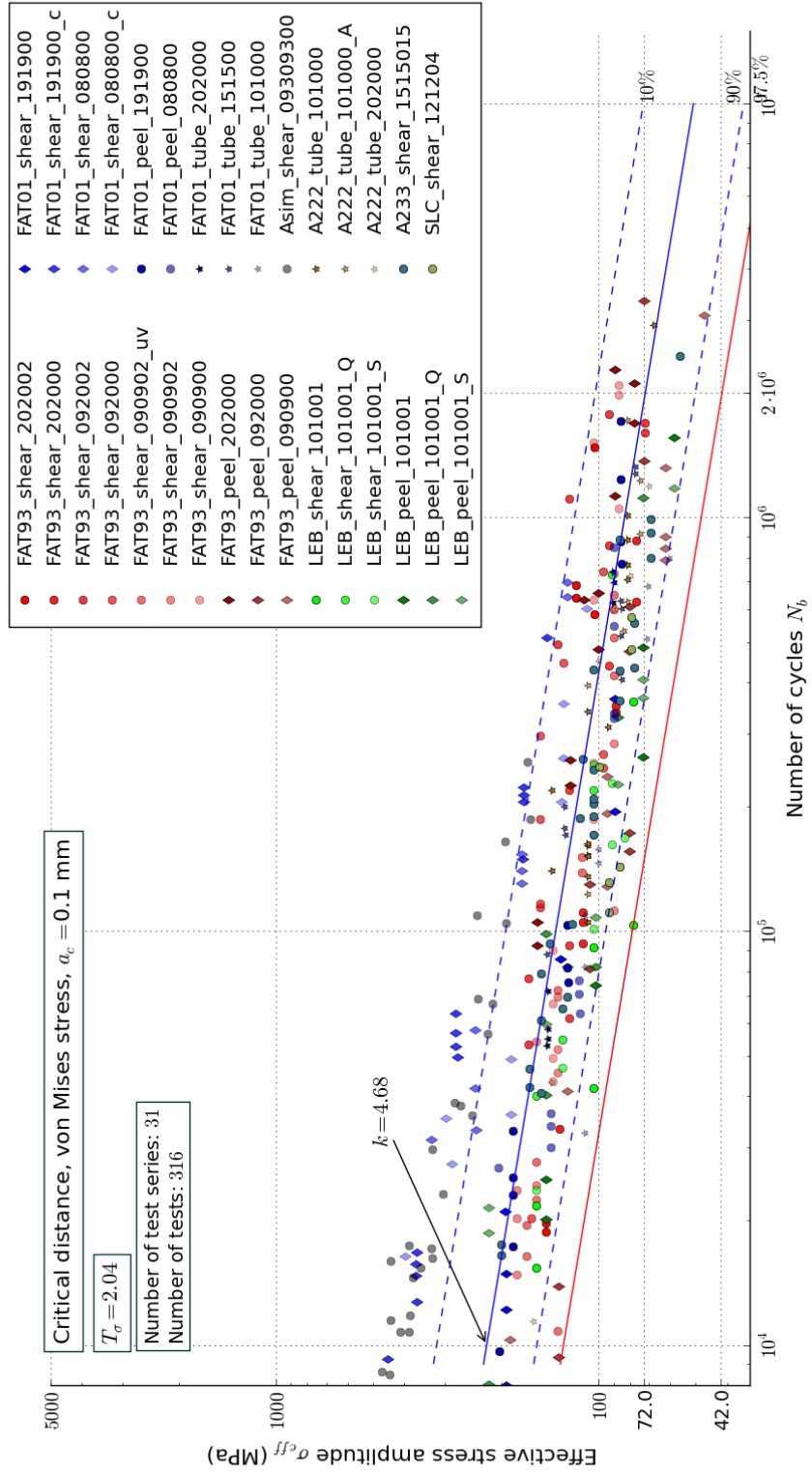
Figure 6.4: Regression curve for effective, von Mises stress from the averaged method, $\rho^* = 0.32$ mm

6.4.3 Critical distance effective stress

The theoretical background of this assessment method, originally proposed by Taylor, is reported in sec. 2.3.1. Also the critical distance assessment method was meant to be performed on the stress field originated from the real geometry of the notch. In this work it is applied to a modified geometry where the weld root notch radius has been fictitiously enlarged to $r_{ref} = 0.05$ mm. The same considerations made for the averaged effective stress can be extended here.
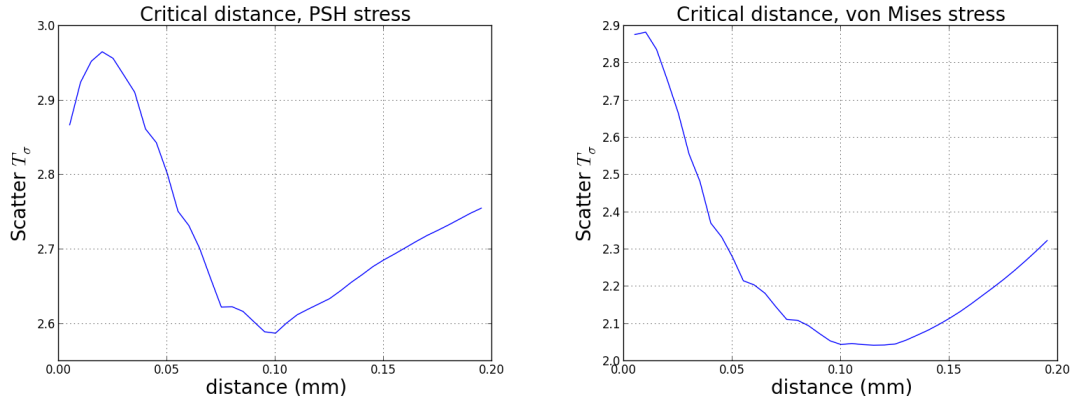
Figure 6.5: Scatter T_σ versus ρ^*

Also on the choice of on which path perform the averaging process there are many resemblances with the averaged effective stress. Several possibilities appears to be meaningful. Therefore also here the kernel was applied to a straight line, perpendicular to the notch surface. Starting from the point where the elastic stress reaches its peak value.

The assessment procedure was performed both with the PSH and the von Mises strength hypothesis. For both the a_c value which produces the lowest scatter was searched. In fig. 6.5, the trend of the scatter T_σ when changing a_c is plotted.

	PSH	von Mises
T_σ	2.59	2.04
$\Delta\sigma_{eff}$ (MPa)	122	88
a_c (mm)	0.1	0.1

Table 6.3: Effective stress range (MPa) values at $N_b = 2 \cdot 10^6$ cycles for curves with $P_s = 97.5\%$, $k = 4.68$, $r_{ref} = 0.05$ mm

In tab. 6.3, the results obtained are reported, while in fig. 6.6 the S–N curve for the von Mises criterion is shown. It is possible to state that the best results are obtained with the von Mises hypothesis, with a scatter of $T_\sigma = 2.04$. Which is also the best best value, in term of scatter obtained in the present work. When the PSH hypothesis is used the scatter increases of the 27%. Those optimum values where obtained for a different ρ^*, also reported in tab. 6.3.

Figure 6.6: Regression curve for effective, von Mises stress from the averaged method, $\rho^* = 0.32$ mm

6.5 Maximum effective stress path

As discussed in sec. 5.3 and after in sec. 6.4, the problem of choosing the right path on which perform the assessment procedure is still an open one. No clues on this topic were found in literature. So different options have been tested. One of those is to pick the path where the effective stress has its maximum value. This, from the design point of view, will surely lead to a conservative estimation of the fatigue life.

Even in this case the averaged and the critical distance effective stress has been performed, with both the PSH and von Mises hypothesis. Then the values of ρ^* and a_c which gives the minimum scatter have been identified. Figs. 6.7 and 6.8 shows the trend of the scatter when varying the distance parameter ρ^* or a_c. It is possible to state that generally this criterion for the choosing of the path lead to a rise in the scatter value whichever method is applied.
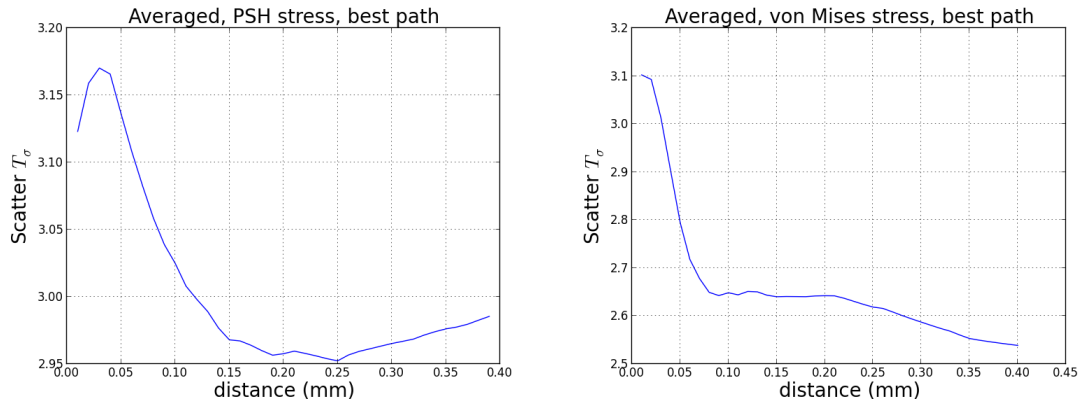
Figure 6.7: Scatter T_σ versus ρ^*, averaged stress
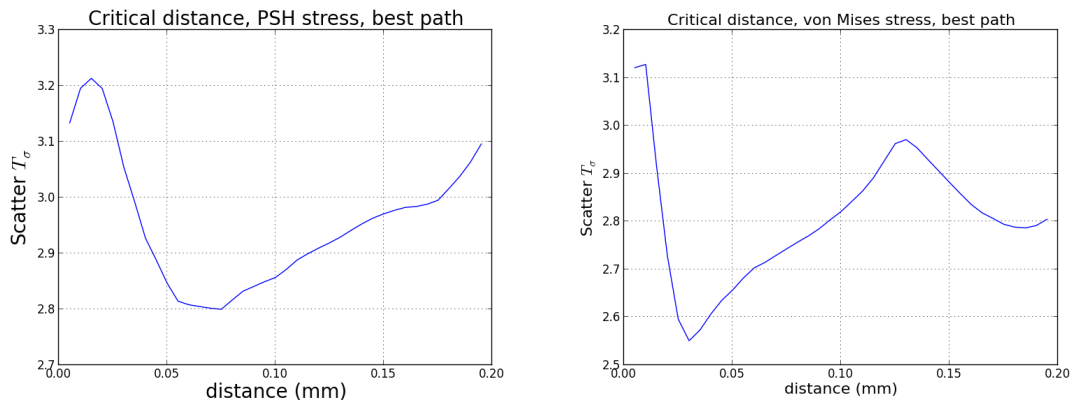
Figure 6.8: Scatter T_σ versus ρ^*, critical distance stress

	PSH	von Mises
T_σ	2.93	2.54
$\Delta\sigma_{eff}$ (MPa)	145	110
ρ^* (mm)	0.25	0.40

Table 6.4: Effective averaged stress range (MPa) values at $N_b = 2 \cdot 10^6$ cycles for curves with $P_s = 97.5\%$, $k = 4.68$, $r_{ref} = 0.05$ mm, maximum effective stress path.

	PSH	von Mises
T_σ	2.80	2.55
$\Delta\sigma_{eff}$ (MPa)	162	188
a_c (mm)	0.075	0.03

Table 6.5: Effective critical distance stress range (MPa) values at $N_b = 2 \cdot 10^6$ cycles for curves with $P_s = 97.5\%$, $k = 4.68$, $r_{ref} = 0.05$ mm, maximum effective stress path.

6.6 Effect of the yield strength of the base material

One of the purposes of this work was to investigate if there is a correlation between the endurable fatigue life of a welded joint and the yield strength of the base material the joint is made from. For this reason the graph in fig. 6.9 has been made. In it the effective stress (on the ordinate),for each test series, has been calculated at $2 \cdot 10^6$ cycles, with the critical distance method for $a_c = 0.1$ mm and the von Mises criterion. Those values have been plotted against the yield stress of the base material (on the abscissa).

Looking at the graph it is possible to state that high yield strength tend to have a somewhat lower endurable fatigue effective stress, compared to the one showed by the mild steel joints. One the possible reasons for this behaviour could be the greater notch sensitivity factor generally showed by high strength steels empathised by the sharpness of the weld root notch.
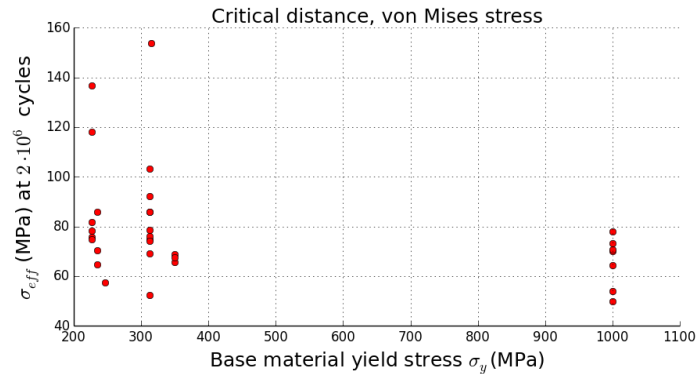
Figure 6.9: Effective stress versus yield strength

6.7   Effects of the stress ratio

An increase of the fatigue life can be expected for loads with a ratio $R \leq 0.5$, under the hypothesis of no or little residual stresses in the joint. Two formulas for taking into account the effects of the stress ratio have been found in the literature, both of them are reported in sec. 2.6 of this work and have been tested on the current database. The first one have been found in the recommendations from the International Institute of Welding [8], the second one was proposed by Sonsino [18]. In the following they will be referred to as IIW and Sonsino respectively.

It has to be stressed that both formulas, were meant to produce a factor $f(R)$ by which increase the fatigue life reference curve. In this work the same factor has been used to reduce the effective stress, in order to make possible a comparison between all the test series.

	no $f(R)$	IIW	Sonsino
Critical distance stress			
a_c	0.1	0.1	0.1
T_s	2.04	2.33	2.19
Averaged stress			
ρ^*	0.25	0.21	0.21
T_s	2.3	2.57	2.44

Table 6.6: Scatter for regression curves obtained with critical distance and averaged stresses (von Mises strength hypothesis), whole database.

	no $f(R)$	IIW	Sonsino
Critical distance stress			
a_c	0.12	0.13	0.125
T_s	2.27	2.33	2.3
Averaged stress			
ρ^*	0.26	0.26	0.26
T_s	2.52	2.57	2.55

Table 6.7: Scatter for regression curves obtained with critical distance and averaged stresses (von Mises strength hypothesis), only plane specimens.

Regression curves for the effective stresses, obtained with the critical distance method and the averaged method, are created. The values of a_c and of ρ^* which produces the smaller scatter are derived. All the results are reported in table 6.6, it is remarkable that the scatter always increases when the stress ratio related factor is accounted for. One of the causes could be the presence in the database of tube specimens with a load ratio $R = -1$, which effective stresses lay generally below the reference curve even when no factor $f(R)$ is considered. When the factor $f(R)$ is accounted for the distance of the tube related points (star marker) from the regression line increases, this effect can be easily noted comparing fig. 6.10 and fig. 6.6 Another relevant aspect of this analysis is that the parametric distances a_c and ρ^* that produce the smaller scatter shown no relevant changes introducing

the $f(R)$ factor.

The same procedure has been repeated excluding from the database all the tube specimens. The obtained results are summarized in table 6.7. The main conclusion that emerges from this data is that for the smaller database with not divided by the factor $f(R)$, the scatter is bigger than for the more complete database. The reason for this is that the tube specimen's points lay very close to the regression line. Speaking of the stress ratio factor, it's effects are very close to the ones observed for the entire database.
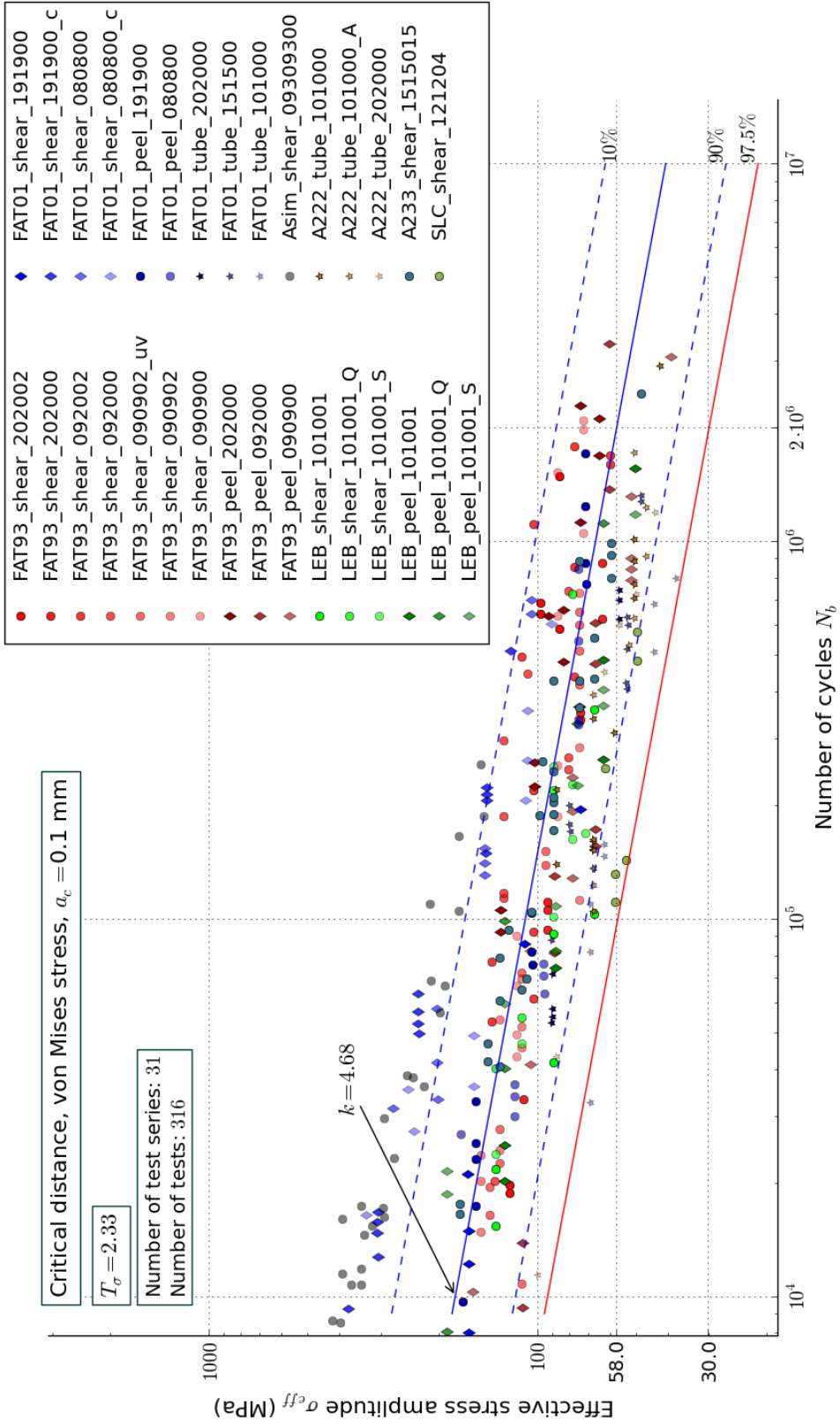
Figure 6.10: Regression curve for effective stress from the critical distance method, $a_c = 0.1$ mm, corrected by $f(R)$ according to IIW

Chapter 7

Conclusions and outlook

7.1 Summary and conclusions

Main purpose of this work was to establish a fatigue life assessment design procedure for thin-walled welded joints. First of all the state of the art on this topic was resumed (chap.2), with special regard to the effective stress theory (sec.2.3), since it was the theoretical background of all the investigations carried out in the present work. Also several other topics were discussed, covering all the steps of the present work, such as the mathematical definition of an S–N curve and the maximum likelihood regression method.

The above mentioned effective stress based methods have been applied to a database of experimental tests, making it possible to investigate the performance of the fatigue life assessment. The general layout is presented from the functional point of view (sec.3.2). The same layout is then translated into an operative structure, which fits better with the possibilities offered by the programming language used to create the database and perform the calculations: Python®.

A number of factors has to be accounted for in the determination of the fatigue strength of a component. Since analysing the effects of every parameter was not possible, in this work it has been chosen to create a database of experimental tests with some common characteristics. Obviously only steel, thin-walled specimens have been selected. Also only specimens where the fatigue crack originates from the weld root have been investigated. Therefore the notch opening angle is always $\omega = 0°$. On the load side the database has been reduced to constant amplitude tests.

It is common practice for fatigue tests on welded joints to be performed with a stress ratio $R = 0.5$ as to reduce the influence of residual stresses. However, tests performed with different values of the stress ratio have been included. For example the tests carried out at the LBF Fraunhofer in the Light E Body project were performed with a stress ratio of $R = 0.1$, in order to prevent failure outside the welded area. Also the test series have selected in order to create a database with a range as wide as possible in terms of yield stress of the base material. Since this was one of the parameters, whose influence was meant to be investigated.

For each specimen the stress field in the notch area has been derived by means of finite element models. It has been decided to model the notch at the weld root with

a keyhole or U-hole shape depending on the width of the gap existing between the plates forming the joint. However, in both cases a reference radius of $r_{ref} = 0.05$ mm has been adopted, having always the same radius allows to easily correlate the obtained stress values. Furthermore, even analysing the micro-sections of the welding, it is not easy to define a standardized procedure capable of stating the real notch radius.

The notch stress field has been reduced into an effective scalar value through properly defined kernels, where the term effective refers to its effectiveness in connection to the fatigue life assessment. Both the kernels deriving from the averaged and critical distance stress concepts have been investigated. They were originally proposed respectively by Neuber and Taylor. The notch stress assessment method has also been performed. The obtained results has been showed as effective stress S–N curves (chap.6). The scatter related to those curves has been chosen as the main performance criterion. Also the problem of which path is the best fitted to perform the effective stress assessment has been discussed. Several possibilities on this matter have been analysed (sec.5.3): a path starting from the point where the elastic stress has its maximum and the path that produces the maximum effective stress.

It has emerged that the critical distance method with $a_c = 0.1$ mm, performed on the von Mises equivalent stress field, is the one leading to the best results in terms of scatter. It also resulted that choosing the path starting from the point where the elastic stress has its maximum generally produces the lowest scatter. The yield stress of the base material was confirmed to be not one of the most significant parameters into assessing the fatigue life of a welded joint. Finally the proposed formulas for taking into account the stress ratio (factor $f(R)$) produced an increase of the scatter when applied to the current database.

Concluding a fatigue design procedure for thin-walled welded joints with root located failure can be proposed. Based on the above mentioned results it should be characterised by:

- keyhole or U-hole shaped notch

- $r_{ref} = 0.05$ mm

- von Mises equivalent stress

- critical distance effective stress, with $a_c = 0.1$ mm

- path starting from the point where the elastic has its maximum

The fatigue strength of such an assessment method for a steel welded component can be summarized as a FAT 88 MPa curve, with a slope of $k = 5$ (fig. 7.1). In the current database the number of experimental points with a failure occurred at a number of cycles greater than the knee point was not big enough. Therefore, only the limited fatigue life region has been investigated. So, no information have been obtained on the position of the knee point and on the slope k^*. However it is conservative to assume a knee point placed at $N_b = 10^7$ cycles and a slope oj $k^* = 22$ behind this point (it equals to a fatigue life reduction of 10% per decade).
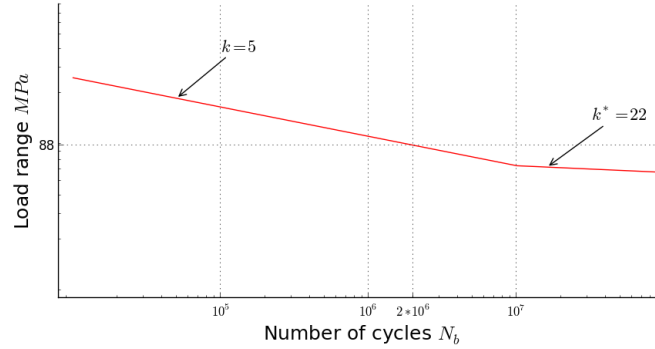
Figure 7.1: Design FAT curve

7.2 Possible future developments

Several developments of the present work are possible. Some of them are discussed here:

- weld toe failure,

- variable amplitude loading,

- yield stress based micro-support length,

- non-linear effective stress kernel.

The first two refers to the possibility to enlarge the experimental database as to include specimens with a fatigue crack originating from the weld toe and tests performed under variable amplitude loading. While the last two concerns the development of the effective stress assessment method itself. It the following each point will be briefly discussed.

Weld toe failure

As previously said the current database contain only specimens for which the crack originates from the weld root. This means that the notch opening angle is always $\omega = 0°$. According to Neuber's analytical solution, the equation of the stress course states [23] (fig. 4.4):

$$\sigma_{\theta,\max} = C\rho^{-p_1} \tag{7.1}$$

where $\sigma_{\theta,\max}$ is the maximum elastic stress in θ direction. When $\omega = 0°$ the exponent assumes the value of $p_1 = 0.5$. For bigger ω values the exponent p_1 is smaller. Thus the stress course is shallower.

This different trend of the stress course over the path could affect the effective stress method, changing the distance parameter (ρ^* or a_c) that produces the smallest scatter.

Variable amplitude loading

As said (sec. 5.1) here only constant amplitude tests have been analysed. It would be interesting to investigate the performance of the effective stress when assessing the fatigue life of a component undergoing a variable amplitude load. Generally this is made by the use of a linear damage accumulation law, such as the one proposed by Palmgren and Miner. In this case no fatigue limit is supposed to occur.

Yield stress based micro-support length

At the current date, there are no fatigue life assessment procedures that take into account the yield strength of the base material. As discussed in sec. 6.6 a correlation between this parameter and the fatigue life could be established. Generally speaking specimens with a higher base material yield stress tend to have a lower fatigue life. This could be taken into account, adopting a variable distance parameter (ρ^* or a_c) as a function of the yield strength:

$$\rho^* = f_1(\sigma_y) \qquad \text{or} \qquad a_c = f_2(\sigma_y). \tag{7.2}$$

Where f_1 and f_2 should be shaped as to produce a decreased distance when the yield stress increases.

Non-linear kernel

In [22] some possible non-linear kernels to define the effective stress are proposed. This could be done both keeping a path as domain for the integral or expanding it to an area around the notch tip. Naturally the kernel should fulfil the same conditions that have been imposed to the linear ones, also described by Zhang in the above cited work. The condition on the functional $\mathcal{F}$ to be linear and continuous is reported in eq. 2.13. Further more it has to be imposed that, for a plain specimen (without a notch), the the effective stress is equal to the nominal one:

$$\sigma_n = \mathcal{F}(\boldsymbol{\sigma}). \tag{7.3}$$

This can be achieved imposing the following condition on the weight function $\mathbf{G}_{\mathcal{F}}(\mathbf{x}, \bar{\mathbf{x}})$:

$$\int_{\Omega} \mathbf{G}_{\mathcal{F}}(\mathbf{x}, \bar{\mathbf{x}}) \, d\Omega_{\bar{\mathbf{x}}} = 1 \tag{7.4}$$

Please note that this condition is the reason for the term $\frac{1}{\rho*}$ in the stress averaging formula by Neuber (eq. 2.17). In that case the weight function assumes the simple form $\mathbf{G}_{\mathcal{F}}(\mathbf{x}, \bar{\mathbf{x}}) = 1$. Then its integral over a line, is simply the length of that line ρ^*. Therefore adding the term $\frac{1}{\rho*}$ to the kernel allows it to fulfil the condition of eq. 7.4.

A non-linear defined effective stress could possibly show a better correlation to the fatigue life experimental data, reducing the scatter of its reference S–N curve. In this perspective an investigation should be needed in order to identify the best non-linear kernel, in terms of weight function shape and integrating

domain. Furthermore a non-linear kernel would be characterized by a weight function containing several numerical parameters, that have to be fixed.

Ringraziamenti

Il ringraziamento più grande va alla mia famiglia che mi ha sempre sostenuto e incoraggiato. Non ci sono parole per esprimere la mia gratitudine nei vostri contronti. Un grande grazie quindi a mamma Angela (di nome e di fatto), papà Raffaele, Rosa e ultima, ma solo temporalmente alla mia Linda. Non sarei mai riuscito a raggiungere questo traguardo senza il vostro aiuto.

Vorrei ringraziare i miei relatori Prof. Ing. Frendo, Prof. Ing. Bertini e Ing. Tomasella per tutto il sostegno che mi hanno dimostrato, ben oltre l'idubbia professionallità.

Many thanks to Ing. PhD Jörg Baumgartner, from the Fraunhofer LBF. Working with you has been a real pleasure, and your teachings have been invaluable to me.

Un ringraziamento all'Ing Gabriele "Perito" Melani, che mi ha introdotto alla nobile arte della simulazione numerica.

Vorrei inoltre ringraziare tutti gli amici, i coinquilini e i colleghi che nel corso degli anni hanno condiviso con me gioie e dispiaceri. Non vi citerò individualmente, ma cercherò di dimostrarvi il mio affetto ogni giorno (potrei iniziare con l'offrirvi una bella panzerottata...).

Infine un grazie a tutti gli appassionati sviluppatori di software gratuito. Grazie anche al loro lavoro, é stato possibilie realizzare questa tesi, escluso le simulazioni agli elementi finiti, esclusivamente mediante l'utilizzo di software a licenza libera.

Parte I

Appendix

Appendice A

Test series data

A.1   Database

Test series label	Specimen	R	Material	σ_y (MPa)	$t1$	$t2$	tests
FAT93_shear_202002	shear	0	St14	313	2.0	2.0	7
FAT93_shear_202000	shear	0	St14	313	2.0	2.0	10
FAT93_shear_092002	shear	0	St14	313	0.9	2.0	13
FAT93_shear_092000	shear	0	St14	313	0.9	2.0	11
FAT93_shear_090902_uv	shear	0	St14	313	0.9	0.9	16
FAT93_shear_090902	shear	0	St14	313	0.9	0.9	13
FAT93_shear_090900	shear	0	St14	313	0.9	0.9	12
FAT93_peel_202000	peel	0	St14	313	2.0	0.9	12
FAT93_peel_092000	peel	0	St14	313	0.9	2.0	14
FAT93_peel_090900	peel	0	St14	313	0.9	2.0	12
LEB_shear_101001	shear	0.1	22MnB5	1000	1.0	1.0	12
LEB_shear_101001_Q	shear	0.1	22MnB5	1000	1.0	1.0	5
LEB_shear_101001_S	shear	0.1	22MnB5	1000	1.0	1.0	8
LEB_peel_101001	peel	0.1	22MnB5	1000	1.0	1.0	7
LEB_peel_101001_Q	peel	0.1	22MnB5	1000	1.0	1.0	9
LEB_peel_101001_S	peel	0.1	22MnB5	1000	1.0	1.0	8
FAT01_shear_191900	shear	0	DC04	227	1.9	1.9	9
FAT01_shear_191900_c	shear	0	DC04	227	1.9	1.9	17
FAT01_shear_080800	shear	0	DC04	227	0.8	0.8	10
FAT01_shear_080800_c	shear	0	DC04	227	0.8	0.8	11
FAT01_peel_191900	peel	0	DC04	227	1.9	1.9	14
FAT01_peel_080800	peel	0	DC04	227	0.8	0.8	13
FAT01_tube_202000	tube	-1	St35	235	2.0	2.0	9
FAT01_tube_151500	tube	-1	St35	235	1.5	1.5	12
FAT01_tube_101000	tube	-1	St35	235	1.0	1.0	10
Asim_shear_09309300	shear	0	J2340 300Y	315	0.93	0.93	28
A222_tube_101000	tube	-1	S 235 G2T	350	1.0	1.0	17
A222_tube_101000_A	tube	-1	S 235 G2T	350	1.0	1.0	8
A222_tube_202000	tube	-1	S 235 G2T	350	2.0	2.0	7
A233_shear_1515015	shear	0.1	Dx52D+Z	246	1.5	1.5	29
SLC_shear_121204	shear	-1	XIP1000	1000	1.2	1.2	8

A.2 Load S–N curves

FAT93
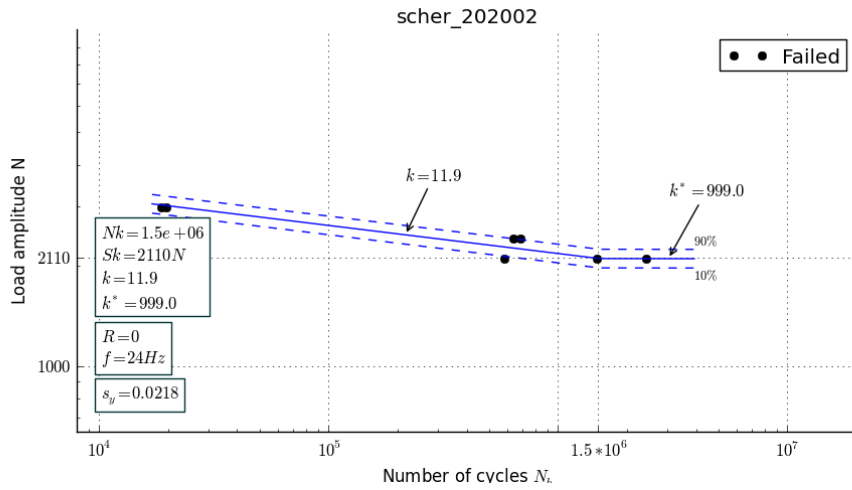
Figura A.1: FAT93_shear_202002
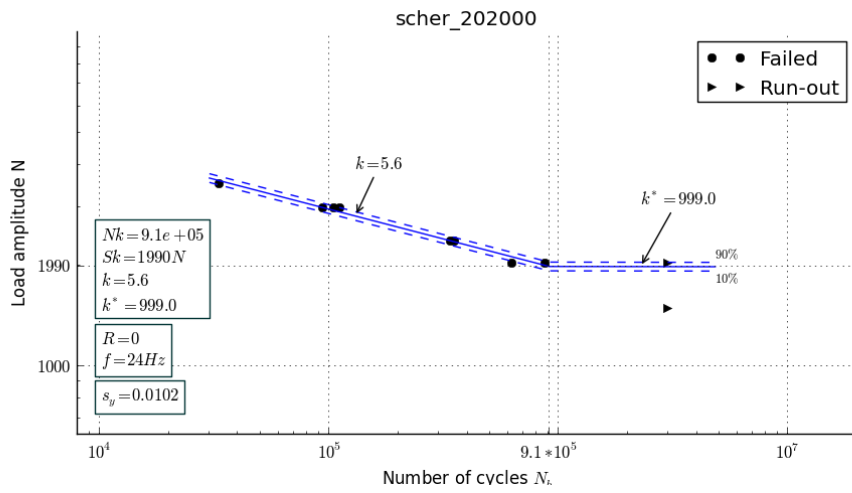
Figura A.2: FAT93_shear_202000
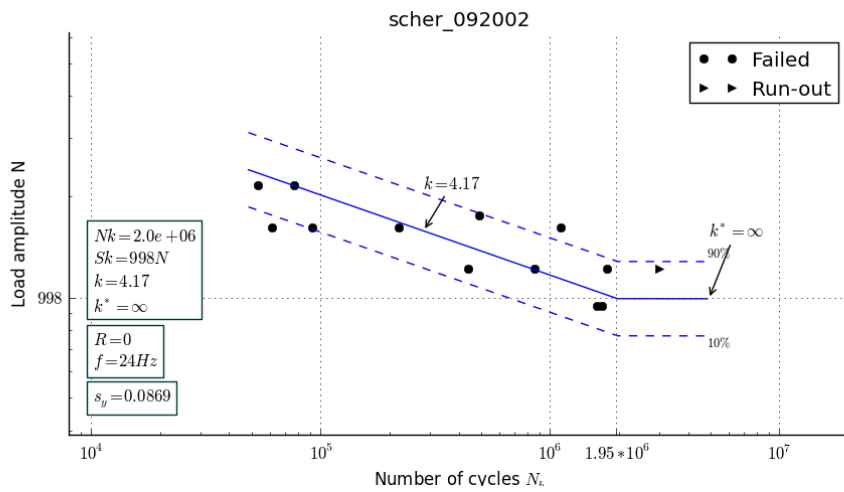
Figura A.3: FAT93_shear_092002

66
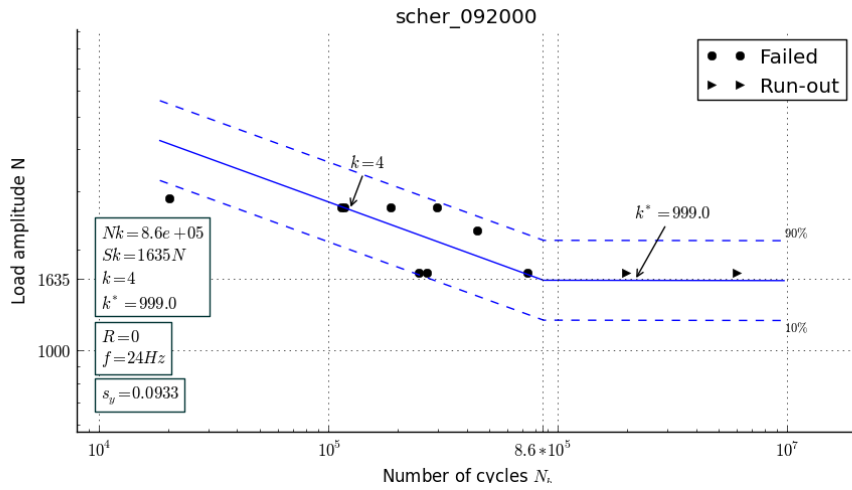
Figura A.4: FAT93_shear_092000
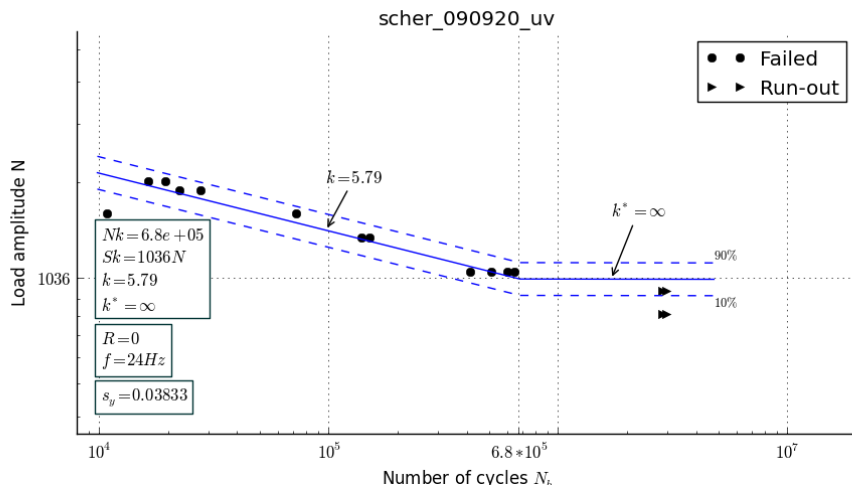
Figura A.5: FAT93_shear_090902_uv
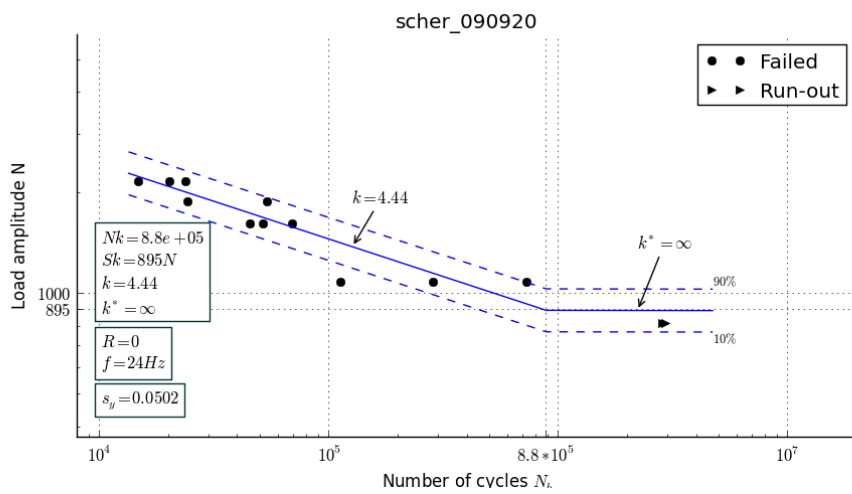
Figura A.6: FAT93_shear_090902

67
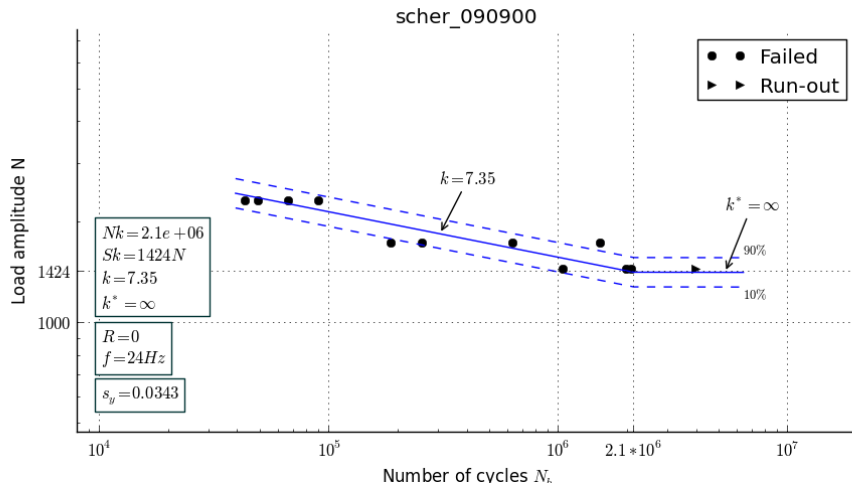
Figura A.7: FAT93_shear_090900
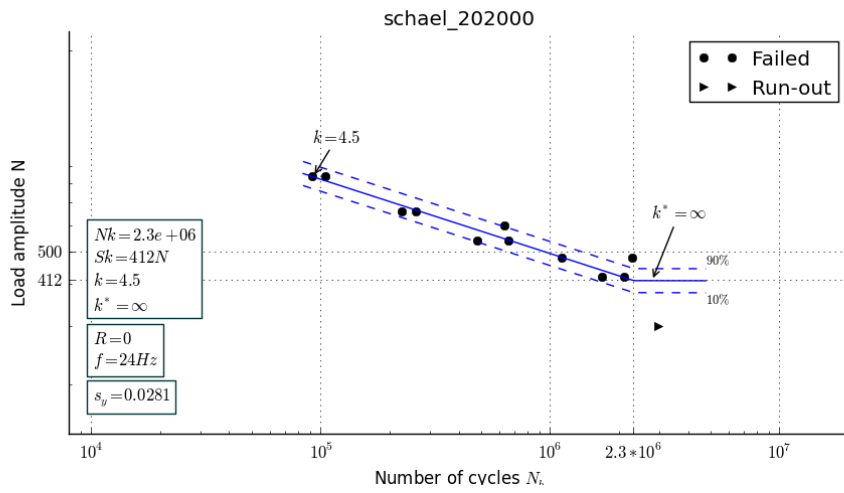
Figura A.8: FAT93_peel_202000
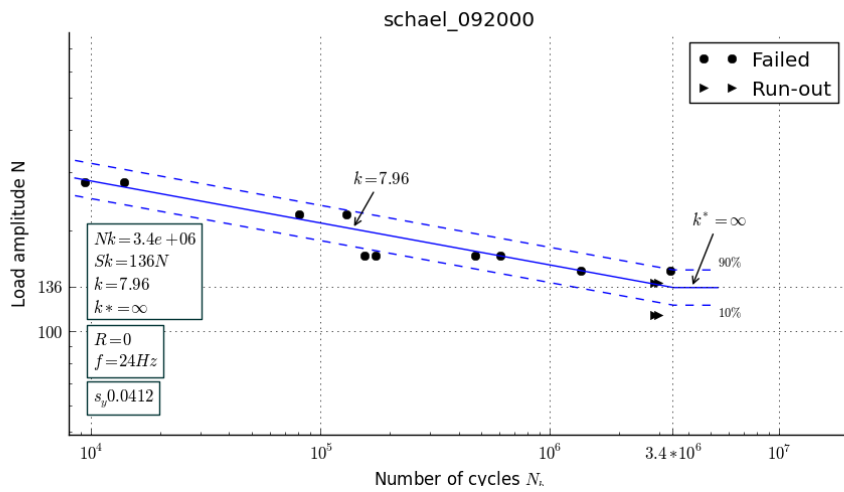
Figura A.9: FAT93_peel_092000
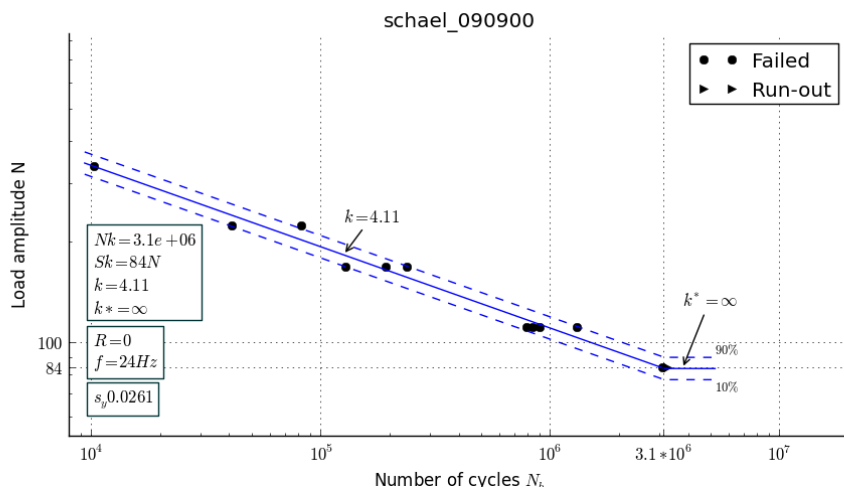
Figura A.10: FAT93_peel_090900

Light E body
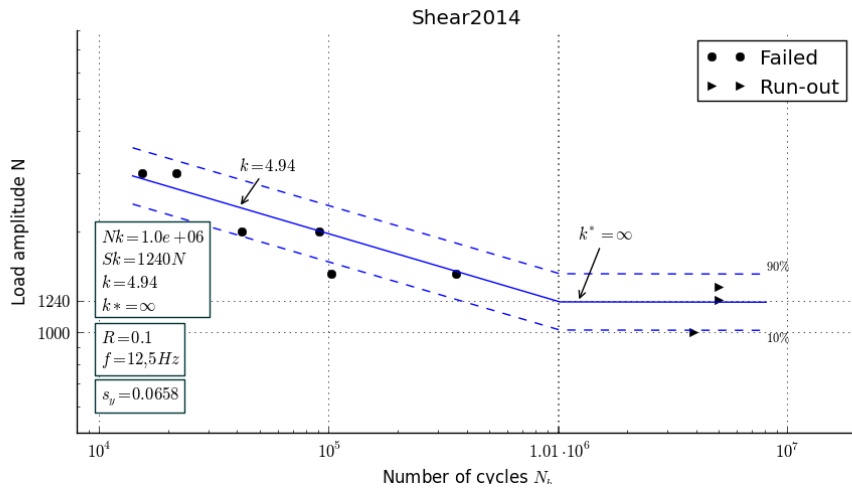
Figura A.11: LEB_shear_101001
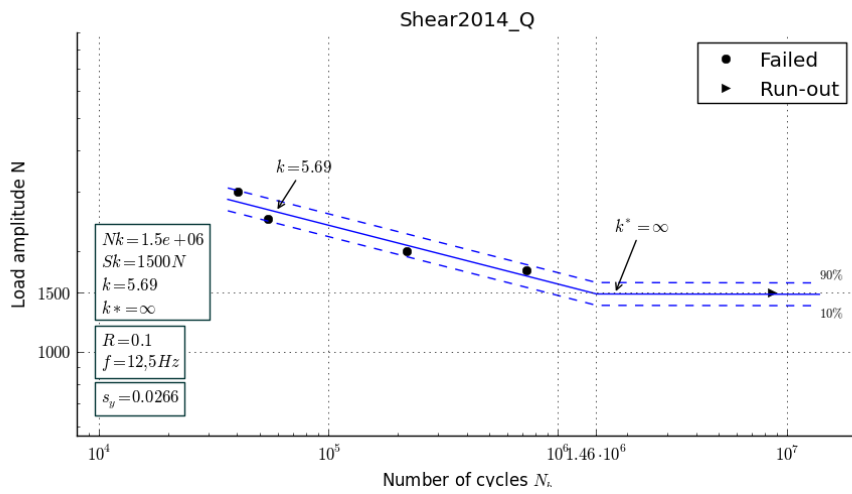
Figura A.12: LEB_shear_101001_Q
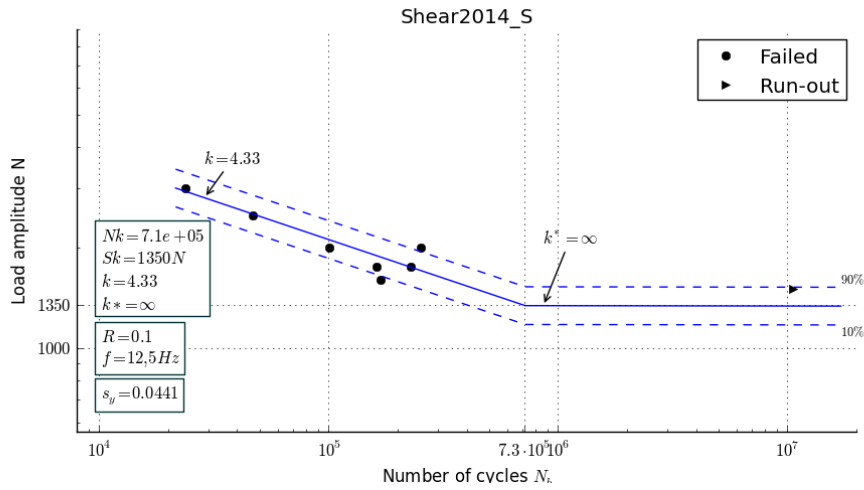
Figura A.13: LEB_shear_101001_S
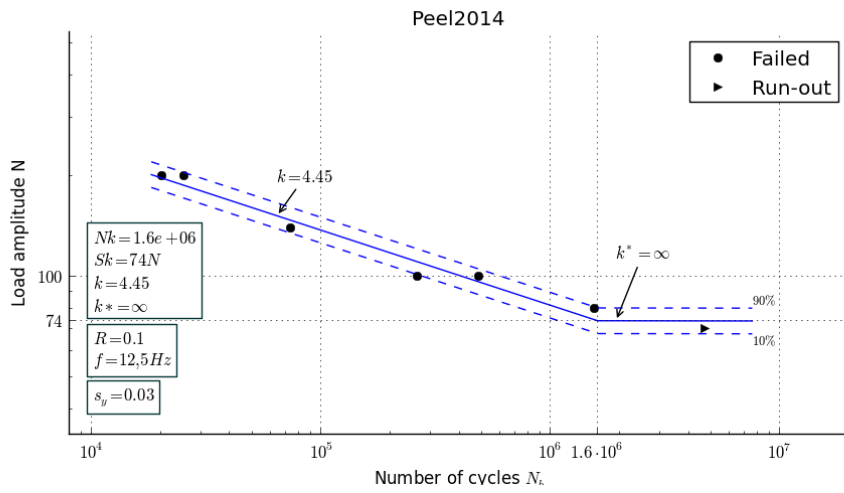
Figura A.14: LEB_peel_101001
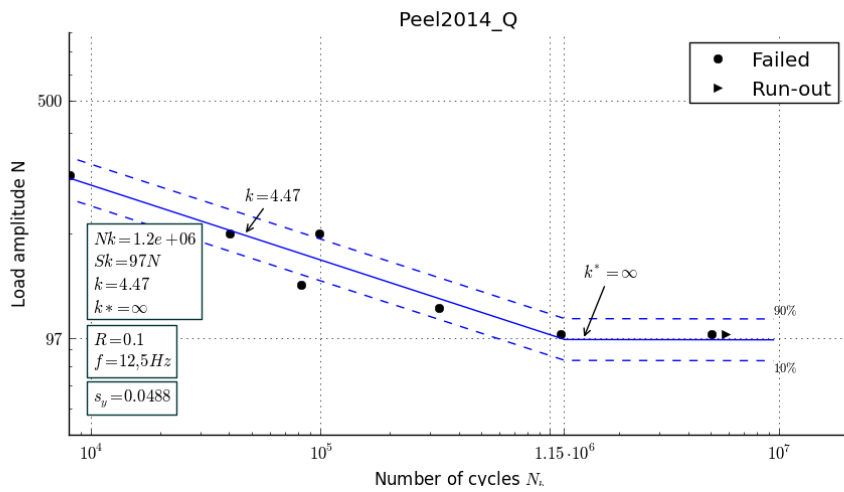
Figura A.15: LEB_peel_101001_Q

71
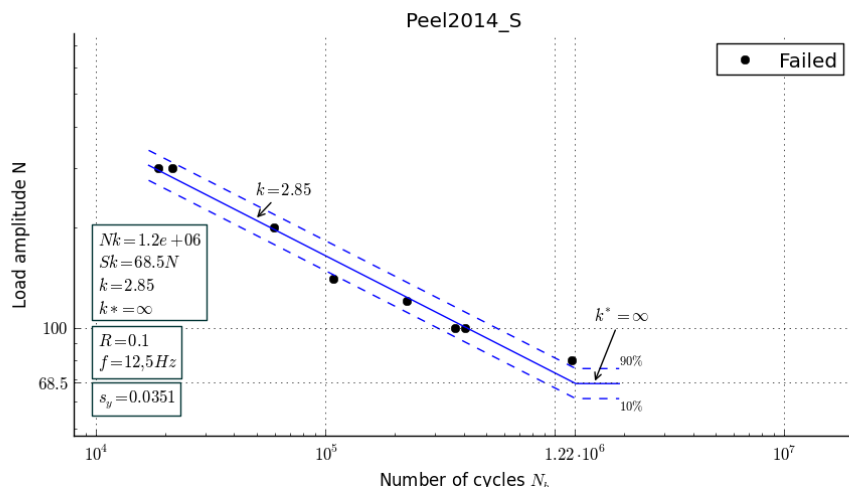
Figura A.16: LEB_peel_101001_S
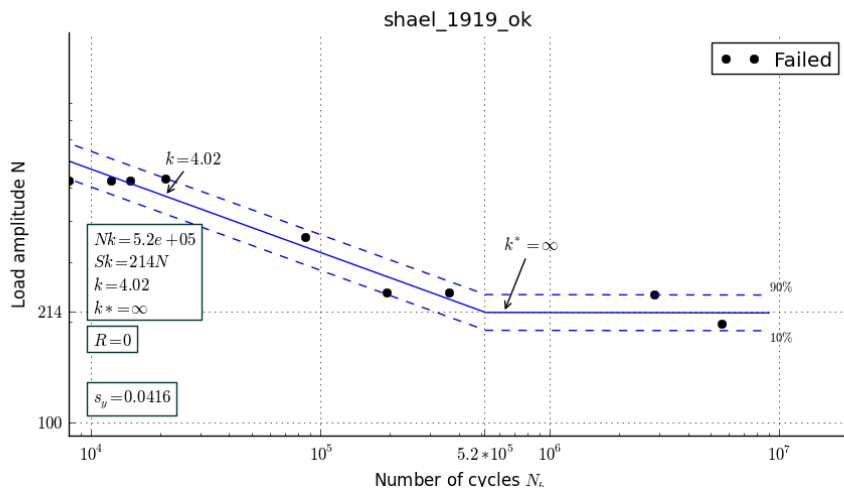
Figura A.17: FAT01_peel_191900
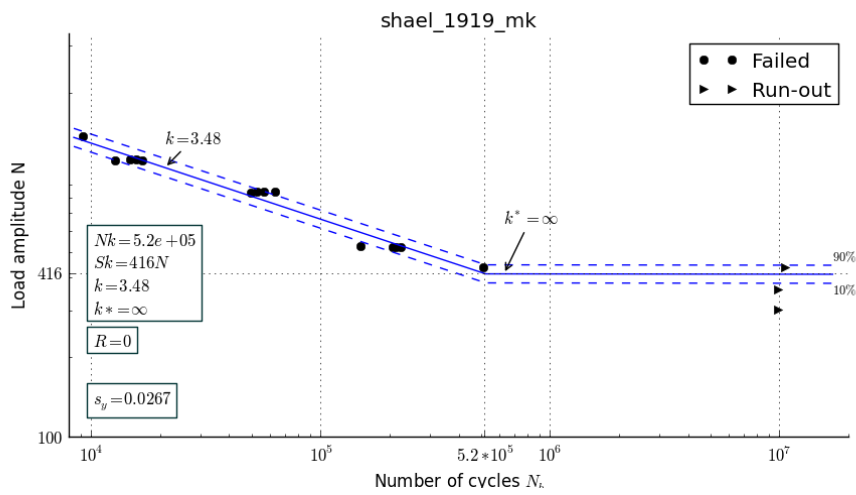
Figura A.18: FAT01_peel_191900_c
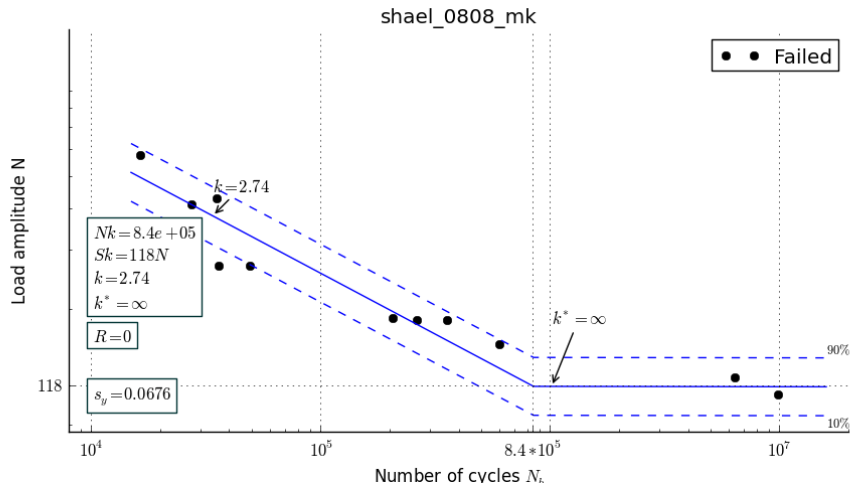
Figura A.19: FAT01_peel_080800_c
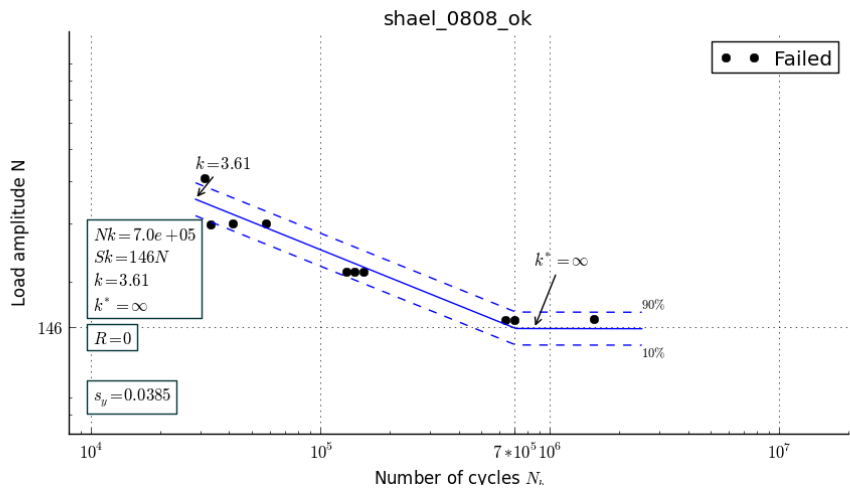
Figura A.20: FAT01_peel_080800
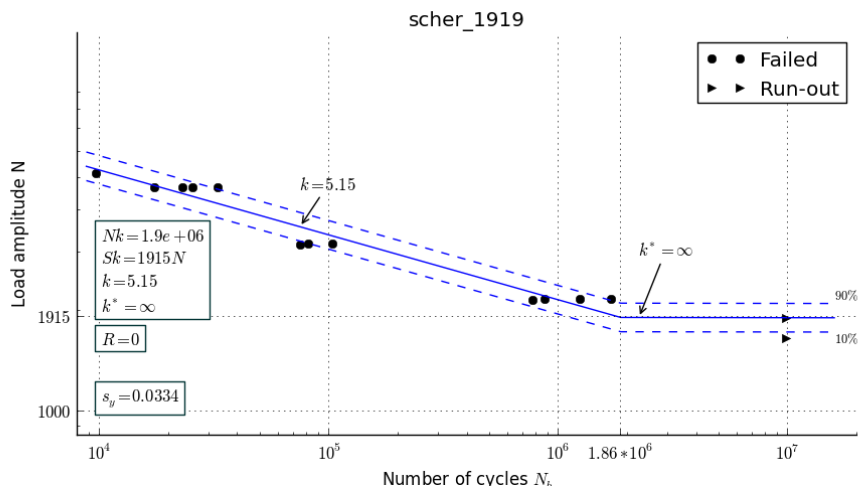
Figura A.21: FAT01_shear_191900

74
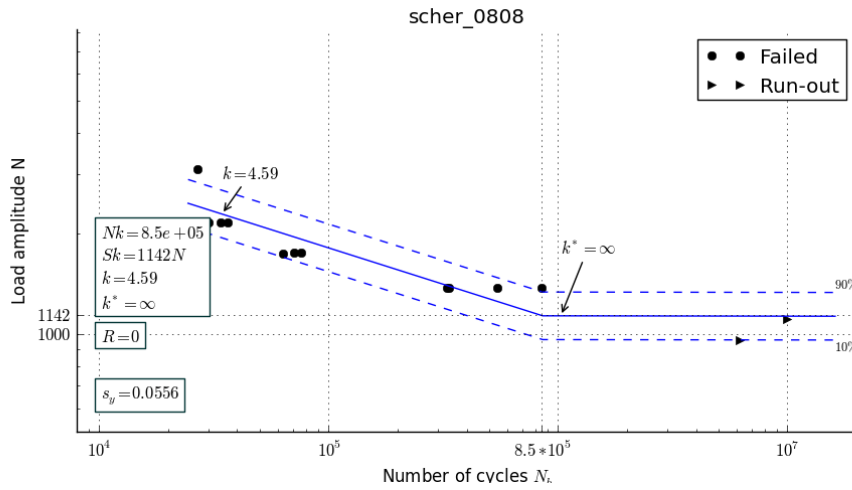
Figura A.22: FAT01_shear_080800
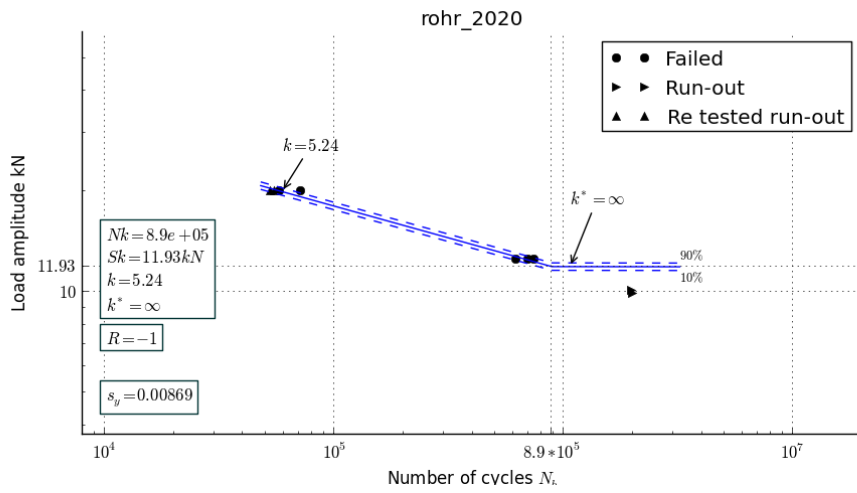
Figura A.23: FAT01_tube_202000
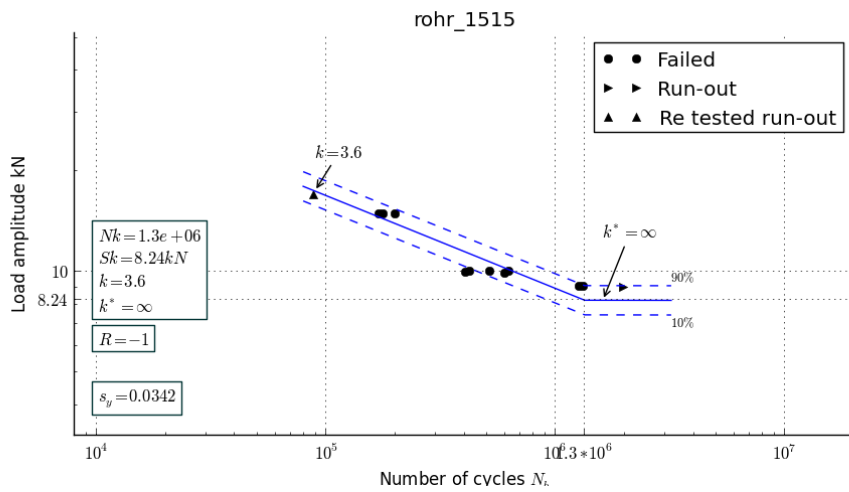
Figura A.24: FAT01_tube_151500

75
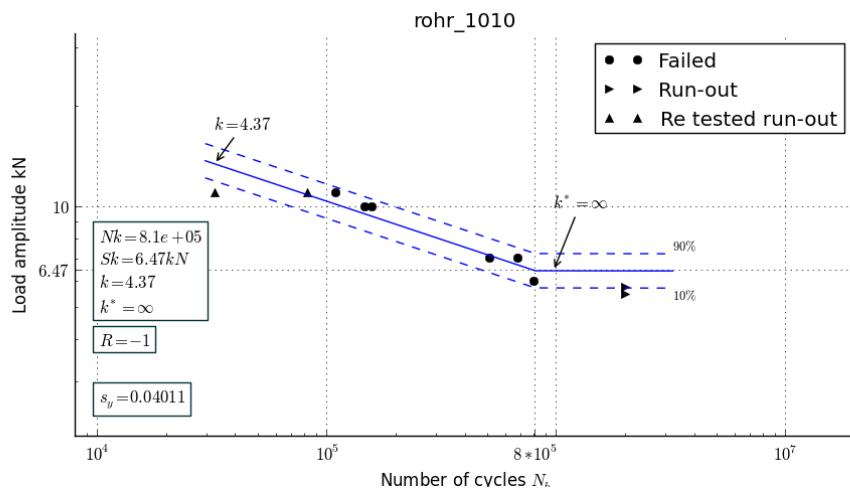
Figura A.25: FAT01_tube_101000

Asim et al.
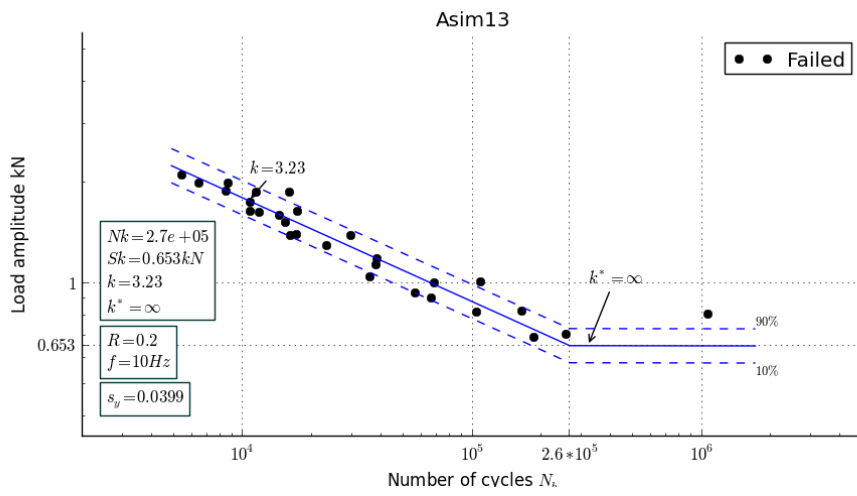
Figura A.26: Asim_shear_09309300

A222
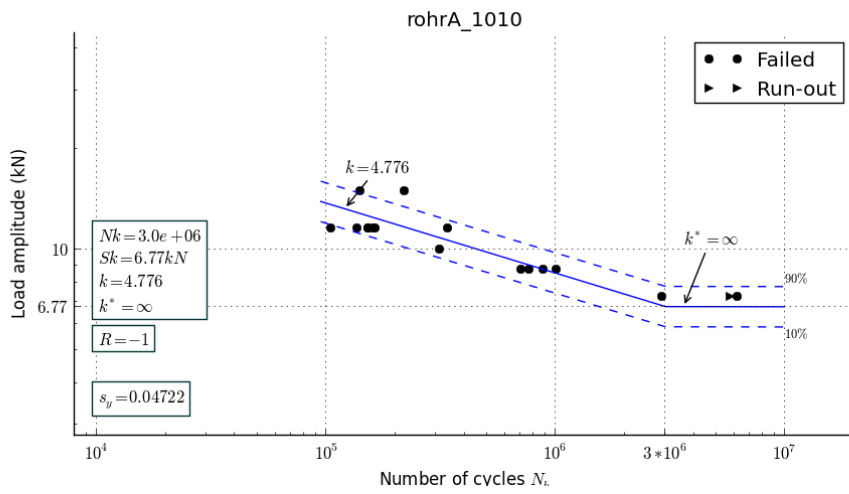
Figura A.27: A222_tube_101000
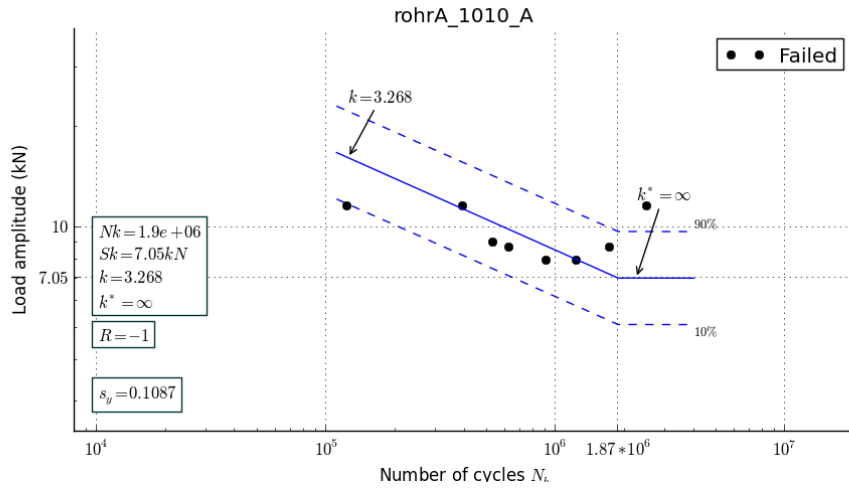
Figura A.28: A222_tube_101000_A
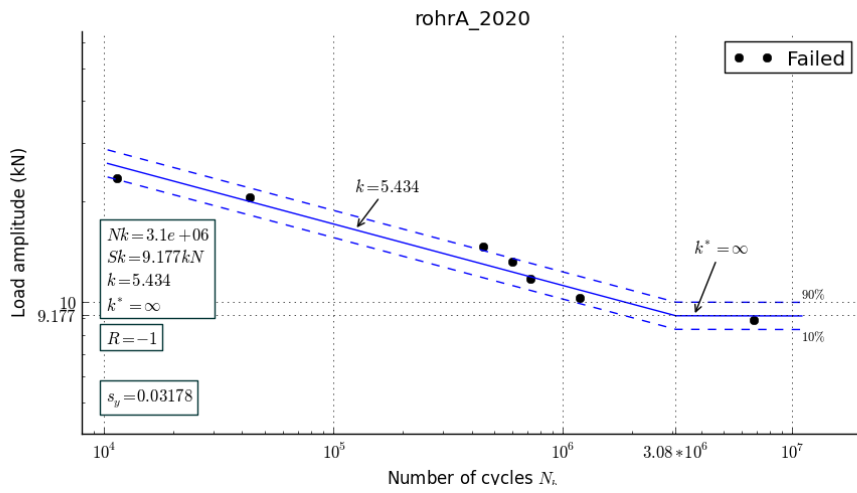
Figura A.29: A222_tube_202000

A233
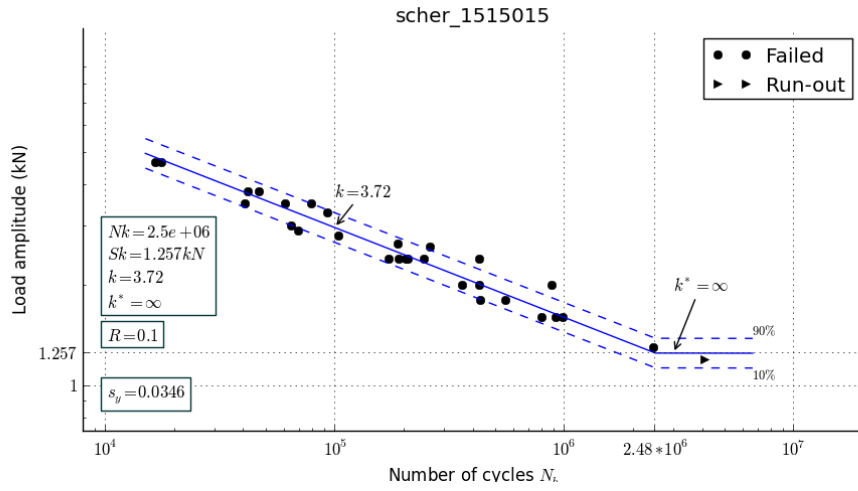
Figura A.30: A233_shear_1515015

SLC
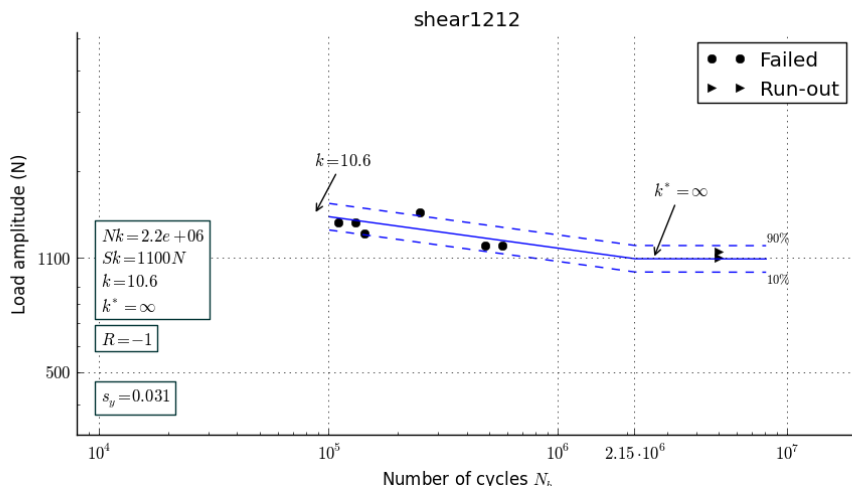
Figura A.31: SLC_shear_121204

Appendice B

Effective stress - Number of cycles curves
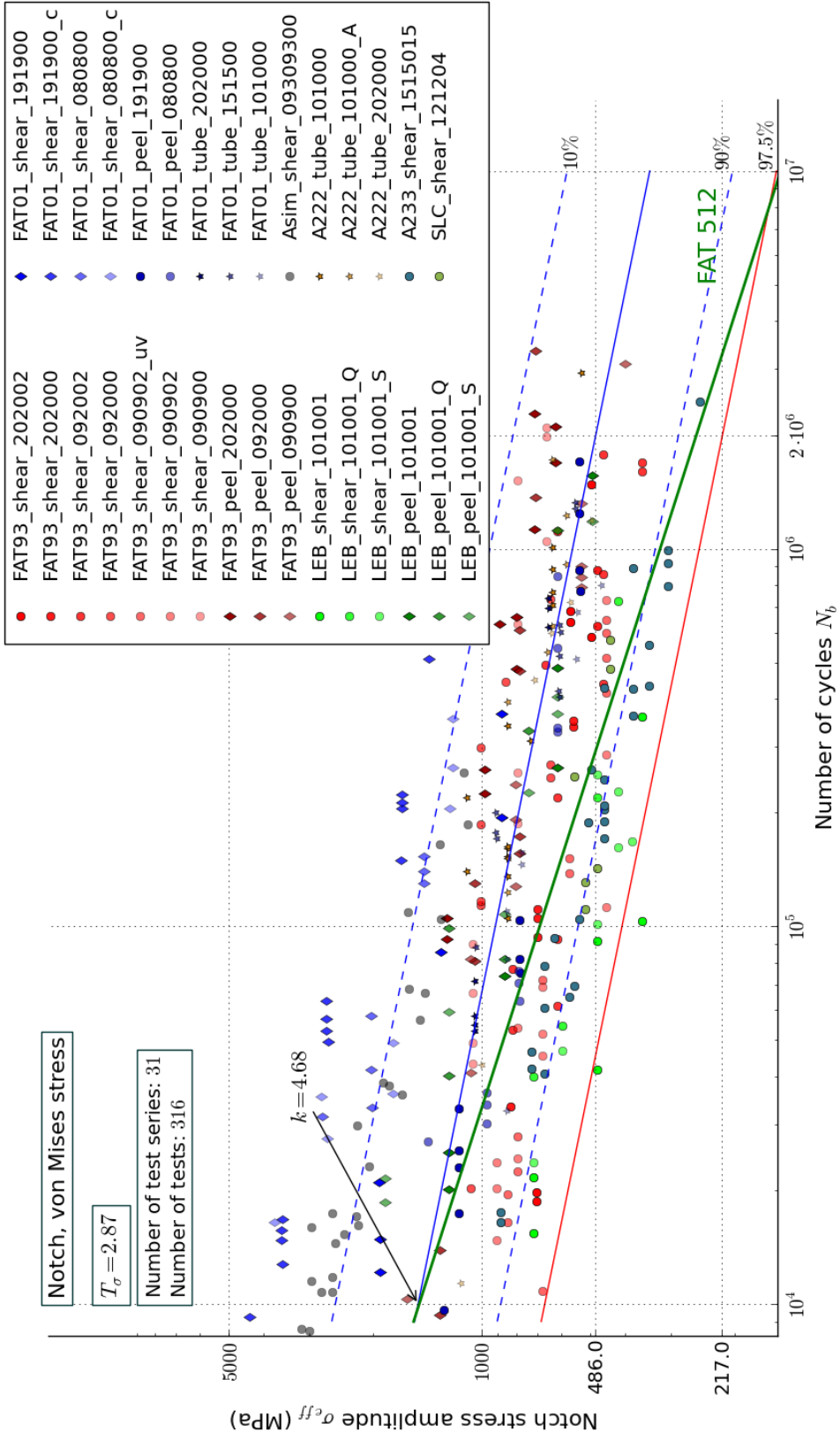
Figura B.1: Regression curve for maximum notch, von Mises stress
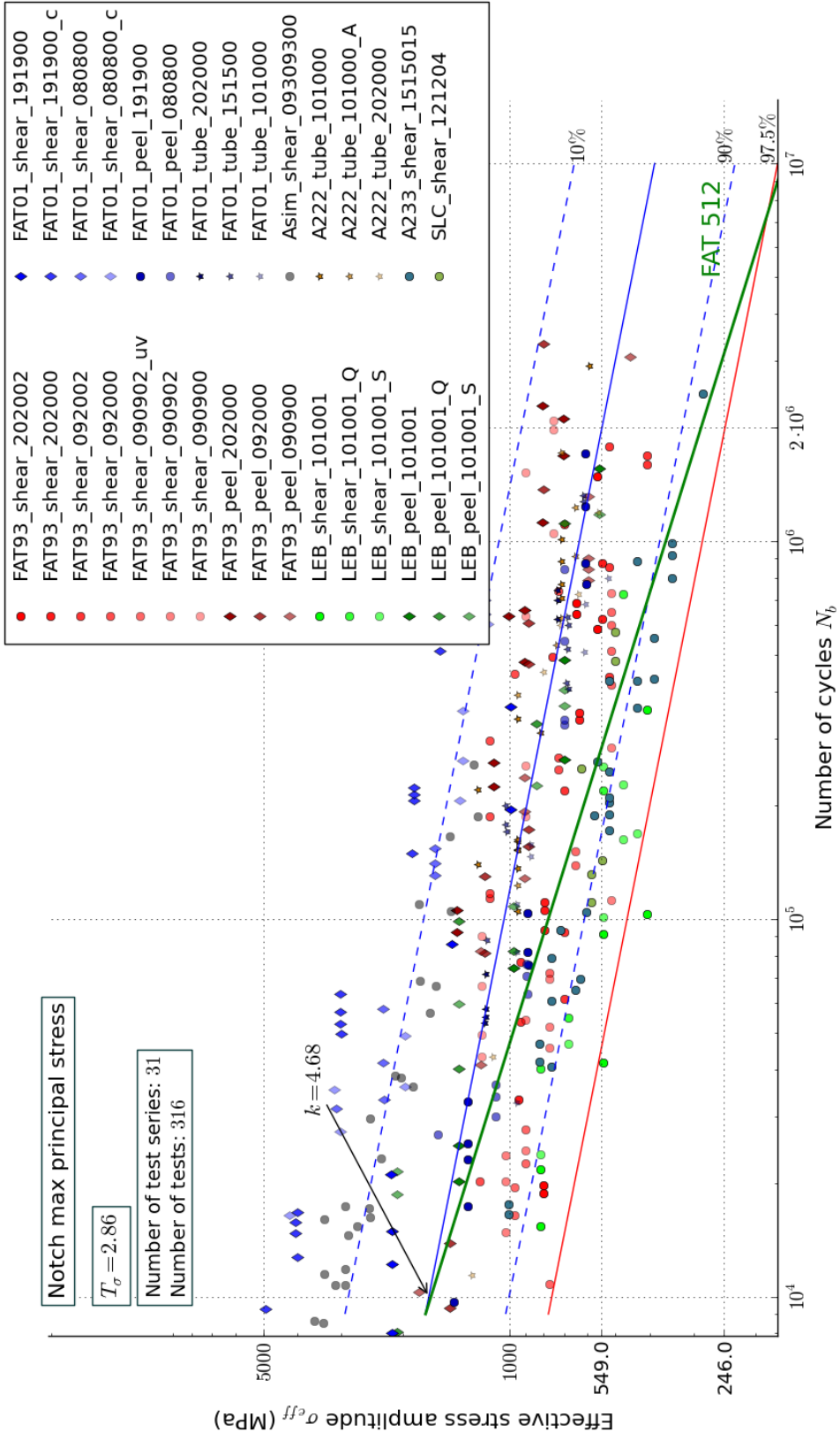
Figura B.2: Regression curve for maximum notch, PSH stress
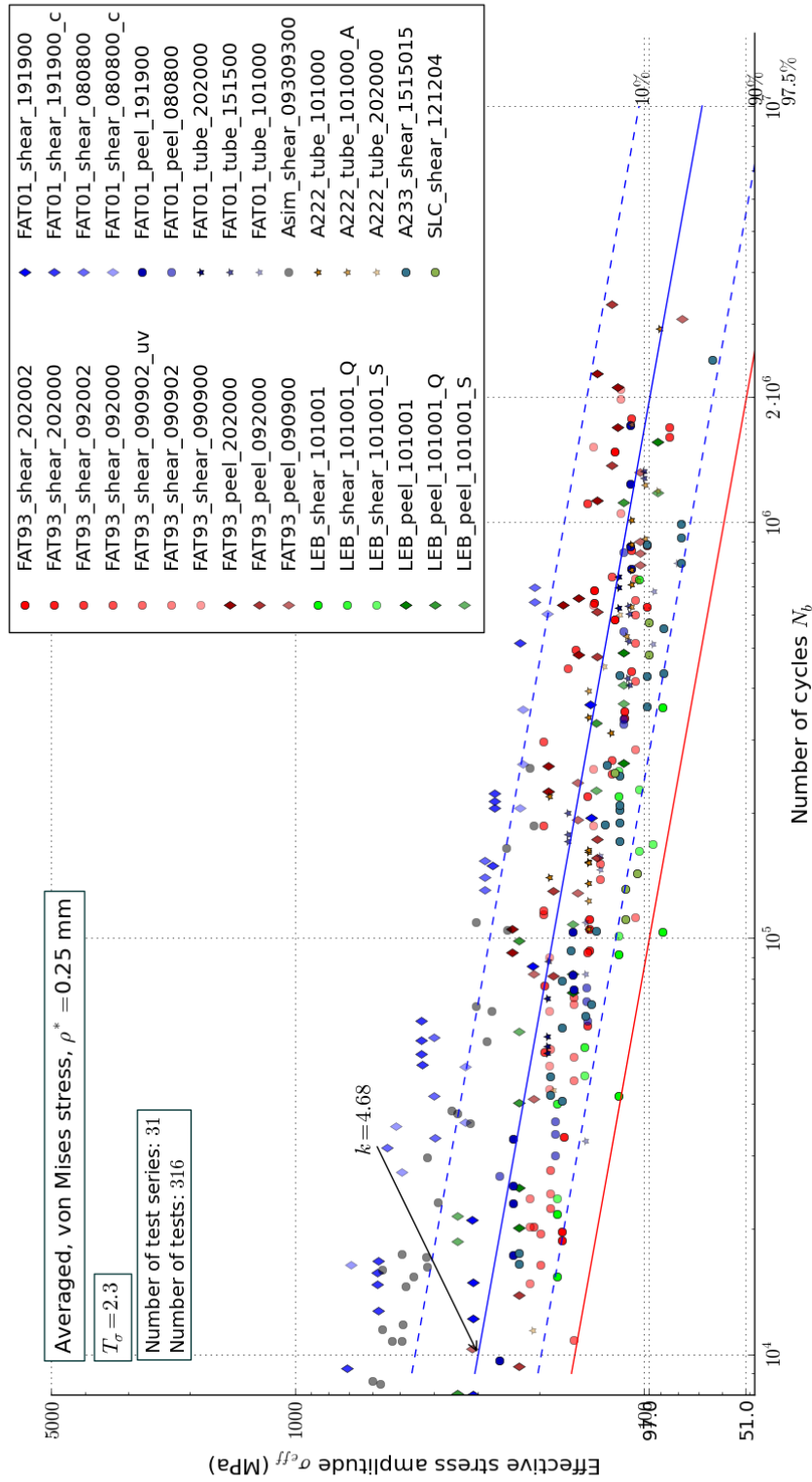
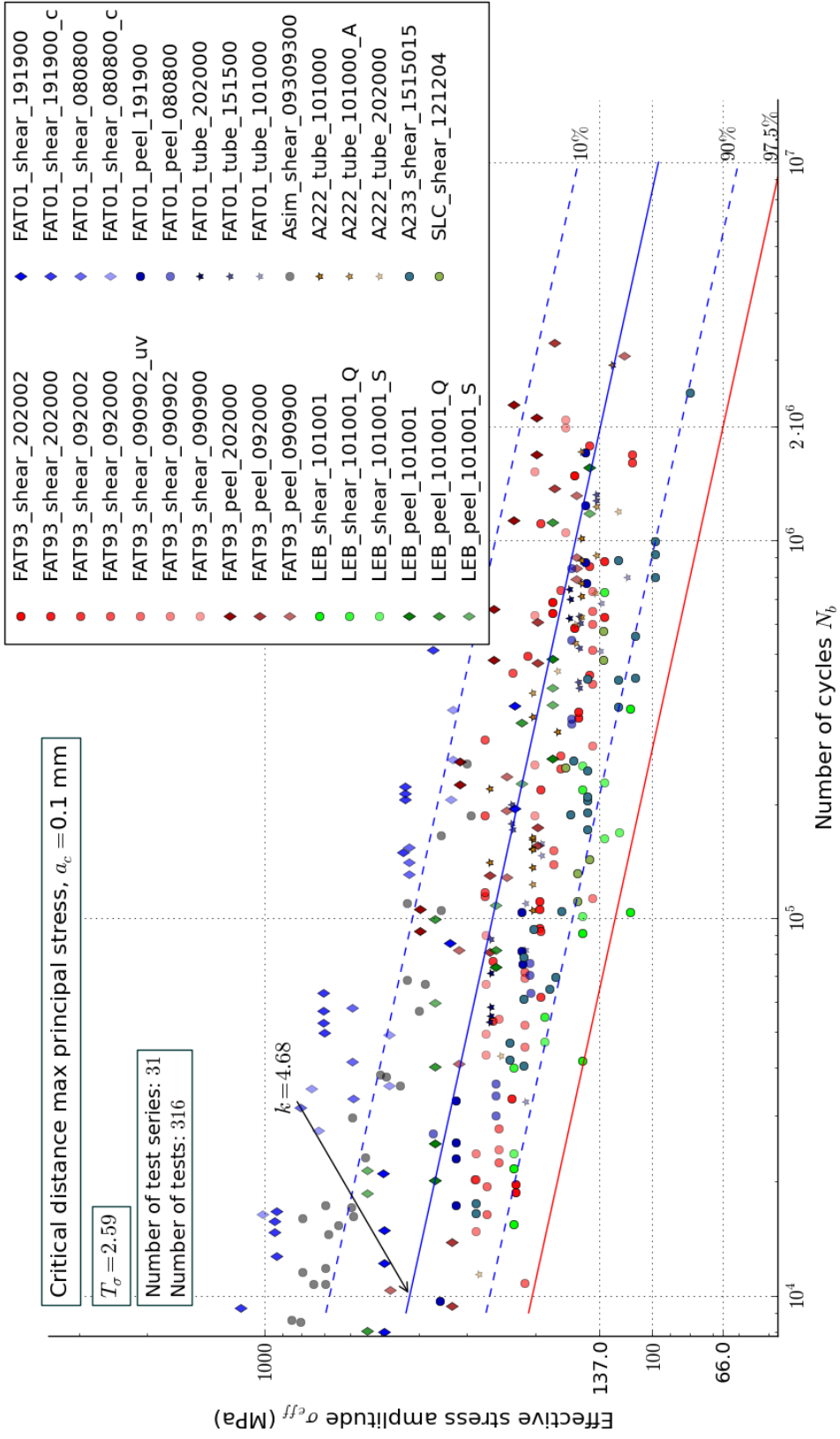Figura B.3: Regression curve for effective, von Mises stress from the averaged method, $\rho^* = 0.25$ mm
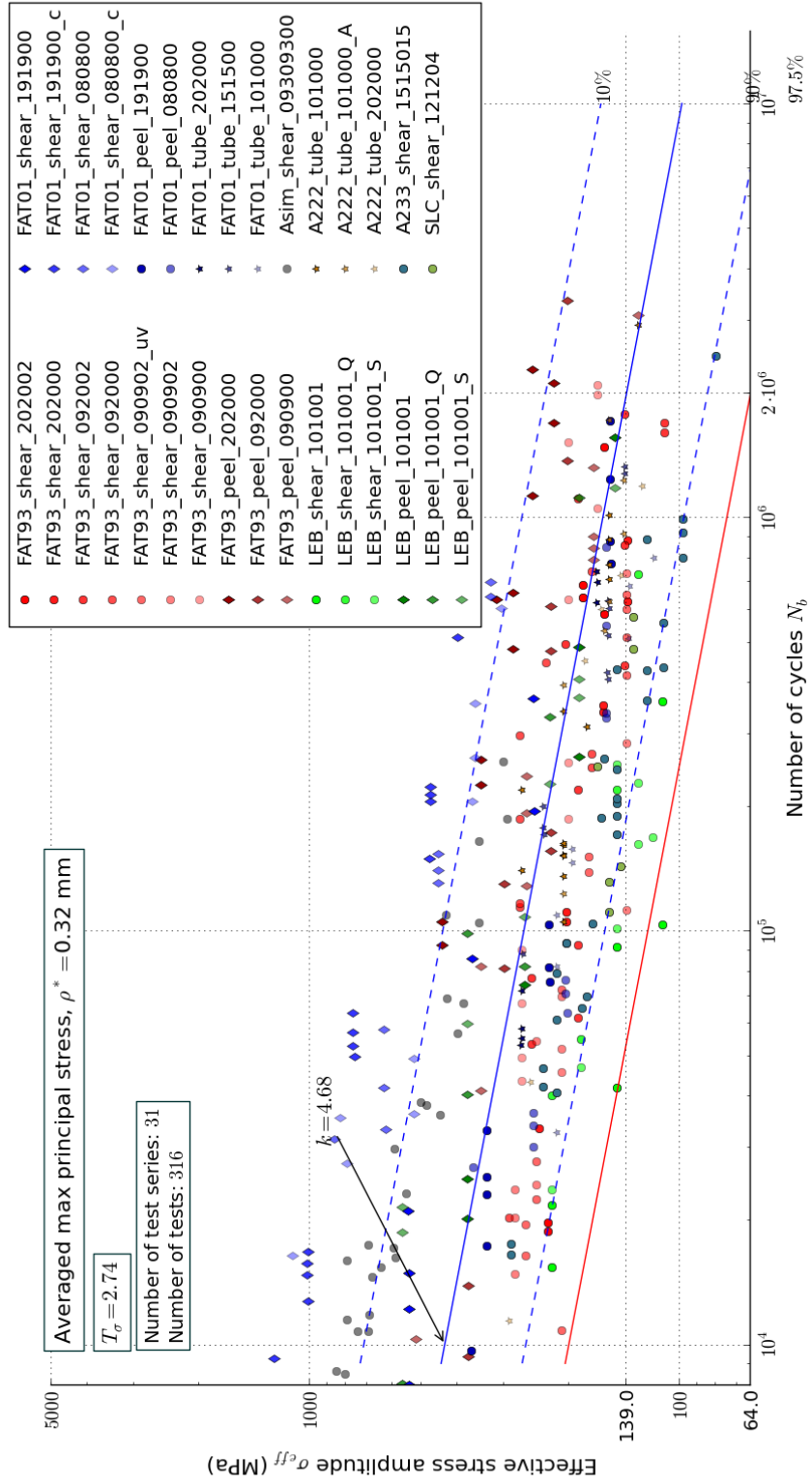
Figura B.4: Regression curve for effective, PSH stress from the averaged method, $\rho^* = 0.32$ mm
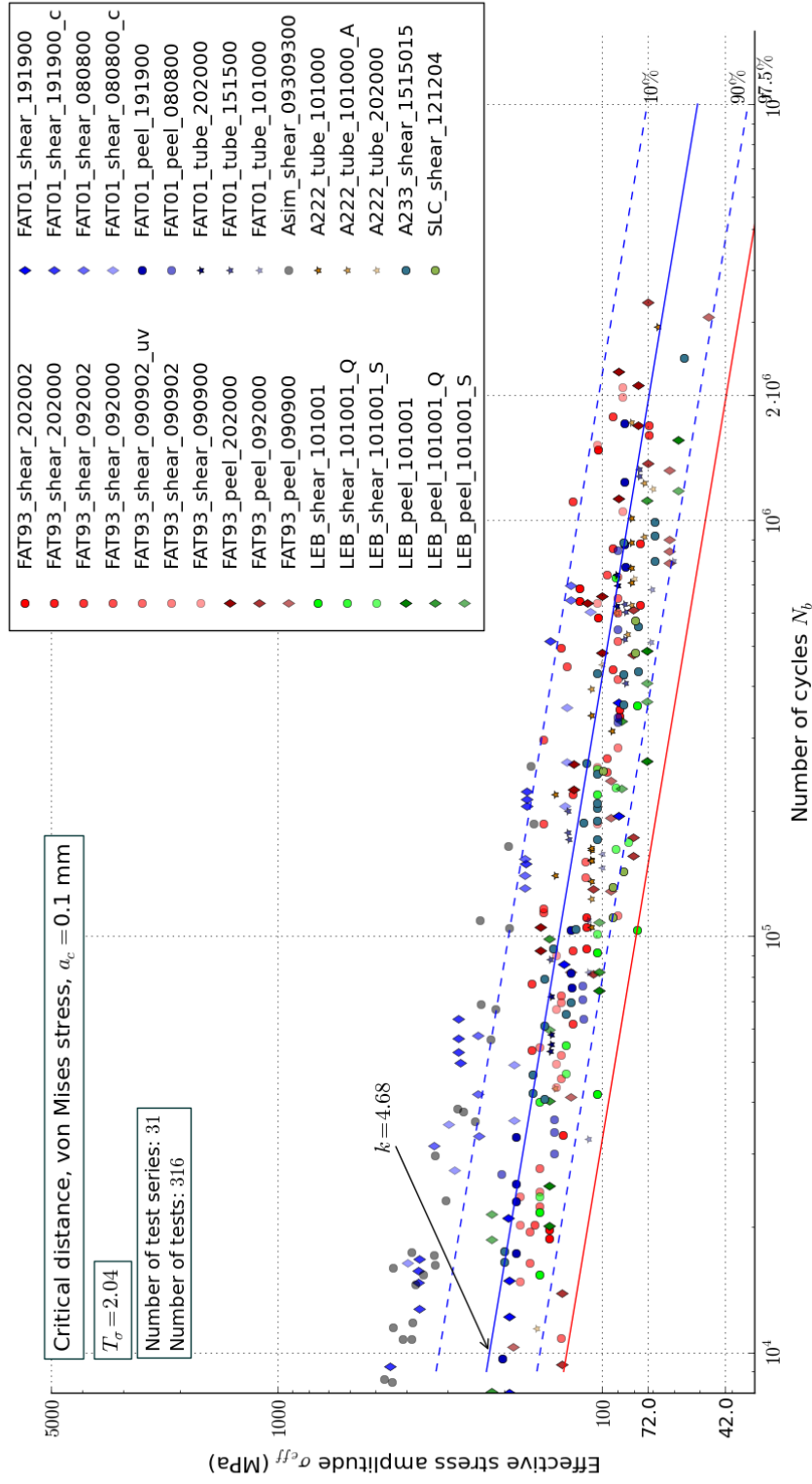
Figura B.5: Regression curve for effective, von Mises stress from the critical distance method, $a_c = 0.1$ mm

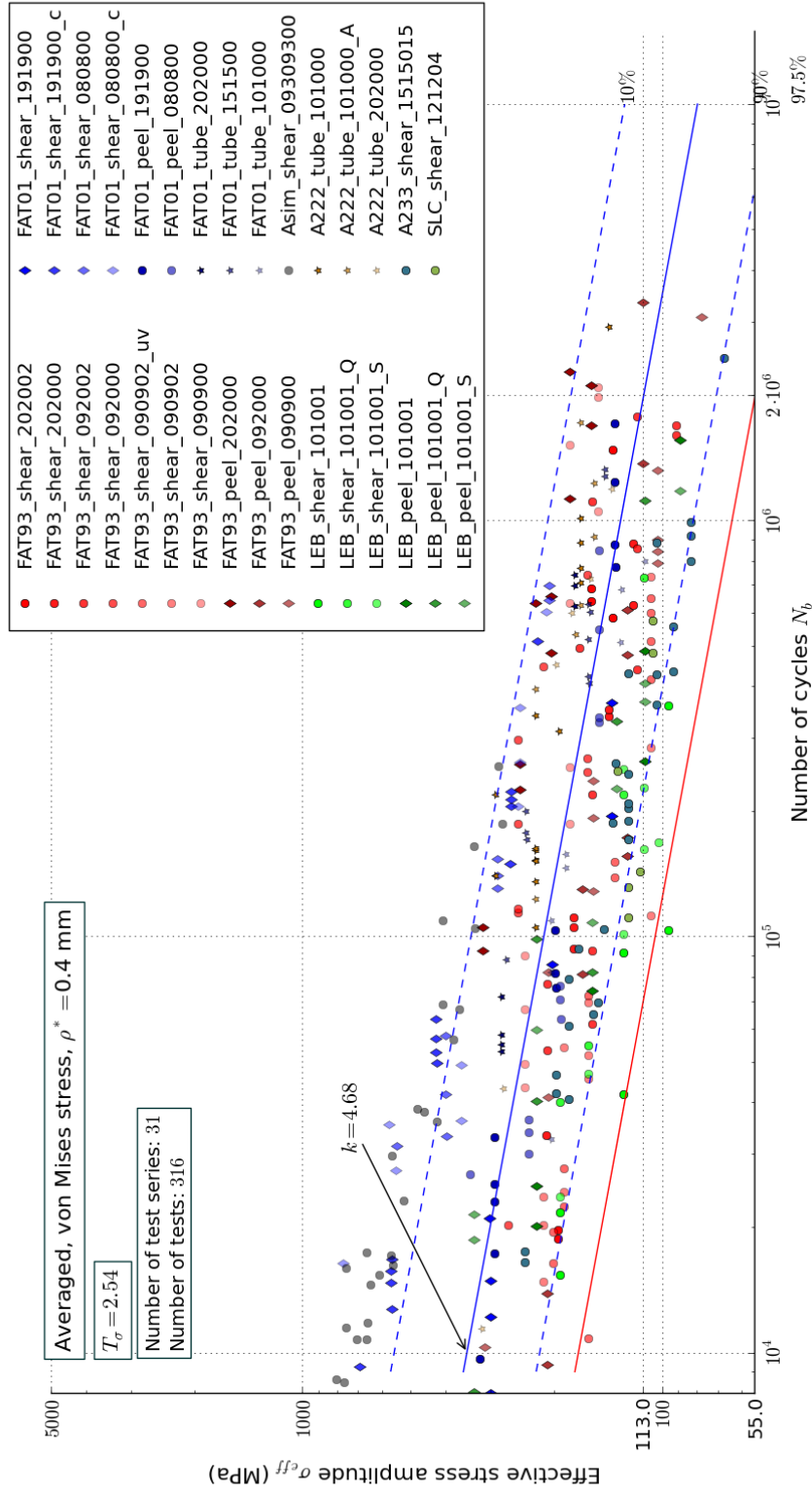Figura B.6: Regression curve for effective, PSH stress from the critical distance method, $a_c = 0.1$ mm

Figura B.7: Regression curve for effective, von Mises stress from the averaged method, $\rho^* = 0.4$ mm. Maximum effective stress path.
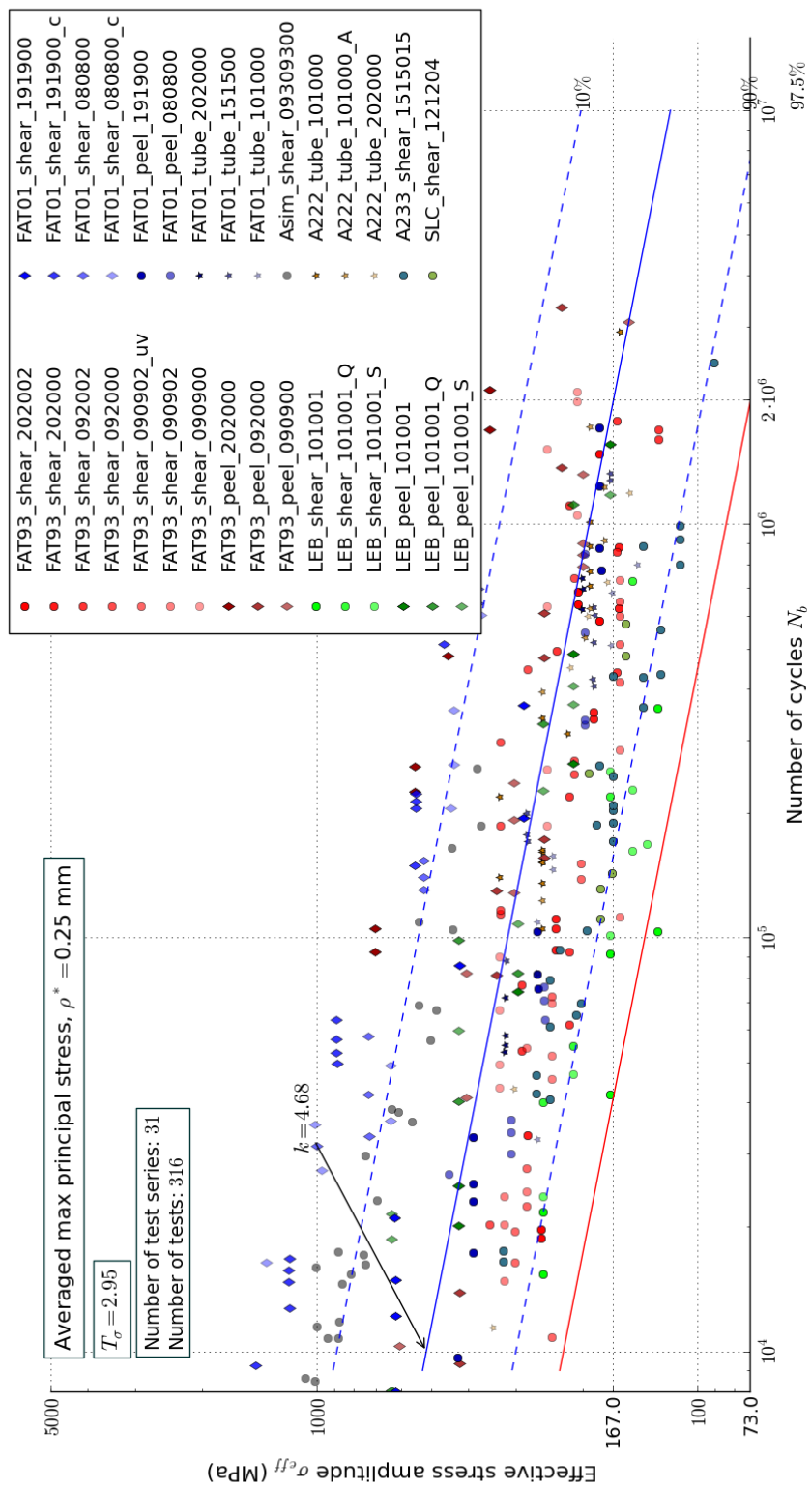
Figura B.8: Regression curve for effective, PSH stress from the averaged method, $\rho^* = 0.4$ mm. Maximum effective stress path.
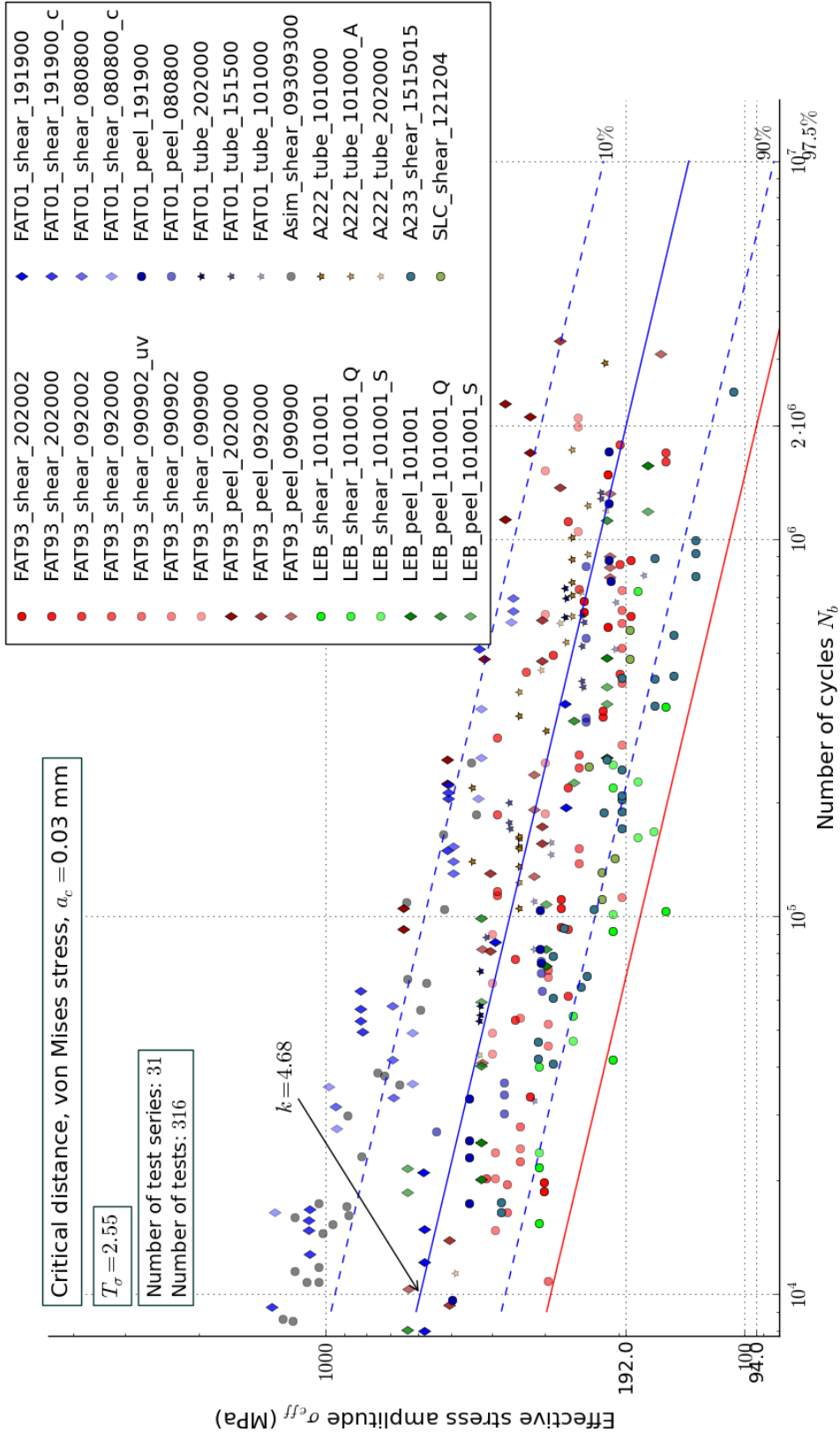
Figura B.9: Regression curve for effective, von Mises stress from the critical distance method, $a_c = 0.03$ mm. Maximum effective stress path.
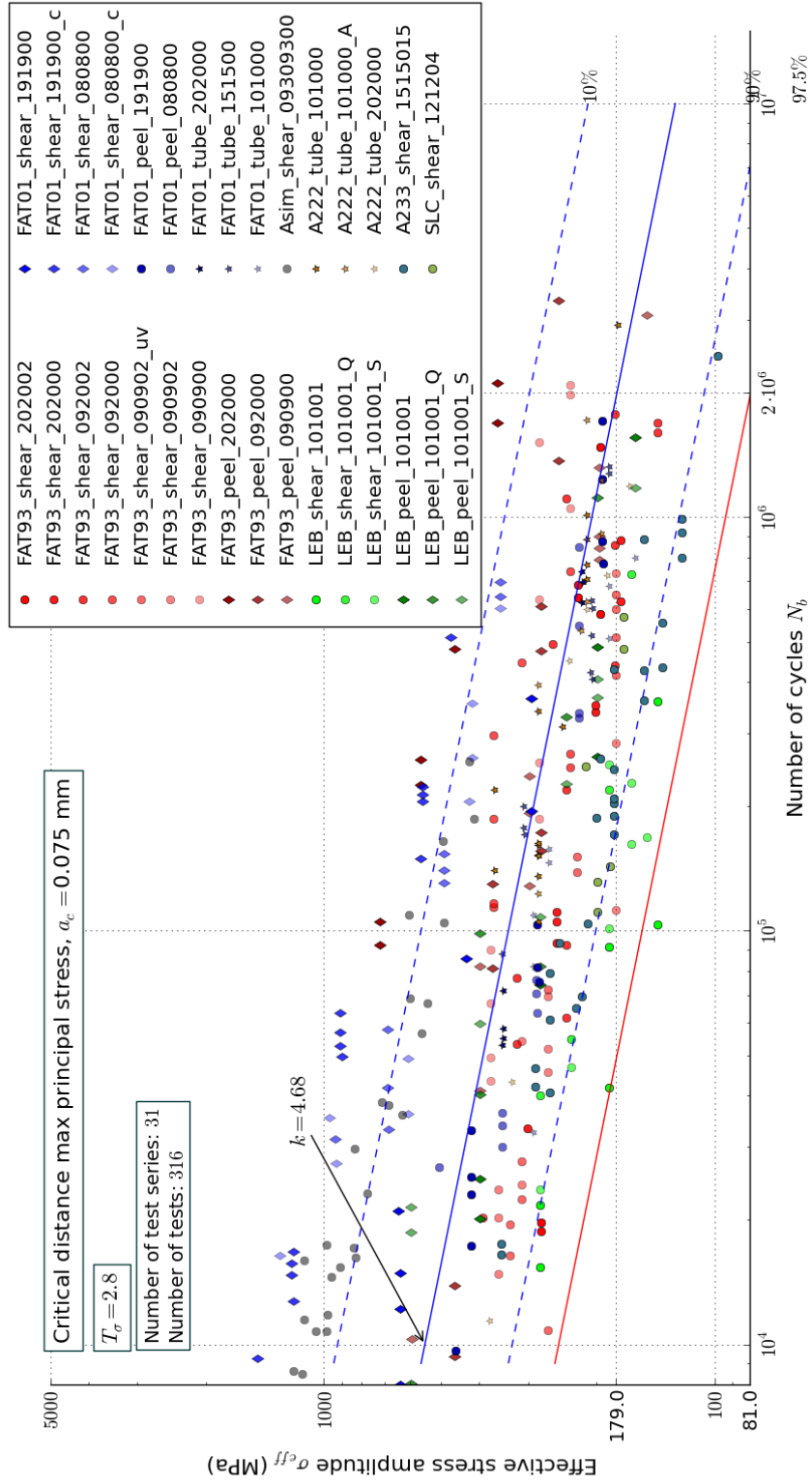
Figura B.10: Regression curve for effective, PSH stress from the critical distance method, $a_c = 0.075$ mm. Maximum effective stress path.
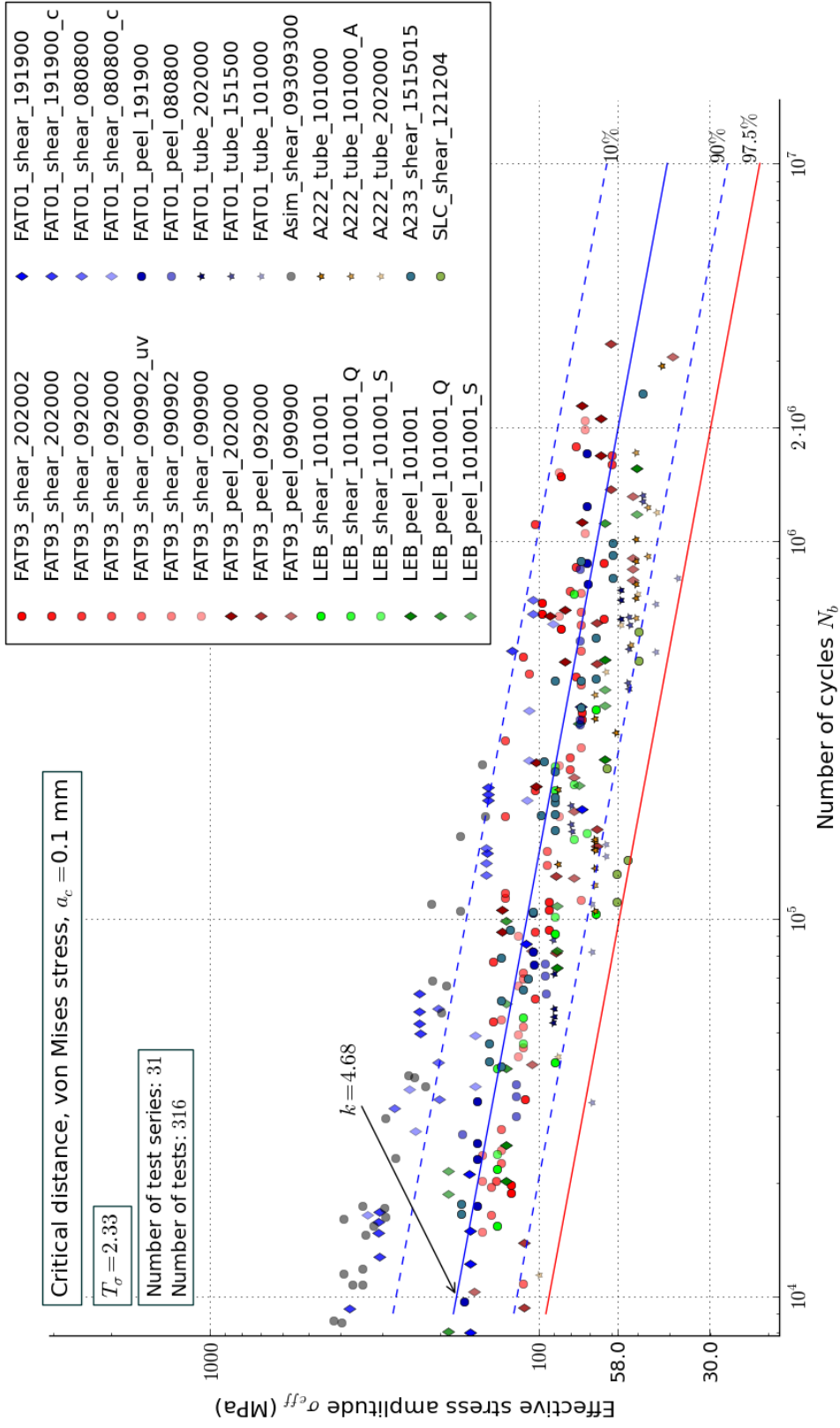
Figura B.11: Regression curve for effective stress from the critical distance method, $a_c = 0.1$ mm, corrected by $f(R)$ according to IIW
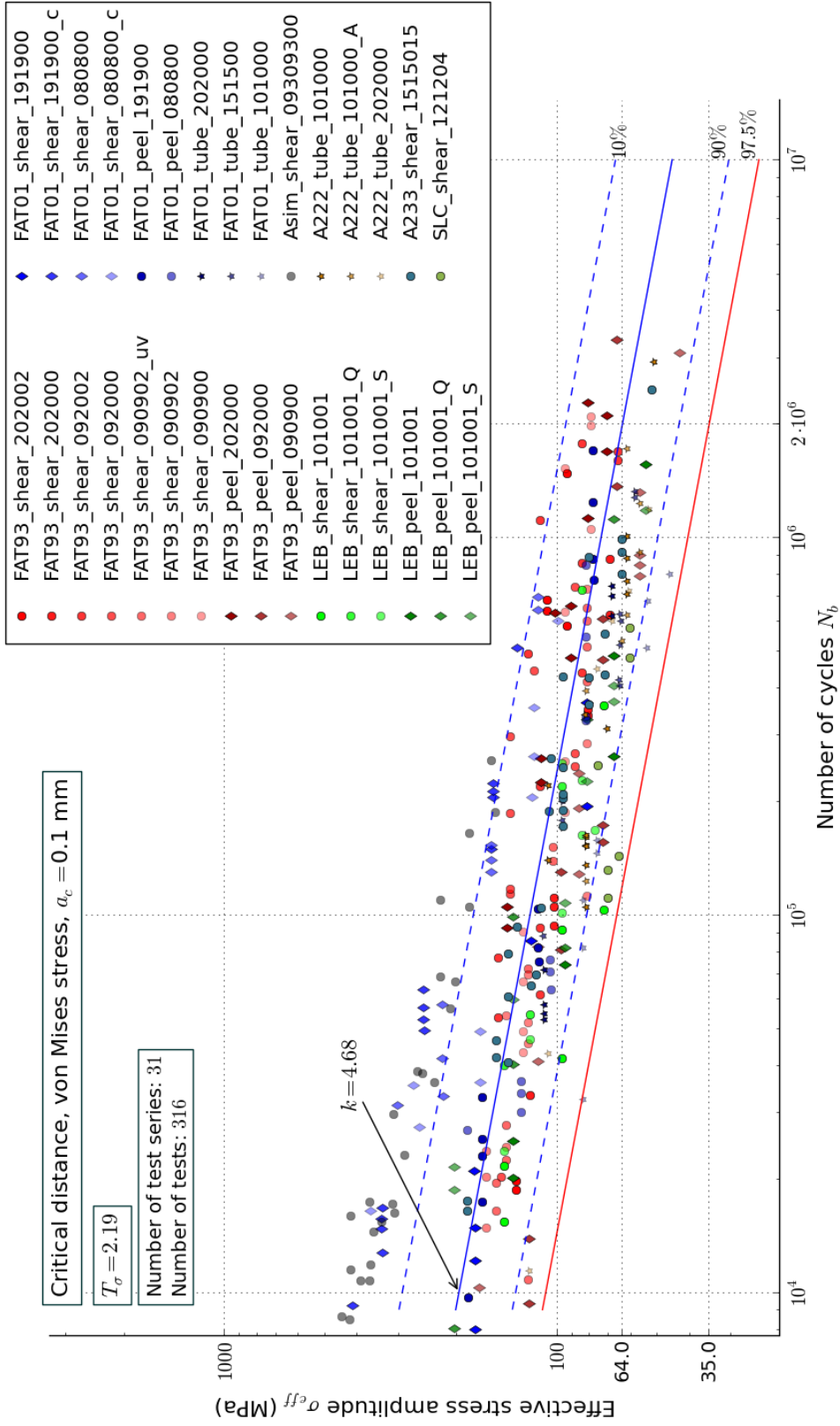
Figura B.12: Regression curve for effective stress from the critical distance method, $a_c = 0.1$ mm, corrected by $f(R)$ according to Sonsino

Bibliografia

[1] Kamran Asim, Kulthida Sripichai, and Jwo Pan. Fatigue behavior of laser welds in lap-shear specimens of high strength low alloy steel sheets. *International Journal of Fatigue*, 61:283–296, 2014. 33

[2] O.H. Basquin. The exponential law of endurance tests. In *Proceedings of American Society of Testing Materials*, volume 10, pages 625–630, 1910. 13

[3] J Baumgartner and T Bruder. An efficient meshing approach for the calculation of notch stresses. *Welding in the World*, 57(1):137–145, 2013. 24, 25

[4] T. Bruder, K. Störzel, and J. Baumgartner. Fatigue assessment of seam welds of automotive components by local stress approaches. *Materialwiss. Werkstofftech.*, 39(10):726–733, 2008. 33

[5] Thomas Bruder, Dennis Fritz, Martin Goede, and Lukas Rafflenbeul. European founded collaborative project superlight-car - towards a new generation of light weight automobiles. In *World Automotive Congress*, volume F2008-04-024, 2008. 34

[6] Matthew Creager and Paul C Paris. Elastic field equations for blunt cracks with reference to stress corrosion cracking. *International Journal of Fracture Mechanics*, 3(4):247–252, 1967. 9

[7] Martin Eibl. *Berechnung der Schwingfestigkeit laserstrahlgeschweißter Feinbleche mit lokalen Konzepten*. PhD thesis, TU Darmstadt, 2003. 33

[8] Adolf Hobbacher. *Fatigue design of welded joints and components: Recommendations of IIW Joint Working Group XIII-XV*. Woodhead Publishing, 1996. 4, 6, 7, 9, 16, 35, 53

[9] AF Hobbacher. The new iiw recommendations for fatigue assessment of welded joints and components–a comprehensive code recently updated. *International Journal of Fatigue*, 31(1):50–58, 2009. 7, 8

[10] GR Irwin. Fracture. encyclopaedia of physics, vol. vi. *Springer-Verlag*, 1:168, 1958. 9

[11] R. C. Juvinall and K. M. Marshek. *Fondamenti della progettazione dei componenti delle macchine*. Edizioni ETS, 2002. 6

[12] M. Beghini L. Bertini. Relazione tecnica rl1262(2010): Metodologie di analisi del comportamento a fatica di carrelli ferroviari saldati: Parte i. *Dipartimento di Ingegneria meccanica nucleare e della produzione, Pisa.* 3, 6

[13] Heinz Neuber. *Kerbspannungslehre*, volume 3. Springer-Verlag Berlin, 1985. 5, 9, 12, 25

[14] Dieter Radaj, Cetin Morris Sonsino, and Wolfgang Fricke. *Fatigue assessment of welded joints by local approaches.* Woodhead Publishing Limited, 2006. 3, 6

[15] Dieter Radaj and Michael Vormwald. Generalised neuber concept of fictitious notch rounding. In *Advanced Methods of Fatigue Assessment*, pages 1–100. Springer, 2013. 9, 12, 13, 23, 24, 27

[16] H. Schmidt, J. Tölle, T. Bruder, H. Hanselka, and O. Hahn. On-line damage detection and monitoring at thin sheet joints for deriving failure criteria. *Matériaux & Techniques*, 99:743–750, 2011. 33

[17] Cetin Morris Sonsino. Course of sn-curves especially in the high-cycle fatigue regime with regard to component design and safety. *Int. J. Fatigue*, 29(12):2246?2258, 12 2007. 32

[18] Cetin Morris Sonsino. A consideration of allowable equivalent stresses for fatigue design of welded joints according to the notch stress concept with the reference radii rref= 1.00 and 0.05 mm. *Welding in the World*, 53(3-4):R64–R75, 2009. 9, 16, 17, 43, 53

[19] Cetin Morris Sonsino, Thomas Bruder, and Dipl-Ing Jörg Baumgartner. Sn lines for welded thin joints?suggested slopes and fat values for applying the notch stress concept with various reference radii. *Welding in the World*, 54(11-12):R375–R392, 2010. 9, 35

[20] CM Sonsino, W Fricke, F De Bruyne, A Hoppe, A Ahmadi, and G Zhang. Notch stress concepts for the fatigue assessment of welded joints–background and applications. *International Journal of Fatigue*, 34(1):2–16, 2012. 9, 41, 43

[21] JE Spindel and E Haibach. The method of maximum likelihood applied to the statistical analysis of fatigue data. *International Journal of Fatigue*, 1(2):81–88, 1979. 14, 15, 16

[22] Genbao Zhang. Method of effective stress for fatigue: Part i–a general theory. *International Journal of Fatigue*, 37:17–23, 2012. 10, 11, 12, 59

[23] Genbao Zhang, Cetin Morris Sonsino, and Ralph Sundermeier. Method of effective stress for fatigue: Part ii–applications to v-notches and seam welds. *International Journal of Fatigue*, 37:24–40, 2012. 23, 25, 26, 58